Blind Adaptive Antenna Arrays for Mobile Communications

by

Paul Petrus

Thesis submitted to the faculty of the
Virginia Polytechnic Institute & State University
in partial fulfillment of the requirements for the degree

MASTER OF SCIENCE
in
Electrical Engineering

APPROVED:

Dr. Jeffrey H. Reed, Chairman

Dr. Theodore S. Rappaport

Dr. Brian D. Woerner

December, 1994

Blacksburg, Virginia

BLIND ADAPTIVE ANTENNA ARRAYS FOR MOBILE COMMUNICATIONS

by

Paul Petrus

Committee Chairman: **Jeffrey Hugh Reed**
Department of Electrical Engineering

ABSTRACT

Adaptive antenna arrays have tremendous potential for increasing the capacity of mobile communications, by reducing co-channel interference, multipath and noise. Blind adaptive algorithms, that is, algorithms which do not require a training sequence, are investigated and compared in this study. These algorithms are tested for common cellular signals. The performances of three blind adaptive algorithms: the Constant Modulus Algorithm (CMA), the Spectral self-COherence Restoral Algorithm (SCORE), and the spectral correlation predictor using a Time-Dependent Adaptive Array (TDAA), are studied. The TDAA is introduced as a new blind algorithm that exploits the cyclostationary property of the signal. Results show that the TDAA is able to out-perform the other blind algorithms for most of the test conditions and provides the optimal MSE solution.

Acknowledgments

I would like to convey my heart-felt thanks to Dr. Reed for providing me with the technical support to complete this research project. He has been always a source of inspiration and a guiding light. I look forward to work with him in years to come.

I am indebted to Dr. Rappaport and Dr. Woerner for their valuable advice. I appreciate their help in carefully reviewing this thesis report.

I thank Dr. Steve V. Schell, Associate Professor, Penn State University, for giving me insight into SCORE and helping me to startup on SCORE algorithm. I also thank Tom. E. Biedka for explaining all intricate details about array processing.

I wish to thank my parents who moulded, shaped, and encouraged me to pursue my higher studies abroad.

I appreciate the help rendered by Joe Liberti, Carl Dietrich, Volker, Rong, Stavros, TPS and Prab Koushik.

I thank all my friends who had put up with me in the past one and a half years.

I thank my creator for the abilities, he has entrusted me with.

Contents

1 Introduction **1**

1.1 Motivation 3

1.2 Overview 5

2 Previous Work in Blind Adaptive Arrays **8**

3 Blind Adaptive Algorithms **14**

3.1 Background Theory 14

3.2 Antenna Array 15

3.2.1 Two-Element Array 15

3.2.2 Extension of the Model 19

3.3 Constant Modulus Algorithm (CMA) 21

3.3.1 Basic Description 21

3.3.2 Adaptive Algorithm 23

3.3.3 Least-Squares CMA Algorithm (LSCMA) 24

3.3.4 Properties of the Constant Modulus Algorithm 26

3.4 Spectral self-COherence REstoral Algorithm (SCORE) 31

3.4.1 Cyclostationarity 31

3.4.2 Exploitation of Cyclostationarity 31

3.4.3 Measure of Cyclostationarity 32

3.4.4 Least Squares SCORE Algorithm 36

3.4.5 Variations of SCORE Algorithm 40

3.4.6 SCORE-Tapped Delay Line Structure 42

3.4.7 Recursive Least Squares SCORE Algorithm Implementation 43

3.5 Time Dependent Adaptive Array 44

3.5.1 Interpretation of this New Blind Adaptive Algorithm 45

3.5.2 Mean-Square Error Analysis for TDAA 45

3.4.4 Recursive Least Squares TDAA Implementation 55

4 Simulation and Performance Analysis 56

4.1 Signal Model 56

4.1.1 AMPS Standard 57

4.1.2 IS-54 Standard 58

4.2 A Simple Statistical Model for Angle of Arrival in Line-of-Sight Multipath Channels 60

4.3 Performance Criteria 68

4.4 Performance of the Adaptive Array on AMPS and IS-54 signals 69

4.5 Implementation of the Algorithms 70
4.5.1 CMA Implementation 70
4.5.2 SCORE-TDL Implementation 71
4.5.3 TDAA Implementation 71
4.6 Problems in Simulating Realistic Conditions 72
4.7 Discussion of the Results 72
4.7.1 Testing CMA on AMPS Signal..... 73
4.7.1.1 Interference from Background Noise 73
4.7.1.2 Interference from Co-Channel Users 78
4.7.1.3 Effects of Increasing the Number of Elements on Interference from Co-channel Users 84
4.7.2 Testing SCORE on AMPS Signal..... 84
4.7.2.1 Cyclostationarity Characteristics of AMPS 86
4.7.2.2 Interference from Background Noise..... 88
4.7.2.3 Interference from Co-Channel Users 90
4.7.2.4 Effects of Increasing the Number of Elements on Interference from Co-channel Users..... 94
4.7.3 Testing TDAA on AMPS Signal..... 94
4.7.3.1 Interference from Background Noise 95
4.7.3.2 Interference from Co-Channel Users..... 95
4.7.4 Testing CMA on IS-54 Signal..... 102
4.7.4.1 Interference from Background Noise 105
4.7.4.2 Interference from Co-Channel Users 105
4.7.4.3 Effects of Increasing the Number of Elements on Interference from Co-channel Users 112

4.8 Summary 115

5 Conclusions and Future Work 117

Appendix. 120

References 121

Vita 127

List of Figures

1. Two-Element Array 16
2. Normalized Gain Response 19
3. Least-Squares SCORE Processor 39
4. Time-Dependent Adaptive Array (Structure 1) 47
5. Time-Dependent Adaptive Array (Structure 2) 51
6. Time Frame Structure of IS-54 Standard Signal 59
7. Constellation Diagram Showing Transition Paths 60
8. The locus of all points where a scatterer might lie which results in a single bounce multipath component with delay τ_i is an ellipse with $a = c\tau_i/2$, $f = d/2$, and $b = \sqrt{f^2 - a^2}$ 63
9. Geometry for Determining θ_a as a Function of θ_d 64
10. The probability density function for the angle of arrival of single bounce multipath components as a function of excess delay for a T-R separation of 4 km 67
11. Delay Profile of the Channel 68
12. Radiation Pattern of the Array as the Algorithm Converges 74

13. Convergence Curves for the Weights of the Array 75
14. Frequency Domain Plots of the Original, Corrupted, and Reconstructed Voice Signals for CNR =4 dB 76
15. Comparison of MSE Curves of CMA Array with a Single Antenna 77
16. A cellular coverage region is split into many different cells where each cell has a base station. The shading in each cell represents the set of channels used in that cell. Cells with the same shading reuse the same channels. The figure shows a mobile subjected to co-channel interference 78
17. Radiation Pattern in the Presence of an Interferer 79
18. Performance Curves for CMA Array in the Presence of Interferers 81
19. Figure Depicting Angle Of Arrivals of Different Users 82
20. Bar Chart of MSE of a Four-Element CMA Array in a Multi-Co-Channel Environment 83
21. Performance Improvement Curves for Increased Number of Elements 85
22. Performance Curve for SCORE-TDL Array in a Noisy Environment 89
23. Post-Demodulated MSE Curves of the SCORE-TDL Array in an Interference Environment 91
24. Pre-Demod MSE Curves of the SCORE-TDL Array in an Interference Environment 92
25. Bar Chart of MSE of the SCORE-TDL Array in a Multi-Co-Channel Environment 93
26. Performance Improvement due to Increased Number of Elements 96
27. Performance Curve for TDAA in a Noisy Environment 98

28. Pre-Demod MSE Curve for TDAA in an Interference Environment 99

29. Post-Demod MSE Curve for TDAA in an Interference Environment..... 100

30. Bar Chart of MSE for TDAA in a Multi-Co-Channel Environment 101

31. The Setup Used to Test CMA Array on IS-54 Signals 103

32. The Structure of the Time Frame for the Desired User and Two Co-Channel Users, Users with the Same Shade Transmit Simultaneously 104

33. Performance Curve for User 1 in a Noisy Environment 106

34. Performance Curve for User 2 in a Noisy Environment 107

35. Performance Curve for User 3 in a Noisy Environment 108

36. Performance Curve for User 1 in an Interference Environment 109

37. Performance Curve for User 2 in an Interference Environment 110

38. Performance Curve for User 3 in an Interference Environment 111

39. Performance Curve for CMA Array on IS-54 Signals in a Multi-Co-Channel Environment 113

40. Performance Curves for CMA Array in an Interference Environment as the Number of Elements Increases 114

41. Performance Comparison Curves for Various Arrays in an Interference Environment 116

List of Tables

1. Examples of Spectrally Self-Coherent Signals 34

2. Frequency Allocation for AMPS Standard 57

3. AOA for Different Users 102

Chapter 1

Introduction

Mobile-radio communication systems are used extensively today. In a mobile environment the propagation channel contains multipath elements that introduce intersymbol interference (ISI) and cause large rapid amplitude changes in the signal envelope. In addition, the signal is further degraded by co-channel interference. The signal is also subjected to noise, but the main problems that limit the capacity of cellular communication are the ISI, adjacent and co-channel interference. Their effect is to degrade the SNR, reducing the capacity, operating range and performance of a radio system.

In order to keep the performance degradation of a radio system to an acceptable level as the radio traffic increases, it is necessary to adopt measures to improve the system capacity. Several techniques have been developed in the past. These techniques fall into one (or a combination) of four categories: adaptive equalizers, anti-multipath modulation techniques, spread-spectrum techniques and antenna arrays.

An array is a system which enhances a signal corrupted by noise, interference, multi-

path and fading. The performance index is the Signal to Noise Ratio (SNR) at the output of the array, and the system acts to maximize the output SNR.

There are several advantages of the adaptive array over a conventional array. The adaptive antenna array senses the interference sources and suppresses them automatically, improving the performance of the radio system, often without the *a priori* knowledge of the interference location. An adaptive array may achieve more reliable communication compared to the conventional array. If a single antenna of the conventional array fails, the sidelobe level and the main lobe width increase, and the main lobe and the null locations are modified. For an adaptive array, graceful deterioration of the SNR results if an element of the array fails. Therefore, more reliable communication as well as an increase in the capacity of a single cell can be achieved. Here we assume that the base station has the adaptive array and the mobile has only a single omni-directional antenna. The reason for this assumption is, the reverse channel is more vulnerable to interference than the forward channel [Gil91], and antennas at the base are more technically feasible than at the mobile with the current technology.

A second advantage of an adaptive array over a conventional array is that there are many cases in which the radiation pattern of the array is determined by close (in terms of wavelength) scatterers, rather than by its own pattern in free space. In such circumstances, an adaptive array is less sensitive, operating better than the conventional arrays.

To obtain high gain and low sidelobe levels for a conventional array, it is necessary to build it within the tight mechanical and/or electrical tolerances. Due to self-correcting mechanism of the radiation pattern, adaptive arrays can be built with lower tolerances and thus at a lower cost.

The conventional technique for adapting an array is to use a training sequence to determine the array combiner weights. However, training sequence directed adaptation

techniques will not produce the optimal solution for a Doppler-shifted signal, since the adaptation algorithm cannot account for the frequency shift. Furthermore in a dynamic environment like the mobile channel, a blind adaptation algorithm (an algorithm that does not require an external training sequence) is necessary to be able to correct the dynamic channel. A blind algorithm adapts by exploiting signal properties like constant envelope, spectral redundancy and so on. The algorithms are classified depending on the property they exploit. This work investigates the relative merits of various blind adaptive array algorithms for improving the performance of mobile communications in the presence of multipath, fading, noise and interference.

1.1 Motivation

Beamforming is the processing used in conjunction with an array of sensors to provide a versatile form of spatial filtering [Edm89]. Antenna beamforming techniques have the potential to overcome the problems stated above, by using the discrete spatial separation of the received signals and digital signal processing techniques to direct nulls in the DOAs of the interferers and beams in the directions-of-arrival (DOAs) of the signals-of-interest (SOIs). However, serious problems exist with the implementation of beamformers in a mobile environment. The numbers, strengths and DOAs of both the SOIs and the interferers in the environment are many times both unknown and time-varying. Any beamformer must therefore learn and track the SOI and the interference parameters necessary to extract the SOIs. In applications where a SOI training signal is not available, the processor has to rely on *blind* techniques to exploit more general properties of the SOI waveform or channel.

Conventional techniques that do not use the SOI waveform for adaptation generally exploit the *spatial-coherence* of the incoming signals, i.e., a property attributed to signals impinging from discrete directions of arrival. These techniques include power-minimization techniques that minimize the output power of the beamformer subject to the linear

constraint of the beamformer look direction, and signal sub-space techniques that exploit the eigenstructure of the received signals [Age89]. These algorithms have their limitations. The power minimization technique generally requires knowledge of the geometry and the sensor characteristics of the array (i.e., calibration data or a special array geometry) in order to design the beamformer constraint, and require an expensive search over the calibration data if the SOI's DOA is not known and a special array geometry is not used. The signal sub-space techniques generally require the knowledge of the covariance of the background noise, and also require a special array geometry or an expensive search over the calibration data for implementation. In addition, all these techniques are sensitive to modeling errors in the calibration data or geometry. Calibration data is expensive to obtain and can be affected by real world conditions, such as temperature, weather, mishandling, etc.

Blind adaptive beamforming answers all these problems. These algorithms do not require a special array geometry or the knowledge of the array manifold or noise covariance matrix to adapt the array. The shortcoming is that a blind adaptive algorithm is developed to exploit a particular property of a class of signals, and it cannot be applied to all signals.

Blind adaptive antenna array algorithms are of particular interest in a mobile environment, because of their ability to adapt their weights without the use of a training sequence and thus are more suited for time-varying channels. These blind adaptive algorithms can mitigate the effects of multipath and fading, which are the causes for fluctuation in the signal level. The algorithms can benefit from multipath components, because they provide extra diversity. These algorithms can mitigate the effects of co-channel interference and thus can increase the cell capacity. Much work has been carried out in the development of blind adaptive array algorithms, but no effort has been made so far to study the relative performance merits of these algorithm subjected to the same conditions. This motivates us to study how different blind algorithms perform in a mobile communi-

cations environment.

1.2 Overview

Blind adaptive algorithms can be classified according to the properties that they exploit. For example, these algorithms might restore certain known properties of the signals like constant modulus or spectral redundancy. In this study we consider the following algorithms. An algorithm that exploits the modulus property is called the *Constant Modulus Algorithm* (CMA) and the one that exploits the spectral redundancy is known as *Spectral self-COherence REstoral algorithm* (SCORE). A new blind adaptive array algorithm called the *time-dependent adaptive array* (TDAA), which uses time-dependent filtering, is proposed.

1.2.1 Constant Modulus Algorithm (CMA)

The CMA exploits the constant modulus property of FM, PSK, or FSK waveforms, by minimizing the modulus variation of the signal at the beamformer output. The CMA can remove the effect of multipath propagation and interference on the transmitted signal by sensing the modulus variation of the received signal introduced by the interferers and noise and adapting to minimize this variation.

1.2.2 Spectral Self-coherence Restoral Algorithm (SCORE)

Most digital communication signals encountered in mobile communications possess underlying statistical periodicities, which are caused by amplitude, phase, frequency modulation or by periodic keying. Although these underlying statistical periodicities are neglected in conventional receiver processors, exploiting cyclostationary properties can bring substantial improvement in the performance of the system. These signals are called

cyclostationary signals, i.e., the statistical parameters vary in time with single or multiple fundamental periodicities.

A key point is that this property can be exploited to discriminate undesired signals and noise. Methods that exploit the property of cyclostationarity require only the knowledge of baud rate, modulation type, carrier frequency, or other signal parameters that characterize the underlying periodicity exhibited by the desired signals. SCORE is a blind adaptive array algorithm that exploits the cyclostationary feature present in the signal. It exploits the spectral redundancy present in the signal due to cyclostationarity.

1.2.3 Time-Dependent Adaptive Array (TDAA)

The time-dependent adaptive array (TDAA) is an extension of the time-dependent adaptive filtering to an adaptive array. A time-dependent adaptive filter (TDAF) is an adaptive filter with a filter response that varies periodically in time. The principle behind the TDAF is to use spectrally correlated portions of the signal of interest (SOI) or/and the signal not of interest (SNOI) to improve the portion of the SOI spectrum corrupted by the interference. When the signal statistics change periodically, a TDAF outperforms a time independent adaptive filter (TIAF) in approximating the optimal time-varying solution [Ree87]. A TDAA exploits spatial, frequency, and time diversities. Blind adaptation is accomplished by configuring the TDAF to predict signals having known spectral correlation characteristics.

1.2.4 Switched Diversity Algorithm

Switched diversity involves switching between transmitting antennas in the base station on the basis of the strength of the signals received by the mobile. Here an implementation of the switched diversity is explained [Win83]. In the forward link, the base station transmits the signal using one of its antenna. The mobile compares the received signal to

the threshold level. When the signal level falls below the threshold, the mobile station tells the base station to switch to the next antenna. After the antenna is switched, the mobile examines the signal level, and if it falls below threshold, the mobile tells the base station to switch to the next antenna again. In the reverse link, the signal from the mobile is combined to detect the output bits and the switch control bits. These switch control bits are used to control the transmitting antennas at the base station. Because it is difficult to distinguish the power of the interference from the SOI, switched diversity has limited applications for interference rejection.

Chapter 2

Previous Work in Blind Adaptive Arrays

Widrow et al. [Wid67] were the first to introduce an LMS adaptive antenna array. They showed that the array can adapt to reject interference without the knowledge of the interference and noise. After the pioneering work on blind equalization by Sato [Sat75], blind equalization for one- and two-dimensional communication systems has become an area of great interest for research and industry applications. Blind equalizers converge without resorting to a known training sequence. For some blind equalizers phase recovery is not necessary. A new self-recovering equalization algorithm was introduced by Godard [God80] for application to phase and amplitude-modulated signals. Both blind adaptive equalization and adaptive antennas continued to be developed in parallel for many years before these signal processing operations were combined.

In the 1980's, many blind adaptive algorithms were developed and eventually applied to train adaptive arrays. The Constant Modulus Algorithm (CMA), introduced by Treichler and Agee [Age83] in 1983 has become one of the most commonly applied blind algorithms. They showed that this adaptive digital filtering algorithm can compensate for

both frequency-selective multipath and interference on constant modulus signals. The first application of CMA to arrays is attributed to Gooch and Lundell [Goo86]. The performance of this algorithm for an FM signal with a tonal interference and for a QPSK data signal with intersymbol interference was presented in this paper. They used the least mean square (LMS) algorithm to train the weights of the FIR filter.

Thereafter extensive studies of this algorithm have been carried out. Treichler and Larimore [Tre85a] analyzed the asymptotic convergence behavior of the weight vector when the norm of the initial weight vector is very large. They also analyzed the convergence behavior of the output modulus to investigate the tone capture effects [Tre85b]. In addition, the abnormal phenomena in the CMA, such as the tone capture and noise capture effects, were studied [Lar85a] [Lar85b]. Recently, Agee proposed a least-squares CMA to improve the convergence speed, but his algorithm is computationally intensive [Age86].

As a new application, Ferrara proposed a CMA structure that can reject strong constant envelope interference from a weak desired signal with known modulus [Fer85]. In this application, the a priori knowledge of the absolute value of the transmitted signal modulus is used. Also, to prevent the CMA from locking to an interference signal, the tap weights of the interference-cancelling are constrained such that its filter weights be symmetric about the center weight with the unity constraint. More recently, Kammeyer et al. modified the CMA in order to be used in a commercial FM stereo broadcasting system for multipath echo cancellation [Kam87]. Recently, several researchers have tried to analyze the performance of CMA. Chan and Shynk analyzed the stationary-point performance of the CMA when the equalizer input signal is a zero-mean, real Gaussian signal [Cha90]. Bershad and Roy analyzed the performance of the 2-2 CMA for Rayleigh fading sinusoids in Gaussian noise assuming Gaussian input signals [Ber90]. Takeo Ohgane [Tak91] analyzed the characteristics of the CMA adaptive array for frequency selective fading compensation in digital land mobile radio communications. It was shown that there is great improvement in BER by employing an adaptive array. The channel was modeled using

two-ray model. It was also shown that the error rate is improved better when the delay difference between the two arriving waves is large. Takeo Ohgane et al. [Tak93] implemented a CMA adaptive array for a high speed GMSK transmission in mobile communications. They implemented a 4-element adaptive array based on the digital beamforming concept to reduce the multipath fading effect in high-speed communications.

Gooch and Lundell [Goo86] were the first to apply the CMA to the adaptive array to reject interference. Simulation results were presented showing the beampattern adapting to the desired signal and placing nulls in the direction of the interferers. Capture analysis was also presented in this paper. Performance of constant modulus adaptive filter for interference cancellation was analyzed by Kwon et al [Kwo92]. They investigated the optimum weight vector that minimizes the performance index of the CMA which is defined as the mean-square difference between the estimated and true modulus. The convergence behavior of the squared output modulus and the performance index was analyzed in this work.

Tugnait et al. [Tug93] came up with a way to improve the convergence of CMA adaptive filters. They used higher-order statistics to estimate the channel and then compute the channel inverse of a specified length to initialize a CMA equalizer. Kikuma et al. [Kik91] used non-steepest descent algorithms (Marquardt method), in contrast to the conventional steepest descent algorithms, to speed up the convergence. The fast covergence of this algorithm makes it useful in a highly dynamic environment like the mobile channel. It was shown that the Marquardt method, a nonlinear least squares method, can reduce the convergence time by a factor of 10 to 100 compared to the steepest descent method. Agee [Age88] also examined the convergence behavior of the CMA arrays in Gaussian interference environments. Simulation results of the performance of the least-squares CMA (LSCMA) array for a mobile channel was presented by Agee et. al. [Age93]. Spatial equalization without beamforming using the CMA for a mobile channel was analyzed by

Sylvie [Syl93], the equalization was performed without temporal processing i.e., acting upon a single snapshot.

Agee, Gardner and Schell [Age88] [Gar86] [Gar91] were the first to use the property of cyclostationarity to help mitigate interference and fading in a mobile environment. They presented three different adaptive processors *least-squares SCORE, auto-SCORE* and *cross-SCORE* processors. Cross-SCORE performs better than the least-squares SCORE, because of its ability to separate signals with same cyclic periodicities. Simulation results show the superior performance of this algorithm in rejecting narrow band and wideband interferers. Gardner et al. [Gar92] discussed the increase in the capacity of a cellular radio by applying blind adaptive spatial filtering. Space/time/frequency division multiplexing access (STFDMA) was proposed in this paper and simulation results show that the cell capacity is increased by a factor of 128 compared to FDMA. This system can accommodate five times as many users as the proposed CDMA scheme using the same bandwidth. Schell and Gardner [Gar93] analyzed the maximum likelihood and common factor-analysis based adaptive spatial filtering for cyclostationary signals. They derived a blind adaptive spatio-temporal filtering for unknown cyclostationary signals in noise in two ways, one by maximizing a constrained conditional likelihood function and by solving a common factor analysis problem. It was shown that the specific choice of free constraint-parameters within the resulting beamformer structure yield the existing cross-SCORE and conjugate cross-SCORE algorithms which blindly adapt an antenna array to extract signals having specified cyclostationary properties from the interference and noise.

A new cost function for adaptive beamformers which uses cyclostationary signal properties was developed by Castedo et al. [Cas93]. This new approach exploits the property of higher order cyclostationarity to generate spectral lines by use of a particular class of nonlinear transformations. They demonstrated that the beamformer can extract the desired signal using only the information from the spectral lines. It was also shown that the interferences can be eliminated even when they exhibit the same cyclostationary prop-

erties as the desired signal.

Shamsunder [Sha93] proposed new bearing and range estimation algorithms which uses cyclostationary of the underlying processes. Direction finding algorithms were proposed for narrowband non-Gaussian signals by exploiting the higher order temporal properties of communication signals. Schell et al. [Sch93] presented a blind adaptive spatiotemporal filtering for wide-band cyclostationary signals. Schell et al [Sch88] applied SCORE algorithm and SCORE extensions to sorting in the rank-L spectral self-coherence environment. This paper investigated the ability of the SCORE algorithm to separate cyclostationary signals from a rank L spectral self-coherence environment where L signals exhibit spectral self-coherence at the same value of frequency separation. It was shown that the signals with spectral self-coherence at the same frequency separation can be separated if their relative self-coherence strengths are different. Agee et al. [Age90] analyzed a blind capture and geolocation of general spatially self-coherent waveforms using multiplatform SCORE. This approach can simultaneously estimate the time difference-of-arrival of multiple temporally-uncorrelated SOIs impinging on multiple receiver platforms, and blindly separate those signals with maximum-attainable SINR at each platform.

Decision-directed algorithms was also investigated by many in the 1980's. Gooch and Sublett [Goo88] described joint spatial and temporal equalization using a decision directed adaptive algorithm. They presented two methods for jointly optimizing the weights of a single-weight per channel adaptive diversity combiner followed by a fractionally-spaced equalizer and showed that this system can reject multipath distortion and co-channel interference for a variety of digital communication system. "Stop and Go" decision directed algorithm for blind equalization and carrier recovery was presented by Picchi and Pratti [Pic87]. They showed that the standard decision-directed estimated gradient adaptation algorithm for joint MSE equalization and carrier recovery, normally utilized in the open-eye condition, can be used for closed-eye start-up condition with no need

of a training sequence. They used a simple flag to tell the synchronizer and the equalizer whether the current output error with respect to the decided symbol is sufficiently reliable to be used.

Switched diversity is another blind adaptive technique which switches the antennas depending on the signal strength. Winters discussed the performance of the switched diversity method with feedback applied to DPSK mobile radio systems. Bit error performance of this array as a function of threshold was presented in this paper [Win83] [Win84]. Methods have been proposed to combine adaptive equalization and diversity to the mobile channel problem. Falconer et al. [Fal90] demonstrated the feasibility of a digital cellular radio system which employs a jointly adaptive decision-feedback equalizer and diversity combiner.

Kailath et al. [Kai93] showed the performance of adaptive arrays for CDMA systems in a multipath environment. Recently Liberti and Rappaport [Lib94] have presented analytical results for capacity improvements in CDMA. Performance improvement provided by adaptive arrays for IS-54 standard signals have been shown by Winters [Win93] [Win94].

Chapter 3

Blind Adaptive Algorithms

3.1 Background Theory

Beamforming

Beamforming signal processing is used in conjunction with an array of sensors to provide a versatile form of spatial filtering. The sensor array collects spatial samples of propagating wave fields, which are processed by the ***beamformer***. A beamformer does spatial filtering to separate signals that have overlapping frequency content but originate from different spatial locations.

Systems designed to receive spatially propagating signals often encounter the presence of interfering signals. If the desired signal and the interfering signals occupy the same temporal frequency band, then linear time-invariant temporal filtering cannot be used to separate the signal from the interferers. However, the desired and interfering signals usually originate from different locations. This spatial separation can be exploited to

separate the desired signal from the interferers using spatial filtering at the receiver. Implementing a temporal filter requires processing of data collected over a temporal aperture. Similarly, implementing a spatial filter requires processing of data collected over a spatial aperture. The beamformer linearly combines the spatially sampled time series from each sensor to obtain a scalar output time series in the same manner that an FIR filter linearly combines temporally sampled data.

Two important characteristics of spatial sampling with an array of sensors are:

1) Spatial discrimination capability depends on the size of the spatial aperture; as the aperture increases, discrimination improves. The absolute aperture size is not important, rather its size relative to wavelength is the critical parameter. A single physical antenna (continuous spatial aperture) capable of providing the requisite discrimination is often practical for high frequency signals because the wavelength is short. However, when low frequency signals are of interest, an array of sensors can often synthesize a much larger spatial aperture than that practical with a single physical antenna.

2) A significant advantage of using an array of sensors, relevant at any wavelength, is the versatility. In many applications, it is necessary to change the spatial filtering function in real time to maintain effective suppression of interfering signals. This change is easily implemented in a discretely sampled system by changing the way in which the beamformer linearly combines the sensor data.

3.2 Antenna Array

3.2.1 Two-Element Array

The first step in describing a plane wave incident to the array is picking a reference

location. The signal received at each sensor in the array will be a time delayed or a time advanced version of the signal at the reference. To demonstrate this concept, consider a two-sensor array as shown in Figure 1. In this example, the first sensor of the array is chosen as the reference position, and the distance between the two sensors is d. Assume a plane wave propagates incident to the array at an angle θ as shown in the Figure 1, i.e., the propagation vector of the plane wave makes an angle θ with the line connecting the two sensors. As labeled on the figure, the wavefront at sensor # 1 must propagate through a distance given by

$$d_{prop} = d\cos(\theta) \tag{1}$$

before it will be detected at sensor # 2. The propagation time is a time delay given by

$$\tau = \left(\frac{1}{c}\right) d\cos(\theta), \tag{2}$$

where c is the velocity of the plane wave.

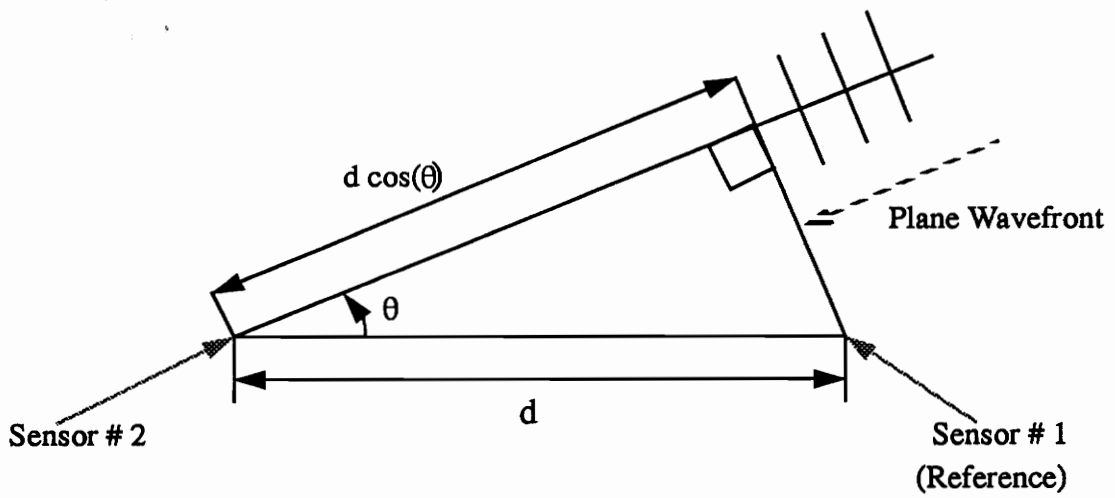

Figure 1. Two-Element Array

Let $\bar{s}_1(t)$ represent the complex representation of the signal received at the sensor # 1 and $\bar{s}_2(t)$ represent the complex representation signal received at the sensor # 2. The relation between the two signals at the sensor is given by

$$\tilde{s}_2(t) = \tilde{s}_1(t-\tau). \tag{3}$$

Given the form for $\tilde{s}_1(t)$

$$\tilde{s}_1(t) = \alpha(t)\exp(j[\omega_c t + \phi(t) + \theta]) = z(t)\exp(j[\omega_c t + \theta]), \tag{4}$$

where $z(t) = \alpha(t)e^{j\omega\phi(t)}$,

we can substitute Eqn. 4 into the equation for $\tilde{s}_2(t)$ to get

$$\tilde{s}_2(t) = \alpha(t-\tau)\,exp(j[\omega_c t - \omega_c\tau + \phi(t-\tau) + \theta]) = z(t-\tau)\,exp(j[\omega_c t - \omega_c\tau + \theta]) \tag{5}$$

.

Assuming a narrowband signal (i.e., the coherence bandwidth of the channel is larger than the signal bandwidth), the information content of the signal is approximately constant over time spans of the order of τ. In other words, we can use the approximation

$$z(t-\tau) \approx z(t), \tag{6}$$

to reduce $\tilde{s}_2(t)$ to the following form:

$$\tilde{s}_2(t) = z(t)\,exp(j[\omega_c t - \omega_c\tau + \theta]) = \tilde{s}_1(t)\,exp(-j\omega_c\tau). \tag{7}$$

Furthermore, by using the relationship between the velocity and the frequency of the waveform, the delay τ can be written as a phase delay.

$$\tilde{s}_2(t) = \tilde{s}_1(t)\,exp\left(-j\omega_c\frac{(d\cos(\theta))}{c}\right) = \tilde{s}_1(t)\,exp\left(-j2\pi\frac{(d\cos(\theta))}{\lambda}\right) \tag{8}$$

Hence the time delay τ corresponds to a phase shift in the signal by $\left(\frac{2\pi d\cos\theta}{\lambda}\right)$ radians.

Changing the direction of arrival of the wavefront can change the relative propagation distance to the array elements. As shown above, the different propagation distances lead to a phase shift between the sensor elements of the array. Consequently, an array is sensitive to the direction of arrival of signals. This sensitivity is characterized by the directional pattern of the array. As an example, consider the two element array of Figure 1 where $d = \frac{\lambda}{2}$. If the output of the array is the simple phasor sum of the outputs of the two array elements, then in baseband representation the output $y(t)$ is given by

$$y(t) = \sum_{1}^{2} s_i(t) = s_1(t)\left[1 + \exp\left(\frac{(-j)\,2\pi\,(d\cos\theta)}{\lambda}\right)\right], \qquad d = \frac{\lambda}{2} \tag{9}$$

$$y(t) = s_1(t)\,[1 + exp\,(-j\pi\cos\,(\theta))\,]\cdot \tag{10}$$

The term in the square brackets determines the directional pattern of the array, $g(\theta)$, also called the gain response of the array. The maximum $g(\theta)$ is for θ at either 90 or 270 degrees. This is easily explained since at 90 and 270 degrees, the signal is striking both elements of the array at the same time instant and the received voltages add in phase. At 0 or 180 degrees, the propagation distance between the two sensors is half of the carrier wavelength, and the two received voltages combine out of phase. Commonly, the directional pattern of an array is reported by a graph that shows that the angle of arrival on the horizontal axis and the directional pattern on the vertical axis scaled so that the maximum value is unity or 0 dB. This scaled quantity, $G(\theta)$, is the normalized gain response of the array. The normalized gain response of the two-element array is shown in Figure 2 below.

The signals received on the two elements for any particular direction of arrival Ψ can be coherently combined for maximum gain if the voltage on the second sensor is phase shifted to compensate for the propagation delay. Mathematically, this corresponds to multiplying the voltage received at the second sensor by a weighting factor w given by

$$w = \exp\left(j2\pi\frac{d\cos\Psi}{\lambda}\right). \tag{11}$$

This process of directing the array at a certain direction is called beamforming. The two variable function $G(\theta, \Psi)$ is used to represent the normalized gain response of the array aimed at a direction of arrival Ψ but evaluated for a direction of arrival θ.

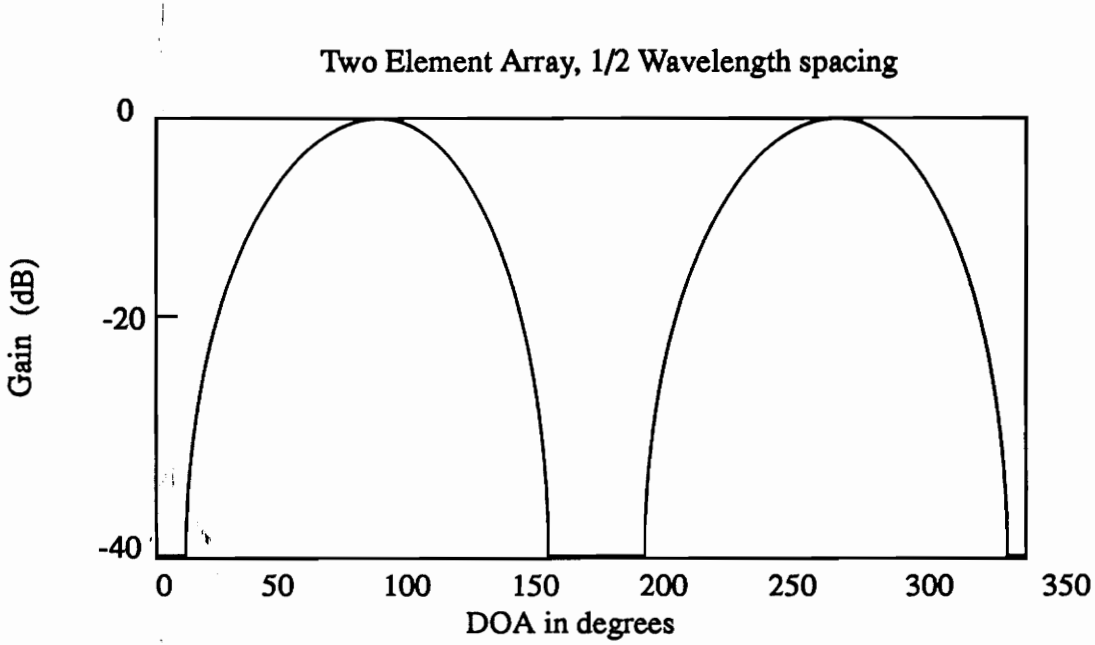

Figure 2. Normalized Gain Response

3.2.2 Extension of the Model

To generalize the description to an M-element array, each element's position is referenced to coordinates in an x-y plane normalized to the wavelength. In this coordinate plane, the origin is located at the selected reference point. As an example, an element located on the positive x axis at a distance of $\frac{\lambda}{2}$ from the origin would be assigned the coordinates (1/2, 0). The set of position coordinates of the array elements are collected

into an (M x 2) position matrix, $\underline{P}$, where the ith row contains the coordinates of the ith element, and the columns contain the x and y components, respectively.

$$\underline{P} = \begin{bmatrix} \underline{P_1}^T \\ \underline{P_2}^T \\ \cdot \\ \cdot \\ \underline{P_M}^T \end{bmatrix} = \begin{bmatrix} P_{1x} & P_{1y} \\ P_{2x} & P_{2y} \\ \cdot & \cdot \\ \cdot & \cdot \\ \cdot & \cdot \\ P_{Mx} & P_{My} \end{bmatrix} \tag{12}$$

Next, the signal direction of arrival is represented by a unit vector, $\underline{u}(\theta)$, which is in the same direction as the propagation vector for the wavefront.

$$\underline{u}(\theta) = \begin{bmatrix} \cos(\theta) \\ \sin(\theta) \end{bmatrix} \tag{13}$$

With these two matrices, $\underline{P}$ and $\underline{u}(\theta)$, the signed distance that the wavefront propagates through from the origin to each sensor is readily calculated by the product of $\underline{P}\,\underline{u}(\theta)$. A negative distance would indicate that the wavefront strikes the sensor before the origin. From the above definitions, the matrix product $\underline{P}\,\underline{u}(\theta)$ represents taking the inner product of each array element's position vector with the direction of arrival vector. The interpretation of this matrix product is a vector of the projections of each position vector along the direction of arrival, Hence, the result of the product $\underline{P}\,\underline{u}(\theta)$ is an (M x 1) matrix of normalized propagation distances from the origin to each array element. Using $s_o(t)$, to represent the complex baseband representation of the signal at the origin as a function of time, the signal at the ith element, $s_i(t)$, can be related back to the origin as follows.

$$s_i(t) = s_o(t) \exp\left(-j2\pi \underline{P_i}^T \underline{u}(\theta)\right) \tag{14}$$

These signals can be collected into a vector

$$\underline{s}(t) = \begin{bmatrix} s_1(t) \\ s_2(t) \\ \cdot \\ \cdot \\ s_M(t) \end{bmatrix} = \begin{bmatrix} \exp\left(-j2\pi \underline{P_1}^T\right)\underline{u}(\theta) \\ \exp\left(-j2\pi \underline{P_2}^T\right)\underline{u}(\theta) \\ \cdot \\ \cdot \\ \exp\left(-j2\pi \underline{P_M}^T\right)\underline{u}(\theta) \end{bmatrix} s_o(t) = \underline{a}(\theta)\, s_o(t) \tag{15}$$

To direct the array at an angle Ψ, a weighting vector $\underline{w}$ is picked to cancel any phase delays between elements such that the composite weighted sum from the array elements along that direction of arrival add in phase.

$$\underline{w} = \begin{bmatrix} w_1 \\ w_2 \\ \cdot \\ \cdot \\ w_M \end{bmatrix} = \begin{bmatrix} \exp\left(j2\pi \underline{u}^T(\Psi)\,\underline{P}_1\right) \\ \exp\left(j2\pi \underline{u}^T(\Psi)\,\underline{P}_2\right) \\ \cdot \\ \cdot \\ \exp\left(j2\pi \underline{u}^T(\Psi)\,\underline{P}_M\right) \end{bmatrix} = \underline{a}^*(\Psi) \tag{16}$$

The output of the array, $y(t)$, is the weighted sum given by

$$y(t) = \underline{w}^T(t)\,\underline{s}(t) = \underline{a}^H(\Psi)\,\underline{s}(t) = \underline{a}^H(\Psi)\,\underline{a}(\theta)\,s_o(t) = MG(\theta,\Psi)\,s_o(t)\,. \tag{17}$$

3.3 Constant Modulus Algorithm (CMA)

3.3.1 Basic Description

Consider a signal $x(k)$, which is a multipath distorted analytic signal, applied to a transversal (tapped delay line) FIR filter with adjustable complex weights. The output of the filter $y(t)$ can be written as

$$y(k) = X^T(k)\,W(i), \tag{18}$$

where $X(k)$ is the vector of data in the filter delay line,

$$X(k) = [x(k)\,x(k-1)\,.....x(k-N+1)]^T, \tag{19}$$

and $W(i)$, the vector of adjustable coefficients, is given by

$$W(i) = [w_0(i)\,w_1(i)\,.....w_{N-1}(i))]^T. \tag{20}$$

The index i indicates that the coefficients or weights are adjustable in time. The assumption is that the weights are going to be updated at each sampling instant so i is replaced by k. The objective of this adaptive filtering is to restore $y(k)$ to the form which, on the average, has a constant modulus. This may be done by choosing the coefficients vector W in such a way as to minimize a positive definite measure of the signal modulus variation, given in some generality by

$$J = d[F((y(k)), F(s(k)))], \tag{21}$$

where d and F are length metric to be defined for a specific algorithm and $s(k)$ is the constant modulus transmitted signal, assumed to be scaled so that $|s(k)|=1$. In this section we choose d and F to yield the function

$$J_{mn} = \frac{1}{4}\left[E\{[|y(k)|^m - 1]^n\}\right], \tag{22}$$

where E denotes statistical expectation, m and n can take value 1 and 2. In the discussion below, m and n both take a value of 2. Note that the length metric F maps $s(k)$ to unity.

Clearly J is just a positive measure of the average amount that the filter output $y(k)$ deviates from the unity modulus condition. The objective in choosing W is to minimize J and in the process to make $y(k)$ as close as to unit length as possible.

3.3.2 Adaptive Algorithm

Given the performance criterion and the filter structure, there are many possible approaches to finding the optimal filter response [Age83]. To ease hardware implementation, we employ here a simple gradient search algorithm to minimize J. The implementation of CMA using gradient search algorithm is computationally less intensive than implementing using least-squares method. In the least-squares algorithm, the inverse of the autocorrelation matrix has to be calculated, which is computationally intensive if the number of elements is large. In particular, assume that W is updated according to the equation

$$w(k+1) = w(k) + \mu \nabla_w J_k, \tag{23}$$

where $w(k)$ is the set of coefficients used to generate outputs $y(k)$, μ is a positive step size, and ∇_w is the gradient operator with the respect to the elements of the vector W.

Using complex matrix calculus, it can be verified that the gradient of J with respect to the weight vector W is given by

$$\begin{aligned} \nabla_w J &= \frac{1}{2} E\{[|y(k)|^2 - 1] \cdot \nabla_w [W^H X^* X^T W]\} \\ &= E\{[|y(k)|^2 - 1] \cdot X^*(k) \cdot X^T(k) W\} \\ &= E\{[|y(k)|^2 - 1] \cdot y(k) X^*(k)\} \end{aligned} \tag{24}$$

The adaptive algorithm is obtained by replacing the true-gradient of Eqn. 24 with an instantaneous gradient estimate given by

$$\hat{\nabla}_w J = \left[|y(k)|^2 - 1\right] \cdot y(k) X^*(k) . \tag{25}$$

Substituting $\hat{\nabla} J$ for ∇J in Eqn. 23, yields the desired algorithm

$$w(k+1) = w(k) - \mu \{ \left[|y(k)|^2 - 1\right] y(k) X^*(k) \}. \tag{26}$$

If the scalar term $\tilde{\varepsilon}(k)$ is defined by

$$\tilde{\varepsilon}(k) \Delta \{ \left[|y(k)|^2 - 1\right] \cdot y(k) \} , \tag{27}$$

then the updating algorithm can be compactly written as

$$w(k+1) = w(k) - \mu \{ \tilde{\varepsilon}(k) \cdot X^*(k) \} . \tag{28}$$

Two interesting things about constant modulus algorithm (CMA). One is its apparent similarity to the complex version of the well known LMS adaptive algorithm [Wid66]. In fact, if $\varepsilon(k) = d(k) - y(k)$ were substituted for $\tilde{\varepsilon}(k)$, where *d(k)* is some externally applied reference, the algorithm reduces to a training sequence directed LMS algorithm. For the CMA algorithm *d(k)* is not required. Rather than using a training signal, it uses the *a priori* knowledge that the transmitted signal has a constant envelope. Note that $\tilde{\varepsilon}(k)$ equals zero if *y(k)* has unit modulus.

3.3.3 Least-Squares CMA Algorithm (LSCMA)

The weights of the antenna array are adapted using least squares CMA [Age86], which provides the maximum likelihood estimate of the transmitted signal waveform if it has a constant modulus (magnitude of the complex envelope). The LSCMA can be interpreted as an alternating projections approach for adapting a set of array weights to minimize the 1-2 *constant modulus cost function* (CMCF).

$$F_{12}(w) = \sum_{m=1}^{N} (|y(m) - 1|)^2 \tag{29}$$

$$F_{12}(w) = \sum_{m=1}^{N} (|y(m) - \delta(m)|)^2$$

$$\delta(m) = \frac{y(m)}{|y(m)|} = sign\{y(m)\}$$

$$y(m) = \underline{w}^H \underline{x}(m)$$

where $\underline{w}$ and $\{x(m)\}_{m=1}^{N}$ are the array combiner weights and the input signal at the time index m, respectively, and $y(m)$ and $\delta(m)$ are the unconstrained and complex-limited array combiner output signals, respectively. The LSCMA adapts $\underline{w}[n]$ to minimize F_{12} for each block of data using the three-step iterative procedure shown below.

The LSCMA algorithm is implemented on a block-update basis. The received data is partitioned into contiguous non-overlapping blocks of data of length N, and LSCMA recursion is applied to each block using weights obtained from the previous block.

Algorithm:

$$\underline{y}([n]) \leftarrow \underline{w}^H[n]\,\underline{x}[n]$$

$$\delta[n] \leftarrow sign\{\underline{y}[n]\}$$

$$\underline{w} \leftarrow \left[\sum_{m=1}^{N} \underline{x}(m)\,\underline{x}^H(m)\right]^{-1} \left[\sum_{m=1}^{N} \underline{x}(m)\,\delta^*(m)\right]$$

3.3.4 Properties of the Constant Modulus Algorithm

1) Shape of the Performance function

An intuitive understanding of the behavior of an adaptive algorithm can often be afforded by examining the shape of the objective or performance function, J in this case [Age 83]. The LMS, for example, has an ensemble average of the squared error that is a hyperparaboloid in the coefficient hyperspace, with dimension equal to the FIR filter order. Such a perspective in the performance function, Eqn. 22, can be found by examining J as a function of the real and imaginary part of $y(k)$. We note that the function J is minimized with a value of zero at any point on a circle with unit radius and centered around the origin.

Two conditions can lead zero gradient situation where the algorithm stops adapting. The first is the contour $|y(k)| = 1$ which represents the desired convergence locus of the algorithm. It should be noted that the point $y(k) = 0$ can also force zero-gradient condition. This potential solution is not a practical solution because of two reasons. First, this solution is not a stable one, because any noise or disturbance can force W away from the zero-gradient point. Second, given a filter input $x(k)$ with non-zero bandwidth the only way to sustain zero output over a large number of samples is to have the weight vector W set to zero. Such a condition can be easily tested and if it exists the weights can be moved away. This zero weight condition is of practical importance only when starting up the filter. Clearly, the traditional all-zero initial vector should not be used.

2) Uniqueness

The constant modulus approach is predicated on the concept of using ~~of using~~ incidental amplitude variations to sense the presence of multipath or interference and control the adaptation of a correction filter. Here we prove that adjusting a filter to remove the inci-

dental AM necessarily yields the proper correction filter. Suppose $s(k) = Ae^{j\theta(k)}$ is a waveform with constant modulus A and that it is convolved with the time invariant channel response $h(l)$, yielding output $y(k)$. The filter $h(l)$ represents the cascade of the channel and the correction filter. It can be shown that for $y(k)$ to have a constant modulus of one, then, under suitable input conditions, $h(l)$ has only one non-zero tap.

Suppose that $h(l)$ has two non-zero taps. If so we may write

$$y(k) = h(m)Ae^{j\theta(k-m)} + h(q)Ae^{j\theta(k-q)} \tag{30}$$

and

$$\frac{|y(k)|^2}{A^2} = |h(m)|^2 + |h(q)|^2 + 2|h(m)||h(q)|\cos\{\theta(k-m) - \theta(k-q) + b - c\} \tag{31}$$

where b and c are the arguments of $h(m)$ and $h(q)$. We desire that $|y(k)|^2 = 1$ for all k, given some choice of A, $h(m)$, $h(q)$. Since all of these will be constant for all k, so must the cosine of the phase difference. This implies that $\theta(k)$ is, at worst, the sum of a term linear in time, plus a term periodic in $(m-q)$. The spectrum of $exp(j\theta k)$ would, in this worst case, be composed of spectral lines only. Thus the only input signal $s(k)$ which can pass through such a two-tap filter without incurring modulus variation is a pathological case carrying no modulation or other intelligence.

Extension to three and more nonzero weights can be done by induction and yields the same result. Only signals with specifically chosen line spectra will emerge from a filter with the constant modulus property intact.

It can be concluded that $h(l)$ must have only one nonzero tap for $s(k)$ with finite non-zero bandwidth, implying that removal of the incidental AM in $y(k)$ forces the impulse

response of the cascaded channel correction filter pair into a simple impulse. Thus, other than the arbitrary choice of which tap in $h(l)$ is employed, and its phase, the frequency response characteristics of the correction filter are uniquely defined by the satisfaction of the constant modulus optimization criterion.

a) Phase Roll

Suppose the chosen nonzero tap of $h(l)$ is $h(l_o)$, where l_o indicates the advance or the delay of the tap. The uniqueness proof does not specify the phase of $h(l_o)$, only that it be the only nonzero tap. This implies that any choice of W, say W_o, which yields a constant modulus $y(k)$, will also suffice if rotated by an arbitrary phase shift. That is, if W_o is satisfactory, then so is

$$W_r = e^{j\phi} W_o. \tag{32}$$

This operation consists of rolling the complex impulse response by ϕ radians, and in turn rotating $y(k)$ to $exp(j\phi)$ to such phase differences. It may be concluded that the bulk phase shift of the adaptive filter is not uniquely determined by the constant modulus performance function J. The impact of this depends on the modulation type of the signal being corrected. In the particular case of FM, it poses no problem since FM reception is sensitive to the derivative of the received phase and is not affected by a constant offset. For the phase-coherent systems, the phase roll must be estimated and removed or an additional feedback loop must be inserted into the adaptive algorithm to reduce and/or correct for the phenomenon.

b) Time shift

The uniqueness proof allows any choice of l_o. This implies that the correction filter can insert arbitrary group delay into the signal without penalty. Just as with the phase roll

ambiguity, the potential presence of an arbitrary delay is usually not a matter of practical concern for a sufficiently large number of coefficients.

3) Comparison with Optimal Joint Estimators

A perspective into the CMA class is provided by contrasting its uniqueness properties with the analysis done in [Tre80]. This reference concerns the application of classical maximum a posteriori probability (MAP) and maximum likelihood (ML) estimation techniques [Tre68][Tre71a][Tre71b] to the specific problem of jointly estimating both the baseband signal-of-interest and the multipath propagation channel. It was shown that even given the received signal in the absence of noise it is sometimes impossible to find which properties of the received signal stem from the signal of interest and which from the channel. This ambiguity leads to the nonuniqueness of the estimator solution and, in some implementations, to instability of the estimator. It is shown in this section that the CMA also leads to nonuniqueness solutions. The differences between the two are useful to examine.

1) The CMA makes no estimate of the signal baseband, while such estimation is vital part of the joint estimators.

2) The MAP and ML techniques require sufficient spectral richness to model the channel uniquely and such uniqueness is required to properly develop an inverse filter. The CMA directly adapts the correction filter.

3) A key difference is the type of null space described by the signal/estimator ambiguity. In the MAP and ML estimator, the null space in the covariance function involves a combination of both signal and channel parameters. Thus, failure to determine the channel exactly leads to lack of the desired knowledge about the message waveform. The CMA performance function stated in Eqn. 21 and Eqn. 22 is designed to force the ambiguous null space into dimensions that are little practical concern in most of signal reception problems. In particular, if the received signal has finite bandwidth, then the null space of this performance function corresponds to phase or time shifts, neither of which impact the

uniqueness of the waveshape of the desired baseband signal.

4) Relationship to the Weiner Filter

Suppose that the filter output $y(k)$ can be written as

$$y(k) = e(k) + y_o(k), \tag{33}$$

where $y_o(k)$ is the complex signal with unit modulus and $e(k)$ is an error vector assumed to be much less than one in length. If so, it can be shown that

$$J = \frac{1}{2}E\{|e(k)|^2\} + \frac{1}{2}E\{|e(k)|^2\cos(2\theta)\}, \tag{34}$$

where θ is the angle between $y_o(k)$ and e(k). If $y_o(k)$ and $e(k)$ are statistically independent processes (e.g., $e(k)$ is additive noise) then the second term is zero and

$$J = \frac{1}{2}E\{|e(k)|^2\}. \tag{35}$$

This indicates that in the vicinity of convergence, minimizing the constant modulus performance function is equivalent to minimizing the mean squared error, and therefore, the CMA will converge to the Weiner filter.

5) AGC Action

For the purpose of analysis, the transmitted signal $s(k)$ has been assumed to be of unit amplitude, neglecting the gains and losses associated with transmission propagation, and reception. In general, the received signal, even if free of noise and interference, will not have unit amplitude. In order to minimize the performance criterion J in Eqn. 21, the filter coefficients are scaled by the adaptive algorithm to introduce the proper gain into the

filter output. In performing this function the adaptive algorithm acts as an automatic gain control (AGC) in addition to its desired task of spectral shaping [Age83].

While a certain amount of AGC action is necessary for the algorithm's proper operation, it is usually undesirable to use the adaptive filter as the only AGC in the receiver chain. In fact, preceding the constant modulus equalizer with an AGC is desirable to limit the dynamic range over which the digitally implemented processor must operate.

3.4 Spectral self-COherence REstoral Algorithm (SCORE)

3.4.1 Cyclostationarity

Conventional statistical signal processing methods treat random signals as statistically stationary, in which case the parameters of the underlying physical mechanisms that generate the signals would not vary with time. But for most man-made signals encountered in communication, telemetry, radar and sonar systems, some parameters do vary periodically with time. In some cases even some multiple incommensurate (not harmonically related) peridiocities are involved. Examples include sinusoidal carriers in amplitude, phase, and frequency modulation systems, periodic keying of amplitude, phase and frequency in digital modulation systems. In most cases, the underlying periodicities can be neglected, but an increased improvement in performance can be obtained by recognizing and exploiting these underlying periodicities. This leads to the to the treatment of random signals as *cyclostationary*, in which the signal parameters vary in time with single or multiple periodicities [Gar86].

3.4.2 Exploitation of Cyclostationarity

The existence of correlation between widely separated spectral components (separa-

tion equal to a cycle frequency α) can be interpreted as *spectral redundancy*. The meaning of the term *redundancy* that is intended here is essentially the same as that used in the field of information theory and coding. Specifically, multiple randomly fluctuating quantities (random variables) exhibit some redundancy if they are statistically dependent, for example, correlated. In speech coding theory, undesired redundancy is removed from the data to increase the efficiency with which it represents information. In the case of error correcting codes, redundancy is introduced to insure reliable transmission of information. Here spectral redundancy is inherently introduced into signals by the modulation process and this be exploited to enhance the corrupted signals. The performance of a signal processor can be substantially improved if it exploits cyclostationarity in its decision making process. The degree of improvement, relative to conventional processors, depends on both the severity of the signal corruption (noise, interference, distortion) and the degree of spectral redundancy in the signal *x(t)*. The degree of improvement also depends on the available data for processing (the collect time). The performance can also be improved by designing the signal to exhibit a sufficient amount of spectral redundancy.

3.4.3 Measure of Cyclostationarity

A scalar waveform is said to be *spectrally self-coherent* [Age88] at frequency separation α if the correlation between *s(t)* and *s(t)* frequency shifted by α is nonzero for some lag τ, that is, if

$$\rho_{ss}^{\alpha}(\tau) \triangleq \frac{\left\langle s\left(t+\frac{\tau}{2}\right)\left[s\left(t-\frac{\tau}{2}\right)e^{j2\pi\alpha t}\right]^{*}\right\rangle_{\infty}}{\sqrt{\left\langle\left|s\left(t+\frac{\tau}{2}\right)\right|^{2}\right\rangle_{\infty}\left\langle\left|s\left(t-\frac{\tau}{2}\right)e^{j2\pi\alpha t}\right|^{2}\right\rangle_{\infty}}} \tag{36}$$

$$= \frac{R_{ss}^{\alpha}(\tau)}{R_{ss}(0)} \neq 0$$

at some value of τ, where $\langle\ \rangle_{\infty}$ denotes infinite time-averaging. Similarly, a signal wave-

forms said to be spectrally self-coherent at frequency separation α if the correlation between *s(t)* and conjugate of *s(t)* frequency-shifted by α is nonzero for some lag τ.

$$\rho_{ss^*}^{\alpha}(\tau) \triangleq \frac{\left\langle s\left(t+\frac{\tau}{2}\right)\left[s^*\left(t-\frac{\tau}{2}\right)e^{j2\pi\alpha t}\right]^*\right\rangle_{\infty}}{\sqrt{\left\langle\left|s\left(t+\frac{\tau}{2}\right)\right|^2\right\rangle_{\infty}\left\langle\left|s^*\left(t-\frac{\tau}{2}\right)e^{j2\pi\alpha t}\right|^2\right\rangle_{\infty}}} \tag{37}$$

$$= \frac{R_{ss^*}^{\alpha}(\tau)}{R_{ss}(0)} \neq 0$$

The function $\rho_{ss}^{\alpha}(\tau)$ and $\rho_{ss^*}^{\alpha}(\tau)$ are referred to here as the spectral self-coherent function and the spectral conjugate self-coherent function of *s(t)*, respectively; and the functions $R_{ss}^{\alpha}(\tau)$ and $R_{ss^*}^{\alpha}(\tau)$ are referred to here as *cyclic autocorrelation function* and *cyclic conjugate autocorrelation function* of *s(t)*, respectively, and are defined by

$$R_{ss}^{\alpha}(\tau) \triangleq \left\langle s\left(t+\frac{\tau}{2}\right)s^*\left(t-\frac{\tau}{2}\right)e^{-j2\pi\alpha t}\right\rangle_{\infty}, \tag{38}$$

$$R_{ss^*}^{\alpha}(\tau) \triangleq \left\langle s\left(t+\frac{\tau}{2}\right)s\left(t-\frac{\tau}{2}\right)e^{-j2\pi\alpha t}\right\rangle_{\infty} . \tag{39}$$

An M-element vector waveform x(t) is said to be *rank* $-L_{\infty}$ *spectrally self-coherent at frequency separation* α or *rank* $-L_{\infty}$ *spectrally conjugate self-coherent at frequency separation* α if the respective cyclic autocorrelation matrix $\boldsymbol{R}_{XX}^{\alpha}(\tau)$ or cyclic conjugate correlation matrix $\boldsymbol{R}_{XX^*}^{\alpha}(\tau)$

$$\boldsymbol{R}_{XX}^{\alpha}(\tau) \triangleq \left\langle x\left(t+\frac{\tau}{2}\right)x^H\left(t-\frac{\tau}{2}\right)e^{-j2\pi\alpha t}\right\rangle_{\infty}, \tag{40}$$

$$\boldsymbol{R}_{XX^*}^{\alpha}(\tau) \triangleq \left\langle x\left(t+\frac{\tau}{2}\right)x^T\left(t-\frac{\tau}{2}\right)e^{-j2\pi\alpha t}\right\rangle_{\infty}, \tag{41}$$

has a rank L_{∞} $(L_{\infty} \leq M)$ at frequency-shift α for some lag τ, where T and H denote

transpose and conjugate-transpose (*Hermitian response*) operations, respectively.

If a real (bandpass representation)signal is considered, the positive and negative frequencies are identical but for a complex phase-shift. Therefore the overall signal is correlated when frequency shifted by twice the carrier frequency f_o, i.e., the signal is spectrally self-coherent at $\alpha = 2f_o$. This correlation can be removed by converting the signal to its analytic representation, i.e., by removing the negative frequency components of the signal. The original negative frequency component of the signal can be created by conjugating the analytical signal, which reflects the signal through the DC axis. The conjugated signal is now correlated with the original signal after a frequency shift of twice the carrier. The original signal exhibits spectral conjugate self-coherence at $\alpha = 2f_o$.

The spectral self-coherence and conjugate self-coherence frequencies for a number of common modulation formats is shown in Table 1 [Age88].

Table 1: Examples of Spectrally Self-Coherent Signals

Complex Modulation Format	Self-Coherence Frequencies	Conj. self-Coherence Freq. (@ 2 x Carrier)
ASK, BPSK	Baud-rate multiple	Baud-rate multiple
QPSK	Symbol-rate multiple	None
MSK, SQPSK	Baud-rate multiple	+/- 1/2 Baud-rate
CPFSK	Symbol-rate multiple	2 x Symbol frequencies
FDM-FM	Pilot-tone multiple	None
DSB-AM	None	2 x carrier
VSB-AM	None	None
SSB-AM	None	None

As seen from the table that most of the common communication signals exhibit cyclostationarity; for instance, all PCM signals exhibit spectral self-coherence at multiples of their baud-rate, and ASK and BPSK signals are in addition spectrally conjugate self-coherent at

twice their carrier frequency.

The function $\left|\rho_{ss^{(*)}}^{\alpha}(\tau)\right|$ can be interpreted as a measure of the relative strength of $s(t)$ contained within $s^{(*)}(t-\tau)e^{j2\pi\alpha t}$, where the optional conjugation (*) is only applied if conjugate self-coherence is being measured. Using the Orthogonal Projection Theorem, $s^{(*)}(t-\tau)e^{j2\pi\alpha t}$ can be represented by

$$s^{(*)}(t-\tau)e^{j2\pi\alpha t} = \left[\rho_{ss^{(*)}}^{\alpha}(\tau)\ e^{-j\pi\alpha t}\right]^{*} s(t) + \varepsilon_s(t)\sqrt{1-\left|\rho_{ss^{(*)}}^{\alpha}(\tau)\right|^2}, \qquad (42)$$

where $s(t)$ and $\varepsilon(t)$ are equal-power orthogonal waveforms ($R_{s\varepsilon_s} = 0$). Therefore, $s^{(*)}(t-\tau)e^{j2\pi\alpha t}$ can be thought of as a scaled and corrupted replica of $s(t)$, with a signal-to-corruption ratio of

$$\Upsilon^2_{SCR}(\alpha,\tau) \triangleq \frac{\left|\rho_{ss^{(*)}}^{\alpha}(\tau)\right|}{\left(1-\left|\rho_{ss^{(*)}}^{\alpha}(\tau)\right|^2\right)} \qquad (43)$$

This ratio varies between zero and infinity as $\left|\rho_{ss^{(*)}}^{\alpha}(\tau)\right|^2$ varies between zero and unity.

The utility of the self-coherence concept can best be seen in the interference environments. Consider the environment where a scalar waveform $x(t)$ is equal to signal of interest $s(t)$ plus an uncorrelated interference $i(t)$, so $x(t) = as(t) + i(t)$. If $s(t)$ is spectrally self-coherent at frequency separation α, then the cyclic-autocorrelation of $x(t)$ is given by

$$R^{\alpha}_{XX}(\tau) = |a|^2 R^{\alpha}_{SS}(\tau) + R^{\alpha}_{ii}(\tau) = |a|^2 R^{\alpha}_{SS}(\tau) \qquad (44)$$

that is, the infinite time-averaged cyclic autocorrelation of x(t) is unchanged by the addition of arbitrary interference, provided that the interference is not spectrally self-coherent

at the same frequency separation α.

A useful interpretation of Eqn. 42 is that the frequency shift and optional conjugation operations completely decorrelate the interference component of $x(t)$, but only partially decorrelate SOI component of $x(t)$. In terms of the decomposition given in Eqn. 40, $x^{(*)}(t-\tau)\,e^{j2\pi\alpha t}$ can be expressed in terms of the signal and interfering components of $x(t)$ by substituting $s(t)$ in the right hand side of Eqn. 42.

$$x^{(*)}(t-\tau)\,e^{j2\pi\alpha t} = \hat{a}s(t) + \hat{i}(t), \tag{45}$$

where

$$\hat{a} = a\rho^{\alpha}_{ss^{(*)}}(\tau)\ {}^{*}e^{j\pi\alpha t}, \tag{46}$$

$$\hat{i}(t) = a\varepsilon_s(t)\sqrt{1-\left|\rho^{\alpha}_{ss^{(*)}}(\tau)\right|^2} + i^{*}(t-\tau)\,e^{j2\pi\alpha t}, \tag{47}$$

and where $\hat{i}(t)$ is uncorrelated with both the $s(t)$ and $i(t)$. Eqn. 44 motivates the development of interference cancellation techniques that uses $x^{(*)}(t-\tau)\,e^{j2\pi\alpha t}$ as the reference signal in a conventional least-squares algorithm.

3.4.4 Least Squares SCORE Algorithm

This simplest SCORE algorithm is developed using the interpretation of spectral self-coherence. A reference signal $r(t)$ is created as follows [Age89]:

$$r(t) \triangleq C^{H}x^{(*)}(t-\tau)\,e^{j2\pi\alpha t}, \tag{48}$$

where the vector C is referred to as the control vector and the optional conjugation (*) is applied if and only if conjugate self-coherence id to be restored by the processor. If $x(t)$ is modeled as follows

$$x(t) = as(t) + i(t), \tag{49}$$

and *s(t)* is the sole received signal component with the spectral self-coherence or conjugate self-coherence at frequency separation α, then Eqns. 45 - 47 can be used to show that *r(t)* decomposes to into a replica of the SOI plus a corruption term that is uncorrelated with both *s(t)* and *x(t)* (and therefore *y(t)*)

$$r(t) = \hat{a}s(t) + \hat{i}(t), \tag{50}$$

where $\hat{a}(t)$ and $\hat{i}(t)$ are given by Eqns. 46 and 47, respectively, with $a = \boldsymbol{c}^H \boldsymbol{a}^{(*)}$ and $i(t) = \left[\boldsymbol{c}^{(*)}\right]^H \boldsymbol{i}(t)$. Eqn. 48 motivates the least-squares SCORE algorithm. We define the least-squares SCORE cost function by

$$F(\boldsymbol{w};\boldsymbol{c}) \quad \triangleq \langle |y(t) - r(t)|^2 \rangle_T, \tag{51}$$

where $y(t) = \boldsymbol{w}^H x(t)$ and *r(t)* is given by Eqn. 50, and where $\langle \cdot \rangle_T$ denotes time-averaging over the interval (0,T). Substituting Eqn. 49 into Eqn. 50 and letting the averaging time grow to infinity yields

$$F = \langle |y(t) - [\hat{a}s(t) + \hat{i}(t)]|^2 \rangle_T \tag{52}$$

$$\rightarrow \langle |y(t) - \hat{a}s(t)|^2 \rangle_\infty + \langle |\hat{i}(t)|^2 \rangle_\infty$$

Because $\hat{i}(t)$ does not depend on **w**, it follows that Eqn. 50 becomes equivalent to the true least-squares cost function and the value of **w** that minimizes Eqn. 49 for infinite averaging time. Minimizing Eqn.50 with respect to $\underline{w}$ produces the maximum-SINR processor as $T \rightarrow \infty$.

Minimizing Eqn. 50 with respect to **w** yields the least-squares SCORE algorithm

$$\boldsymbol{w}_{sc} = \hat{\boldsymbol{R}}_{xx}^{-1} \hat{\boldsymbol{R}}_{xr}, \tag{53}$$

where $\hat{R}_{xx}^{-1}$ and $\hat{R}_{xr}$ are the sample autocorrelation matrix and the cross-correlation vector computed over [0,T]. If $i(t)$ is not spectral self-coherent at α, the autocorrelation and crosscorrelation are not a function of i, then as $T \to \infty$ Eqn. 51 converges to

$$w_{sc} \to R_{xx}^{-1} \; R_{xr} \tag{54}$$

$$= R_{xx}^{-1} \; R_{xx}^{\alpha}(\tau)\, c e^{-j\pi\alpha\tau}. \tag{55}$$

If only $s(t)$ is spectrally self-coherent at α, then as $T \to \infty$, $R_{xx}^{\alpha}(\tau)$ reduces to a rank-1 matrix with form

$$R_{xx}^{\alpha}(\tau) = a\left[a^{(*)}\right]^{H} R_{ss^{(*)}}^{\alpha}(\tau) \tag{56}$$

and Eqn. 54 reduces to

$$w_{sc} \to R_{xx}^{-1} \; \left(a\left[a^{(*)}\right]^{H} c\right) R_{ss^{(*)}}^{\alpha}(\tau) \; e^{-j\pi\alpha\tau} \tag{57}$$

$$= g_{sc} R_{xx}^{-1} \, a \, R_{ss}, \quad [\quad g_{sc} = \left[a^{(*)}\right]^{H} c \rho_{ss^{(*)}}^{\alpha}(\tau)\, e^{-j\pi\alpha\tau} \; . \tag{58}$$

That is, w_{sc} reduces to the maximum-SINR (or scaled least-squares) weight vector given by

$$w_{max} \propto R_{ii}^{-1} \; a \propto R^{-1}{}_{xx} a R_{ss}, \tag{59}$$

where g_{sc} is the gain constant. Note that w converges to the maximum-SINR solution for any value of c, as long as c is not orthogonal to $a^{(*)}$.

The least-squares SCORE processor block diagram is shown in Figure 3. The refer-

ence signal *r(t)* is generated by linearly combining, delaying, conjugating (if conjugate self-coherence is being exploited), and frequency-shifting the data received by the array. The reference signal is then used as a training signal to adapt the processor vector w using a least-squares algorithm. The only control parameters used in the processor are the control vector **c**, the delay τ, the conjugation control, and the frequency-shift α; Note that α and the conjugation control are the primary parameters.

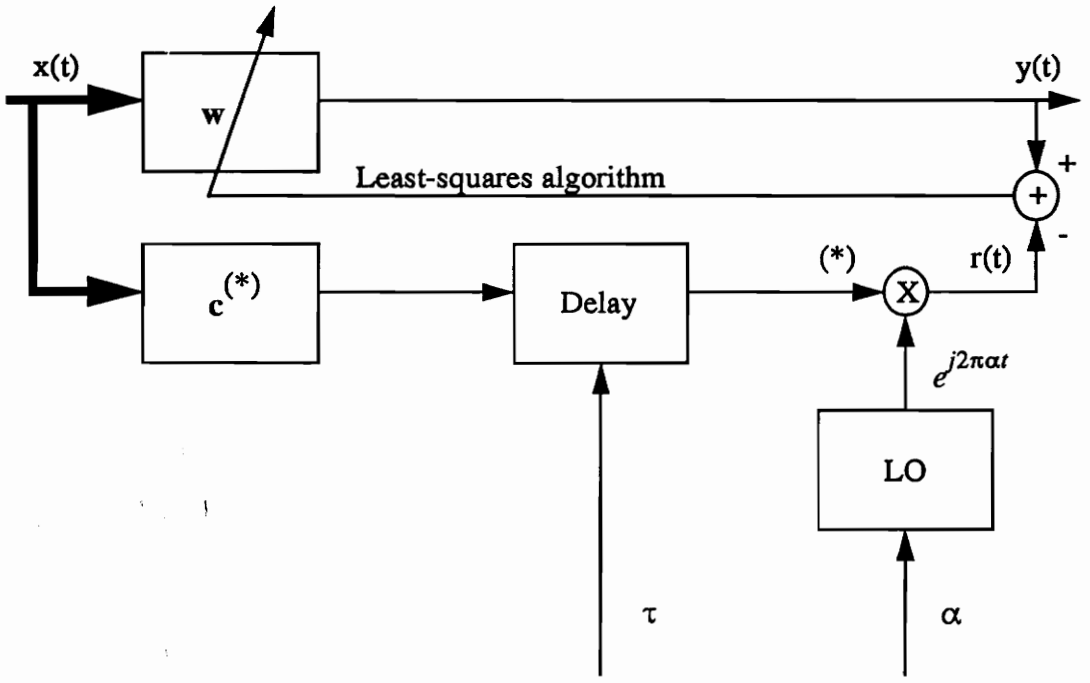

Figure 3. Least-Squares SCORE Processor (Thick line represents the input from the antenna elements)

Theoretically various values α and τ are possible, because in theory these parameters need only to be chosen to yield a nonzero value for g_{sc} in Eqn. 57. In addition, the frequency-shift parameter α need not be related in any way to the bandwidth or sampling rate of the receiver system; however, to implement the processor in the digital form and if α is large, care should be taken to prevent aliasing.

Practically α should be chosen to exploit spectral correlation that requires less averaging time to mitigate the effect of noise. From Figure 3 it is clear that the least-squares SCORE processor can be generalized in many ways. For instance, the delay operation can be replaced by a more general filtering operation, by generating *r(t)* using

$$r(t) = c^H \hat{x}^{(*)}(t) e^{j2\pi\alpha t}, \quad \hat{x}(t) = h((t) \bullet x(t), \tag{60}$$

where *h(t)* is the control filter impulse response and $\bullet$ denotes convolution. The optimum weight vector then converges to

$$w_{sc} \rightarrow g_{sc} R^{-1}{}_{xx} a R_{ss}, \quad g_{sc} = \left[a^{(*)}\right]^H c \rho^{\alpha}{}_{ss^{(*)}} \sqrt{\frac{R_{ss}}{R_{\hat{s}\hat{s}}}}, \tag{61}$$

where $\hat{s}(t)$ is the filtered SOI. The convergence of the filter depends on the strength of the spectral self-coherence $\rho^{\alpha}_{ss^{(*)}}$ being restored by the processor.

The critical dependence of the SCORE processor on the precision of the target α can be eased somewhat by the particular choice of averaging window used to calculate the finite-time correlation matrices $\hat{R}_{xx}$ and $\hat{R}_{xr}$. If a growing rectangle window is used to calculate $\hat{R}_{xr}$, for instance, then the processor will eventually reject the SOI if there is any error in specifying α [Age89]. In many environments, the self-coherence of the SOI is not always known exactly, for instance if the SOI undergoes a Doppler shift there is no way of knowing the exact α. Also, the signal environment may be dynamic due to the changing interference, multipath, and noise. So to make the SCORE processor robust, exponential decay windows can be used to compute $\hat{R}_{xr}$.

3.4.5 Variations of SCORE Algorithm

Cross-SCORE is another algorithm which performs better than LS-SCORE. This

algorithm maximizes the cross-correlation coefficient between $\hat{s}(n)$ and $\boldsymbol{c}^H \boldsymbol{x}(n-\tau)$. This algorithm solves the problem of how $\boldsymbol{c}$ has to be chosen to minimize convergence time. Without resorting to prior knowledge of the spatial characteristics of $s(n)$ or $i(n)$, a direct method is to maximize $|\hat{\rho}_{sr}|^2$ with respect to $\boldsymbol{w}$ and $\boldsymbol{c}$. This algorithm can estimate multiple SOI with same cyclic features, based on the spectral self-coherence strength. The Cross-SCORE can be easily be implemented as follows.

$$\boldsymbol{c} \leftarrow g_c \hat{\boldsymbol{R}}_{rr}^{-1} \hat{\boldsymbol{R}}_{rx} \boldsymbol{w}$$

$$\boldsymbol{w} \leftarrow g_w \hat{\boldsymbol{R}}_{xx}^{-1} \hat{\boldsymbol{R}}_{xr} \boldsymbol{w}$$

---

where g_c, and g_w are used to normalize the power of $y(t)$ and $r(t)$ at each step in the algorithm.

Phase-SCORE is a version which exploits the phase information in the cyclic feature strengths, to distinguish multiple SOIs with identical self-coherence strengths. For example in a CDMA system, all the users occupy the same band and they have identical baud rate, chip rate and code repetition rate. If the users are operating in an asynchronous mode, the cyclic correlation coefficients will have different phases even if the feature strengths are the same. The algorithm can be stated as follows.

$$\hat{\boldsymbol{R}}_{xx}^{\alpha}(\tau)\, \boldsymbol{w} = \lambda \hat{\boldsymbol{R}}_{xx} \boldsymbol{w}$$

---

where λ is the dominant eigenvalue.

3.4.6 SCORE-Tapped Delay Line (SCORE-TDL) Structure

The SCORE algorithm is implemented using recursive least-squares algorithm. The algorithm operates on samples of data instead of blocks of data. SCORE has one weight per antenna element, but it was noted that SCORE on AMPS does not work satisfactorily. The reason is that the array is not able to resolve the spectral correlation features created by two closely spaced SATs. To resolve the closely spaced SAT components, large scale time-averaging is needed, and a good estimate of the statistics is obtained.

A slight modification to this basic SCORE algorithm was made by introducing a tapped-delay line to each antenna element. There are 16 taps in each of the element. This new structure, SCORE-Tapped Delay Line (SCORE-TDL), gives far better results compared to the basic SCORE structure. This structure has frequency selection capability due to the presence of the tapped-delay line. This capability enables this structure to reduce the interference and noise. Thus consistent statistical estimation requires less integration time with the TDL version of SCORE. The estimated output is a frequency-shifted version of the original signal. The frequency shift is equal to the SAT tone. The TDL shapes the non-frequency shifted array inputs to estimate a frequency shifted version of the input signal. Because AMPS consists of replicated spectrum of the original FM voice signal, this approach works well. A beam is formed in the direction of the SOI because this condition will also minimize the MSE. The frequency shift in the output of the array is not a problem in AMPS, because the demodulated output signal has a DC component which does not affect the voice signal. This will be a problem for digital signals, that can also be compensated for.

The mechanism for its operation is different from SCORE. The new structure is frequency-selective and extracts the sidelobe, creating a distorted version of the AMPS signals. However the distorted version reproduces faithfully the voice signal upon demodulation. This SCORE-TDL converges faster than the basic SCORE, because the

mainlobe is used as the training signal to extract the sidelobes. This mainlobe has a higher SIR than the sidelobe, which is used as the training sequence in the basic SCORE algorithm.

3.4.7 Recursive Least Squares SCORE Tapped Delay Line Algorithm (RLS-SCORE-TDL) Implementation

Implementation of least-squares SCORE-TDL involves estimating the tap-weight vector and the estimation involves the computation of the inverse of the autocorrelation matrix. If the length of the tap weight vector is large then the inverse operation is time consuming. For a narrowband model of the antenna array, the computation complexity using least-squares SCORE-TDL or RLS-SCORE-TDL is the same. But for wideband model, it is certainly advantageous to use RLS-SCORE-TDL. The implementation steps of the algorithm for a wideband model is given below.

Algorithm:

Initialize the algorithm by setting

$$\boldsymbol{P}(0) = \delta^{-1}\boldsymbol{I}, \quad \delta = \text{a small positive constant}$$

$$\hat{\boldsymbol{w}}(0) = \boldsymbol{0}$$

M is the number of elements in the array

L is the number of taps in the tapped delay line attached to each element

For each instant of time, $n = 0, 1, 2, \ldots\ldots$, compute

$$\boldsymbol{c} = [1 \quad 0 \quad 0 \quad \ldots \quad M] \qquad \boldsymbol{k}(n) = \lambda + \pi(n) \cdot \boldsymbol{x}(n)$$

$$\boldsymbol{x} = \boldsymbol{X} \cdot \boldsymbol{c}$$

$$\boldsymbol{K}(n) = \frac{\pi^{H}(n)}{\boldsymbol{k}(n)}$$

$$\pi(n) = \boldsymbol{x}^{H}(n)\boldsymbol{P}(n-1)$$

$$\boldsymbol{d} = (\boldsymbol{X} \cdot \boldsymbol{c}) \cdot e^{j2\pi\alpha t}$$

$$\alpha(n) = \boldsymbol{d}(N/2) - y(n)$$

$$\hat{\boldsymbol{w}}(n) = \hat{\boldsymbol{w}}(n-1) + \boldsymbol{k}(n) \cdot \alpha^*(n)$$

$$\boldsymbol{P}'(n-1) = \boldsymbol{K}(n) \cdot \pi(n)$$

$$\boldsymbol{P}(n) = \frac{1}{\lambda}(\boldsymbol{P}(n-1) - \boldsymbol{P}'(n-1))$$

$$y = \hat{\boldsymbol{w}}^H \boldsymbol{X}$$

3.5 Time Dependent Adaptive Array (TDAA)

The time-dependent adaptive array is a combination of the time-dependent optimal filter and adaptive array. A TDAA exploits spatial, frequency, and time diversities. A time-dependent adaptive filter (TDAF) is an adaptive filter implementation of the time-dependent optimal filter, with a filter response that varies periodically in time. The principle behind time-dependent optimal filter is to use spectrally correlated portions of the signal-of-interest (SOI) or/and the signal-not-of-interest (SNOI) to improve the portion of SOI spectrum corrupted by the interference. When the signal statistics change periodically, a TDAF outperforms a time independent adaptive filter (TIAF) in approximating the optimal time-varying solution [Ree87] [Ree88]. The idea behind the TDAA is that correlated, but different data can be obtained from each spatially separated array element through frequency shifting the data at each antenna element. The TDAA can be blindly adapted by configuring the TDAA as a predictor. That is, the TDAA predicts signals which exhibit a particular form of spectral correlation.

An implementation of the time-dependent adaptive array is shown in Figure 4. There are M elements in the array and the array exploits L cyclic periodicities. There are N signals coming from arbitrary directions. The advantage of a TDAA over the conventional array is that not as many antenna elements are required to achieve a given performance level. This is desirable from both an operational point of view and from a cost point of view. A second advantage is that it is possible to derive new blind array algorithms based on the spectral correlation characteristics of the SOI and interference.

3.5.1 Interpretation of this New Blind Adaptive Algorithm

Here we introduce a new array structure and a blind adaptation algorithm. This new adaptation algorithm can be viewed as a power minimizer structure which tries to minimize the mean-squared-error. This technique behaves as a beamformer if the elements estimate the SOI and the error is the SNOI. Otherwise, if the elements estimate the SNOI, then the structure can be viewed as a null-steering array. Two structures, one for narrowband signals and the other for wideband signals are introduced. The time-dependent adaptive array can be implemented by a bank of frequency shifters and filters as is done in temporal filtering. The MSE and BER performances of these structures are better than CMA and SCORE arrays. TDAA achieves the optimal MSE and it does an optimal combining when both interference and noise are present.

3.5.2 Mean-Square Error Analysis for TDAA

Let $\hat{y}$ be the output vector of the array and x is the input vector to the array. The objective is to find $h(t)$, the impulse response of the filter, that minimizes the mean-squared-error

$$MSE = \lim_{z \to \infty} \frac{1}{z} \int_{-z/2}^{z/2} (y(t) - \hat{y}(t))^2 dt, \tag{62}$$

where

$$\hat{y}(t) = \int_{-\infty}^{\infty} \boldsymbol{h}(t-u)\,\boldsymbol{x}(u)\,du, \tag{63}$$

and the MSE is the mean-squared-error based on time-averaging as opposed to an ensemble averaging. The optimal $\boldsymbol{h}(t)$, which is a vector of size (M x 1), occurs when the gradient of the MSE with respect to the filter is zero:

$$0 = \lim_{z \to \infty} \frac{1}{z} \int_{-z/2}^{z/2} (y(t) - \hat{y}(t))\,\boldsymbol{x}^*(t-u)\,dt \quad \text{for all } u, \tag{64}$$

where * represents the complex-conjugate operation. The value of $\boldsymbol{h}(t)$ which satisfies the above condition is the Wiener solution. In this case $\boldsymbol{h}(t)$ is a time-dependent array.

Consider the case where the filter is allowed to be almost periodically time-varying. Therefore

$$\boldsymbol{h}(t,u) = \left[\left(\sum_{n=0}^{L-1} g_{n1}(t-u)\,e^{j2\pi\alpha_n u}\right), \left(\sum_{n=0}^{L-1} g_{n2}(t-u)\,e^{j2\pi\alpha_n u}\right), \ldots \right. \tag{65}$$

$$\left. \ldots \left(\sum_{n=0}^{L-1} g_{nM}(t-u)\,e^{j2\pi\alpha_n u}\right)\right]$$

where g_{ni} represents the weight of the filter corresponding to the element i, and periodicity n. So $\boldsymbol{h}(t)$ is a vector of size M x 1. The argument t is the output time and the argument u is the input time. For convenience, $\tilde{\alpha}$ is defined a set of desired periodicities, where α_n is a member: $\{\alpha_n \in \tilde{\alpha}; n = 0, 1 \ldots\ldots, L-1\}$. The estimate $\hat{y}(t)$ is now

$$\hat{y}(t) = \int_{-\infty}^{\infty} \boldsymbol{h}(t,u)\,\boldsymbol{x}(u)\,du\ . \tag{66}$$

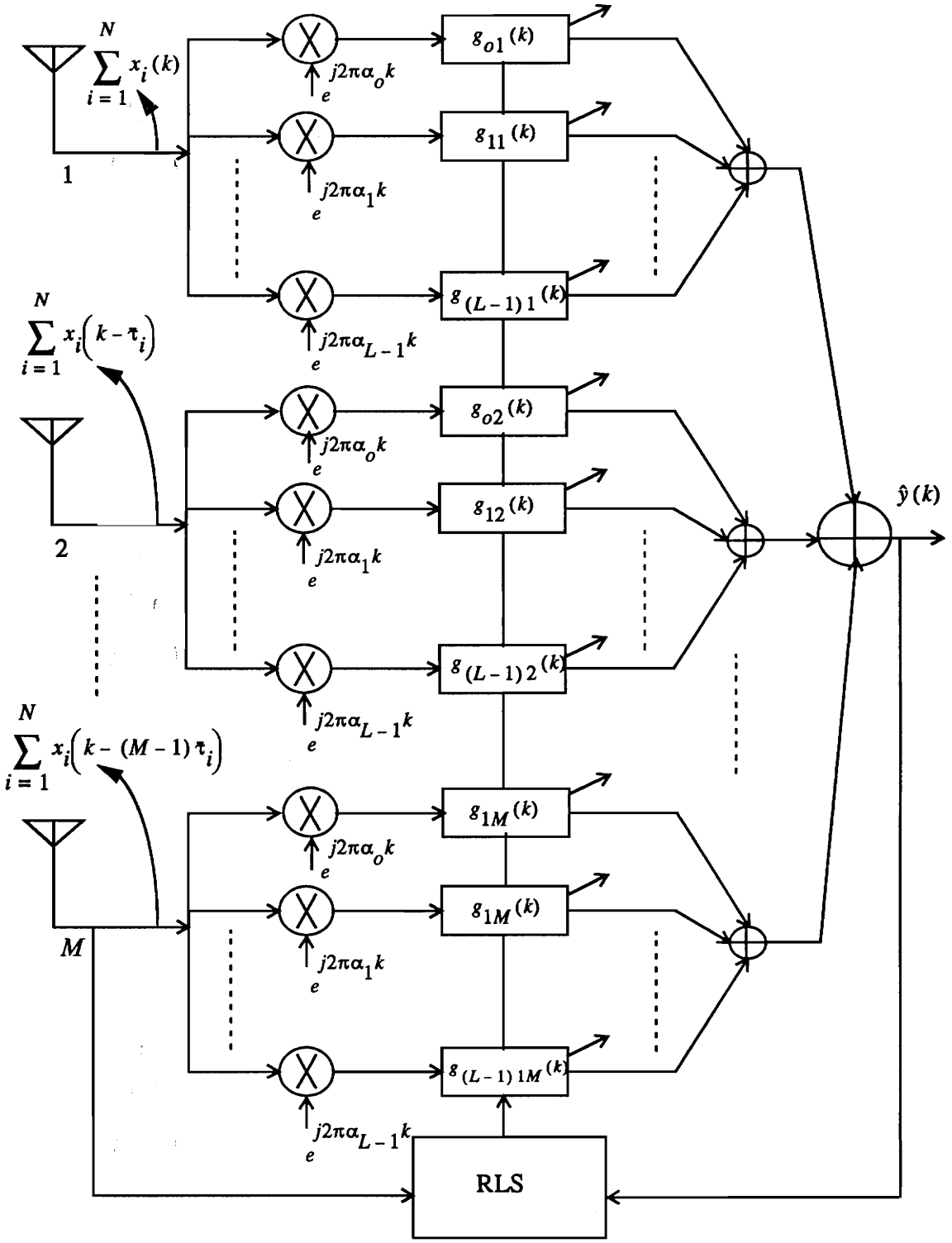

Figure 4. Time-Dependent Adaptive Array (Structure 1)
($\bar{\tau}_i$ is the normalized discrete delay corresponding to τ_i)

Substituting Eqn. 65 in Eqn. 66, we get

$$\hat{y}(t) = \int_{-\infty}^{\infty} \left[\sum_{n=0}^{L-1} g_{n1}(t-u)\, e^{j2\pi\alpha_n u} \right] [x_1(u) + x_2(u) + \ldots\ldots + x_N(u)]\, du$$

$$+ \int_{-\infty}^{\infty} \left[\sum_{n=0}^{L-1} g_{n2}(t-u)\, e^{j2\pi\alpha_n u} \right] [b_{11}(u) \bullet x_1(u) + b_{12}(u) \bullet x_2(u) + \ldots\ldots$$

$$\ldots\ldots + b_{1N}(u) \bullet x_N(u-\tau_N)]\, du \qquad (67)$$

$$\ldots + \int_{-\infty}^{\infty} \left[\sum_{n=0}^{L-1} g_{nM}(t-u)\, e^{j2\pi\alpha_n u} \right] [b_{M1}(u) \bullet x_1(u) + b_{M2}(u) \bullet x_2(u) + \ldots\ldots$$

$$\ldots\ldots + b_{MN}(u) \bullet x_N(u-\tau_N)]\, du$$

where b_{ij} represents the channel impulse response associated with the *i*th antenna element and *j*th signal. Eqn. 67 is the output if the signal is wideband. If the signal is narrowband and it is in the far-field, then $b_{mn}(t) = \delta(t-\tau_i)$,

$$\hat{y}(t) = \int_{-\infty}^{\infty} \left[\sum_{n=0}^{L-1} g_{n1}(t-u)\, e^{j2\pi\alpha_n u} \right] [x_1(u) + x_2(u) + \ldots\ldots + x_N(u)]\, du$$

$$+ \int_{-\infty}^{\infty} \left[\sum_{n=0}^{L-1} g_{n2}(t-u)\, e^{j2\pi\alpha_n u} \right] [x_1(u-\tau_1) + x_2(u-\tau_2) + \ldots\ldots + x_N(u-\tau_N)]\, du$$

$$\ldots + \int_{-\infty}^{\infty} \left[\sum_{n=0}^{L-1} g_{nM}(t-u)\, e^{j2\pi\alpha_n u} \right] (x_1(u-\tau_1(M-1)) + x_2(u-\tau_2(M-1)) + \qquad (68)$$

$$\ldots + x_N(u-\tau_N(M-1))]\, du$$

where τ_i is the delay associated with the propagation of the plane wave due to the ith signal from one element to the next.

$$\hat{y}(t) = \sum_{n=0}^{L-1} g_{n1}(t) \bullet \left[x_1(t)\, e^{j2\pi\alpha_n t}\right] + \sum_{n=0}^{L-1} g_{n1}(t) \bullet \left[x_2(t)\, e^{j2\pi\alpha_n t}\right] + \ldots + \sum_{n=0}^{L-1} g_{n1}(t) \bullet \left[x_N(t)\, e^{j2\pi\alpha_n t}\right] \quad (69)$$

$$+ \sum_{n=0}^{L-1} g_{n2}(t) \bullet \left[x_1(t-\tau_1)\, e^{j2\pi\alpha_n t}\right] + \sum_{n=0}^{L-1} g_{n2}(t) \bullet \left[x_2(t-\tau_2)\, e^{j2\pi\alpha_n t}\right] + \ldots + \sum_{n=0}^{L-1} g_{n2}(t) \bullet \left[x_N(t-\tau_N)\, e^{j2\pi\alpha_n t}\right]$$

$$\ldots + \sum_{n=0}^{L-1} g_{nM}(t) \bullet \left[x_1(t-(M-1)\tau_1)\, e^{j2\pi\alpha_n t}\right] + \sum_{n=0}^{L-1} g_{nM}(t) \bullet \left[x_2(t-(M-1)\tau_2)\, e^{j2\pi\alpha_n t}\right] + \ldots + \sum_{n=0}^{L-1} g_{nM}(t) \bullet \left[x_N(t-(M-1)\tau_N)\, e^{j2\pi\alpha_n t}\right]$$

where $\bullet$ represents the convolution operation.

When the signal is narrowband, the correlated portions of the spectrum of the signal at each element are not different. Therefore the weights $g_{ki}(l), g_{k(i+1)}(l), \ldots\ldots g_{k(i+M-1)}(l)$ differ by complex constants, and these complex constants are the same for different values of l. So, the weight matrix has columns that are dependent.

$$\hat{y}(t) = \sum_{n=0}^{L-1} g_{n1}(t) \bullet \left[\sum_{i=1}^{N} x_i(t)\, e^{j2\pi\alpha_n t}\right] + \sum_{n=0}^{L-1} g_{n2}(t) \bullet \left[\sum_{i=1}^{N} x_i(t-\tau_i)\, e^{j2\pi\alpha_n t}\right] + \ldots + \sum_{n=0}^{L-1} g_{nM}(t) \bullet \left[\sum_{i=1}^{N} x_i(t-(M-1)\tau_i))\, e^{j2\pi\alpha_n t}\right] \quad (70)$$

and $g_{n2}(t) = C_2 g_{n1}(t)$,....,$g_{nM}(t) = C_M g_{n1}(t)$, where C_2, ..., C_M are complex constants. So Eqn. 70 becomes,

$$\hat{y}(t) = \sum_{n=0}^{L-1} C_1 g_{n1}(t) \bullet \left[\sum_{i=1}^{N} x_i(t) e^{j2\pi\alpha_n t} \right] + \sum_{n=0}^{L-1} C_2 g_{n1}(t) \bullet \left[\sum_{i=1}^{N} x_i(t-\tau_i) e^{j2\pi\alpha_n t} \right] + \ldots \tag{71}$$

$$\ldots + \sum_{n=0}^{L-1} C_M g_{n1}(t) \bullet \left[\sum_{i=1}^{N} x_i(t-(M-1)\tau_i)) e^{j2\pi\alpha_n t} \right],$$

$$\hat{y}(t) = \sum_{j=1}^{M} C_j \left[\sum_{n=0}^{L-1} g_{n1}(t) e^{j2\pi\alpha_n t} \bullet \left[\sum_{i=1}^{N} x_i(t-(j-1)\tau_i) \right] \right]$$

where $C_1 = 1$, and $g_{n1}(t)$ is the response of the first filter which is used as a basis to represent the responses of the other filters in Structure 1. From Eqn. 71, the TDAA (Structure 1) reduces to the Structure 2 shown in Figure 5. This is true because since the time-dependent filter for each antenna elements is dependent, and so the Structure 1 can be reduced to the Structure 2. Note that an adaptive implementation of Structure 2 is more complex, because it involves optimizing the product of unknown variables. However, for analysis purposes Structure 2 is convenient. The Structure 2 can be sub-optimized by fixing the front section of the array constant and optimize the back section of the array. In the same way, the back section can be fixed constant and optimize the front section of the array. The gradient of the error ∇_n can be obtained by substituting the above equation into Eqn. (62) and taking the derivative with respect to $g_{ij}(t)$. The gradient of the error for a particular coefficient of the time-varying filter series is given by

$$\nabla_\beta = \int_{-\infty}^{\infty} \lim_{z \to \infty} \frac{-2}{z} \int_{-z/2}^{z/2} (y(t) - \hat{y}(t)) x^*(t-u) e^{-j2\pi\beta(t-u)} \, dtdu \, , \tag{72}$$

where β can take any value that α_n can assume. The optimal value for $g_\beta(t)$ occurs when the gradient is zero.

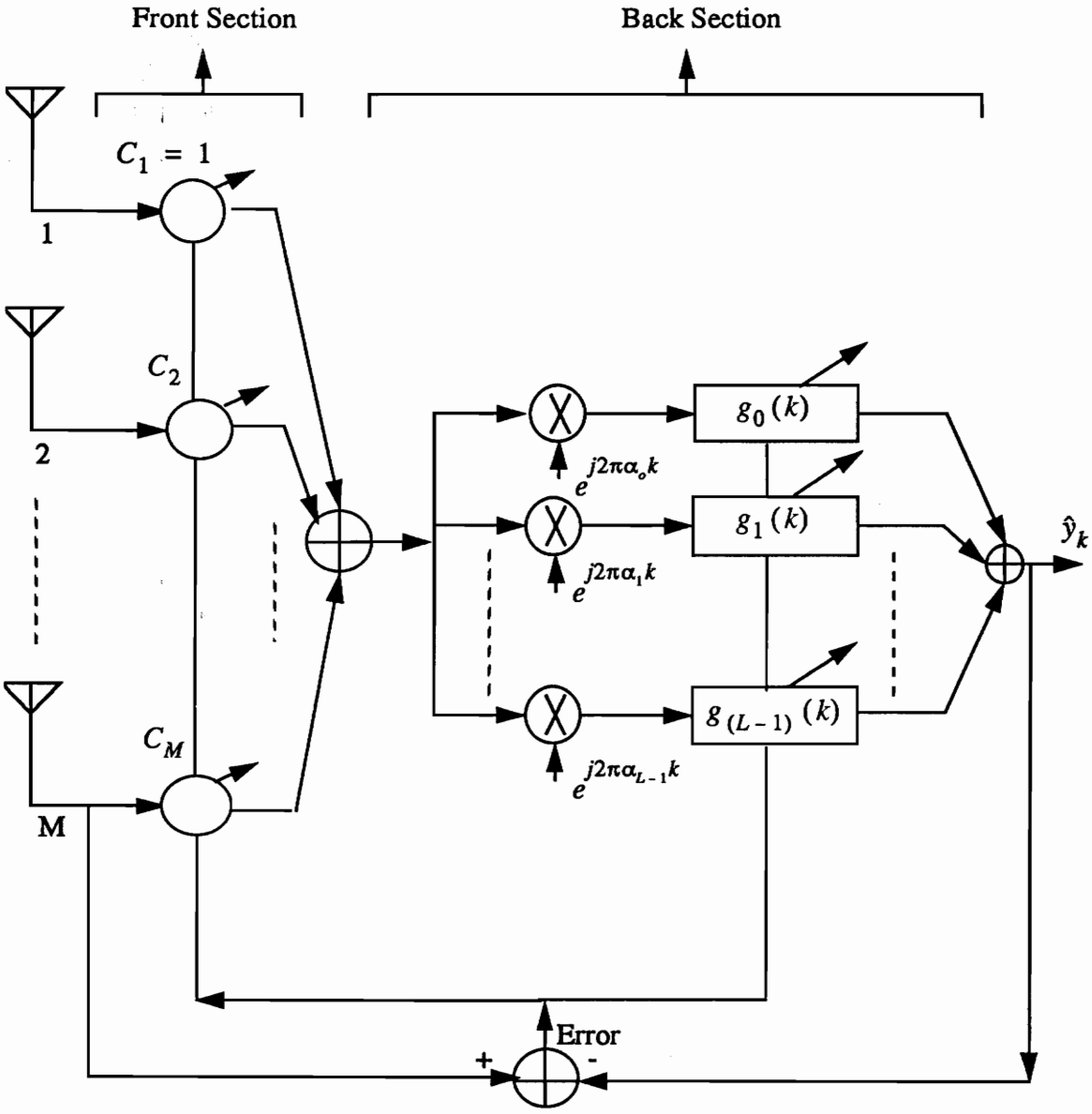

Figure 5. Time-Dependent Adaptive Array (Structure 2)

$$0 = \nabla_{\beta} \tag{73}$$

$$0 = \lim_{z \to \infty} \frac{1}{z} \int_{-z/2}^{z/2} (y(t) - \hat{y}(t)) x^*(t-u) e^{-j2\pi\beta(t-u)} \, dt \qquad \text{for all } u$$

The above equation requires that the estimation error must be uncorrelated with the data frequency shifted by β. This is the same as

$$\lim_{z \to \infty} \frac{1}{z} \int_{-z/2}^{z/2} y(t) x^*(t-u) e^{-j2\pi\beta(t-u)} \, dt = \lim_{z \to \infty} \frac{1}{z} \int_{-z/2}^{z/2} (\hat{y}(t)) x^*(t-u) e^{-j2\pi\beta(t-u)} \, dt \tag{74}$$

The right-hand side of Eqn. 74 can be expressed as

$$\sum_{l=1}^{N} \left[\sum_{n=0}^{L-1} g_{n1}(u) \bullet \left[K_1 R_{x_l}^{\beta-\alpha_n}(u) + K_2 e^{j2\pi(\beta-\alpha_n)\tau_l} R_{x_l}^{\beta-\alpha_n}(u) + \ldots\ldots + K_M e^{j2\pi(\beta-\alpha_n)(M-1)\tau_l} R_{x_l}^{\beta-\alpha_n}(u) \right] \right] \tag{75}$$

where $K_1 = C_1 e^{j\pi(\alpha_n+\beta)u}$, $K_1 = C_2 e^{j\pi(\alpha_n+\beta)u}$,...., $K_M = C_M e^{j\pi(\alpha_n+\beta)u}$, and

$R_x^{\beta-\alpha_n}(u)$ is the cyclic autocorrelation for cycle frequency $(\beta - \alpha_n)$ and is defined as

$$R_x^{\beta-\alpha_n}(u) = \lim_{T \to \infty} \left(\frac{1}{T} \int_{-\infty}^{\infty} x(t + (u/2)) x^*(t - (u/2)) e^{-j2\pi(\beta-\alpha)t} dt \right) \tag{76}$$

The left-hand side of Eqn. 74 is equal to

$$e^{j\pi\beta u} R_{yx}^{\beta}(u) \, . \tag{77}$$

From Eqns. 75 and 77

$$e^{j\pi\beta u} R_{yx}^{\beta}(u) = \sum_{l=1}^{N} \left[\sum_{n=0}^{L-1} g_{n1}(u) \bullet \left[K_1 R_{x_l}^{\beta-\alpha_n}(u) + K_2 e^{j2\pi(\beta-\alpha_n)\tau_l} R_{x_l}^{\beta-\alpha_n}(u) + \ldots\ldots - \right. \right.$$
$$\left. \left. + K_M e^{j2\pi(\beta-\alpha_n)(M-1)\tau_l} R_{x_l}^{\beta-\alpha_n}(u) \right] \right] \tag{78}$$

In the frequency-domain

$$S_{yx}^{\beta}(f-\beta/2) = \sum_{l=1}^{N} \sum_{n=0}^{L-1} G_{n1}(f) S_{x_l}^{\beta-\alpha_n}\left(f - \frac{(\alpha_n+\beta)}{2}\right) \left[C_1 + C_2 e^{j2\pi(\beta-\alpha_n)\tau_l} + \ldots\ldots\ldots + \right.$$
$$\left. + \ldots\ldots + C_M e^{j2\pi(\beta-\alpha_n)(M-1)\tau_l} \right] \tag{79}$$

where $S_{yx}^{\beta}(f) = \int_{-\infty}^{\infty} R_{yx}^{\beta}(\tau)\, e^{j2\pi f\tau} d\tau$.

Solving either Eqns. 78 and 79 involves L unknowns i.e., exploiting L periodicities. The value of L is infinity if the signal is band unlimited. But usually L takes a value which is finite and small, because $S_{yx}^{\beta}(f)$ and $S_x^{\beta}(f)$ are significant only for a finite number of values of β.

The MSE is the correlation of the estimation error and $y(t)$

$$MSE = \lim_{z\to\infty} \frac{1}{z} \int_{-z/2}^{z/2} (y(t) - \hat{y}(t))\, y^*(t)\, dt \tag{80}$$

Substituting Eqn. 68 in Eqn. 80,

$$MSE = R_y^0(0) - RR,$$

$$RR = \int_{-\infty}^{\infty}\left(\sum_{l=1}^{N}\left[\sum_{n=0}^{L-1} g_{n1}(u) \bullet \left[\left(K_1 R_{x_l}^{\beta-\alpha_n}(u)\, e^{j\pi\alpha_n}\right)^* + \left(K_2 e^{j2\pi(\beta-\alpha_n)\tau_l} R_{x_l}^{\beta-\alpha_n}(u)\, e^{j\pi\alpha_n}\right)^* + \ldots\ldots \right.\right.\right.$$

$$\left.\left.\left. + \left(K_M e^{j2\pi(\beta-\alpha_n)(M-1)\tau_l} R_{x_l}^{\beta-\alpha_n}(u)\, e^{j\pi\alpha_n}\right)^* \right]\right] du \qquad (81)$$

Using Parseval's theorem, MSE in the frequency domain

$$MSE = \int_{-\infty}^{\infty} [S_y(f) - [R]]\, df$$

$$R = \sum_{l=1}^{N}\left[\sum_{n=0}^{L-1}\left(G_{n1}(f)\left(S_{yx}^{\alpha_n}\left(f-\frac{\alpha_n}{2}\right)\right)^*\right)\left[C_1 + C_2 e^{j2\pi(\beta-\alpha_n)\tau_l} + \ldots\ldots\right.\right. \qquad (82)$$

$$\left.\left. \ldots\ldots + C_M e^{j2\pi(\beta-\alpha_n)(M-1)\tau_l}\right]\right]$$

The term inside the square bracket is the contribution from the signal-of-interest. MSE reduces as the number of spectral periodicities exploited increases. MSE can be viewed as a measure of signal to interference plus noise ratio (SINR).

3.5.3 Recursive Least Squares TDAA Implementation

The recursive least squares implementation [Hay91] of TDAA is described below and corresponds to Structure 1 (Figure 4).

Algorithm:

Initialize the algorithm by setting

$$\boldsymbol{P}(0) = \delta^{-1}\boldsymbol{I}, \quad \delta = \text{small positive constant}$$

$$\hat{\boldsymbol{g}}(0) = \boldsymbol{0}$$

M is the number of elements in the array, T is the number of taps in each tapped delay line, L is the number of periodicities exploited, $\boldsymbol{x}$ is the input data vector of size [1 x TML], $\hat{\boldsymbol{g}}$ is the weight vector of size [1 x TML], $\boldsymbol{a}$ is the frequency-shift vector of size [1 x TML], $\boldsymbol{c}$ is the control vector of size [1x TML], λ is the forgetting factor, $\boldsymbol{d}$ is the reference vector, and $\boldsymbol{y}$ is the output vector.

For each instant of time, $n = 0, 1, 2, \ldots\ldots$, compute

$$x_1(n) = (\boldsymbol{x}' \cdot \boldsymbol{a})$$

$$m(n) = x_1^{H}(n)\,\boldsymbol{P}(n-1)$$

$$k(n) = \lambda + m(n) \cdot \boldsymbol{x}(n)$$

$$K(n) = \frac{m^{H}(n)}{k(n)}$$

$$\boldsymbol{d}(n) = (\boldsymbol{x}' \cdot \boldsymbol{c})$$

$$\alpha(n) = \boldsymbol{d}(n) - y(n)$$

$$\hat{\boldsymbol{g}}(n) = \hat{\boldsymbol{g}}(n-1) + k(n) \cdot \alpha^{*}(n)$$

$$\boldsymbol{P}'(n-1) = \boldsymbol{K}(n) \cdot m(n)$$

$$\boldsymbol{P}(n) = \frac{1}{\lambda}(\boldsymbol{P}(n-1) - \boldsymbol{P}'(n-1))$$

$$y(n) = \hat{\boldsymbol{g}}^{H} \cdot \boldsymbol{x}$$

Chapter 4

Simulation and Performance Analysis

This chapter describes the simulation procedure to test the algorithms described in Chapter 3. The standards which are of interest include the *Advanced Mobile Phone System standard* (AMPS), that is the current North American analog FM standard, and the IS-54 (the new U. S. Digital Cellular (USDC) standard). This chapter discusses the channel model used in the simulation and the performance criteria used. The relative performance evaluation of these algorithms under different scenarios is also presented. All simulations in this thesis were performed on Sun Microsystems SPARC 10/40 workstations using the MATLAB signal processing software and custom scripts.

4.1 Signal Model

This section discusses the features of the AMPS and the IS-54 standards that are used in the simulations to test the algorithms.

4.1.1 AMPS Standard

AMPS is the analog US cellular standard [EIA90] employing Frequency Division Multiple Access (FDMA). Voice signals are FM modulated and the control channel is FSK modulated. The signals occupy the frequency band 824-849 MHz for the reverse channel and 869-894 MHz for the forward channel. The channel bandwidth is 30 kHz. The control channel uses a data rate of 10 kbps. Channel number 1 has the mobile transmit channel at 825.030 MHz and the corresponding base transmit channel at 870.030 MHz. The channel allocation is shown in the table below.

Table 2: Frequency Allocation for AMPS Standard

System	Width in MHz	Channel Number 'N'	Mobile Center Frequency in MHz	Base Center Frequency in MHz
A	10	1 to 333	825+0.030*N	870+0.030*N
B	10	334 to 666	825+0.030*N	870+0.030*N
A'	1.5	667 to 716	825+0.030*N	870+0.030*N
B'	2.5	717 to 799	825+0.030*N	870+0.030*N
None	-	990	824.01	869.01
A"	1	991 to 1023	825+0.030*(N-1023)	870+0.030*(N-1023)

System A is the wireline system and B is the non-wireline systems. A', B', A" are the systems which provide the channels for future use. To supervise the connection on the traffic channel the Supervisory Audio Tone (SAT) and the Signaling Tone (ST) are added. SAT assumes a frequency of 5970 or 6000 or 6030 Hz. The SAT is added to the voice transmission at the base station. A mobile must detect, filter, and demodulate the transmitted voice signal with this tone. Transmission of the SAT must be suspended during transmission of wideband data on the reverse voice channel, but must not be suspended when

signaling tone is sent.

To control spectral splatter into the adjacent channels pre-emphasis and de-emphasis are used. Companding is also used to improve the quality of voice transmission.

4.1.2 IS-54 Standard

IS-54 (*Interim Standard* 54) is a cellular system standard set by the Electronic Industries Association (EIA) in 1990 [EIA90]. The IS-54 standard is implemented as a dual mode standard to allow support for the current analog AMPS standard. The IS-54 standard occupies the same band as the existing AMPS signals with the same 30 kHz spacing between adjacent cells. AMPS channels will be converted to IS-54 channels as the demand for the new IS-54 channels increases. Each IS-54 channel contains a time-division multiplexed signal operating at 48.6 kbps and carries three users' signals. The timing structure is shown in Figure 6.

The frame duration is 40 ms and is divided into six 6.67 ms slots. One time slot carries 324 bits, including 260 bits of user data and 12 bits of system control information. The remaining 52 bits carry a time synchronization signal (28 bits), a digital verification color code (12 bits). In addition, the mobile-to-base direction contains a 6 bit guard time interval where no energy is transmitted, followed by a 6 bit ramp interval to allow the transmitter to reach its full power level. Each user is allowed two slots per frame in the half rate structure. Eventually, speech coding technology is expected to progress to the point that only one slot per user per frame will be needed. This full rate signal structure will allow the data rate to be reduced from 13 kbps to 6.5 kbps.

The 28 bit synchronization signal contains a known bit pattern that allows the receiver to establish bit synchronization and train an adaptive equalizer. There are six different synchronization codes, one for each time slot, that serve to help the receiver lock

onto the correct time slot.

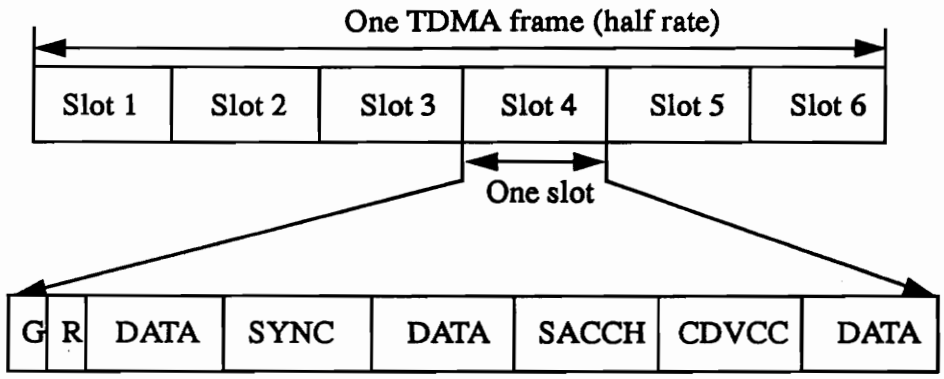

Slot Format for Mobile to Base

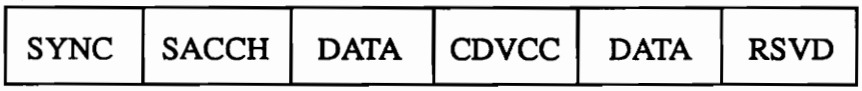

Slot Format for Base to Mobile

G = Guard time
R = Ramp up time
RSVD = Reserved bits
CDVCC = User signature
SACCH = Control information
SYNC = Synchronization information

Figure 6. Time Frame Structure of IS-54 Standard Signal

Each base is assigned a digital verification color code. This code keeps a receiver from locking onto a signal from a distant cell. Note that this sequence by itself is probably insufficient to train an adaptive filter to compensate for flat fading.

The modulation technique for the IS-54 standard is Differential Quaternary Phase Shift Keying (DQPSK). It is also called $\pi/4$ DQPSK. This modulation type resembles 8 PSK except that only phase transitions of $\pm\pi/4$ and $\pm 3\pi/4$ are allowed. The constellation diagram of $\pi/4$ DQPSK is shown in Figure 7. The signal is shaped by a root cosine filter present at both the receiver and the transmitter. The roll-off factor is 0.35.

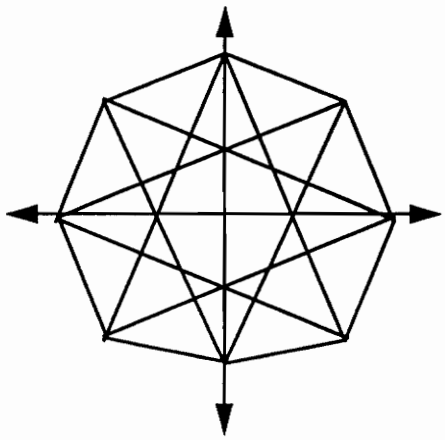

Figure 7. Constellation Diagram Showing Transition Paths

IS-54 operates in the frequency band 824-849 MHz for the reverse link and 869-894 MHz for the forward link. Pre-emphasis and de-emphasis are used. Companding is also used as in AMPS.

4.2 A Simple Statistical Model for Angle of Arrival in Line-of-Sight Multipath Channels

A typical model for the multipath channel is given by Rappaport [Rap89] as

$$h(t) = \sum_{i=0}^{N} A_i e^{j\phi_i} \delta(t - \tau_i) \ , \tag{83}$$

where A_i is the magnitude of a multipath component, ϕ_i is the phase of the multipath component and τ_i is the delay associated with that component. The statistics of N, A_i, and τ_i are given by the work of Seidel and Rappaport [Sco90] [Rap94]. This model is adequate for modelling systems which use omnidirectional antennas. In general, each multipath component also has an angle-of-arrival associated with it. This information is necessary when considering the performance of communication systems employing directional antennas at the receiver.

To develop a simple statistical model for angle of arrival (AOA) in multipath environments, we first make the assumption that the transmitter uses an omnidirectional antenna [Lib95]. If a line-of-sight path exists between the transmitter and the receiver, then the first arriving component will arrive at a time $\tau_0 = d/c$ where d is the distance between the transmitter and receiver (T-R separation) and c is the speed of light which is 3×10^8 meters/sec.

Let us consider a subsequent multipath component which arrives at time τ_i. As noted earlier by Seidel and Rappaport, if the component is the result of a single reflection (a single bounce path), then the scatterer which caused the reflection must lie on an ellipse with major axis half length a, and minor axis half length b as shown in Figure 8. The quantities a, b, and f_{focus} are given by:

$$f_{focus} = \frac{d}{2}, \tag{84}$$

$$a = \frac{c\tau_i}{2} \ , \tag{85}$$

$$b = \sqrt{a^2 - f_{focus}^2}. \tag{86}$$

Then the scatterer which resulted in a single-bounce multipath component arriving at time τ_i must lie at coordinates (x, y) such that x and y satisfy

$$\frac{x^2}{a^2} + \frac{y^2}{b^2} = 1. \tag{87}$$

This is due to the fact that r_1, the distance from the scatterer at (x, y) to the transmitter at $(-f_{focus}, 0)$, and r_2, the distance from the point (x, y) to the receiver at $(f_{focus}, 0)$, sum to $2a = c\tau_i$ at every point (x, y) on the ellipse. Let us assume that there is an angle of departure θ_d that is taken by a particular ray as it leaves the transmitter. The angle of arrival at the receiver is θ_a.

Based on the geometry of Figure 9, we may write the following equations

$$r_1 = a + f_{focus}\cos\gamma, \tag{88}$$

$$r_2 = a - f_{focus}\cos\gamma, \tag{89}$$

$$r_1\cos(\theta_d) + r_2\cos(\theta_a) = 2f_{focus}, \tag{90}$$

$$r_1\sin(\theta_d) = r_2\sin(\theta_a). \tag{91}$$

Substituting Eqn. 88 and 89 into Eqn. 90 yields

$$a(\cos\theta_d + \cos\theta_a) + f_{focus}\cos\gamma(\cos\theta_d - \cos\theta_a) = 2f_{focus}, \tag{92}$$

and substituting Eqn. 88 and 89 into Eqn. 91 gives:

$$\cos\gamma = \frac{a}{f_{focus}}\left(\frac{\sin\theta_a - \sin\theta_d}{\sin\theta_a + \sin\theta_d}\right). \tag{93}$$

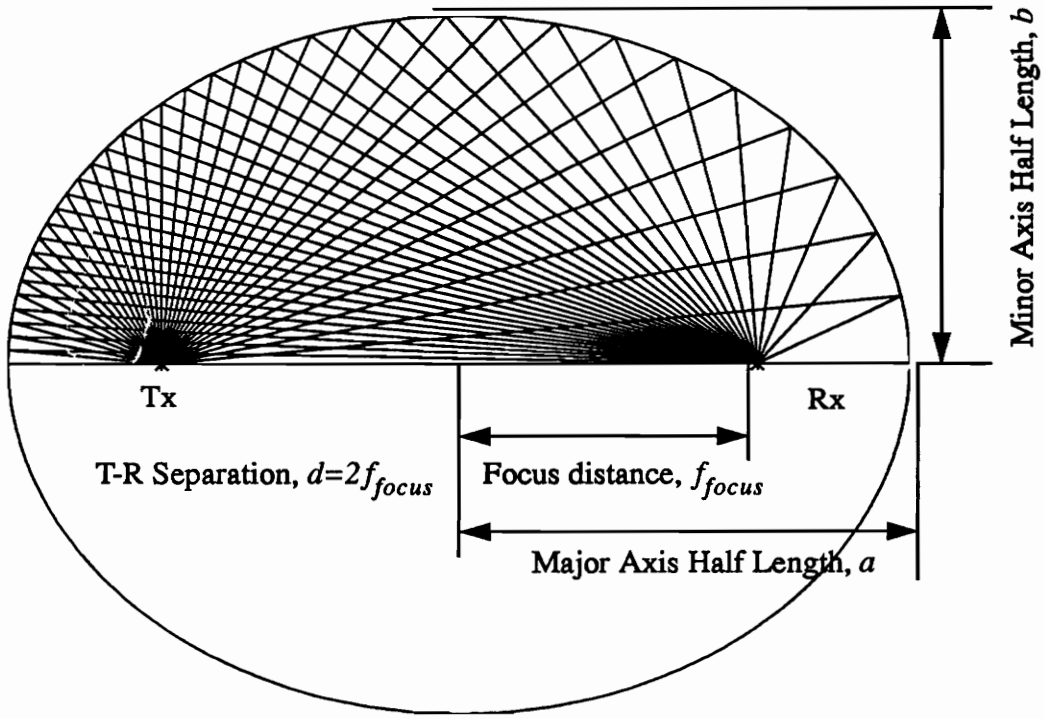

Figure 8. The locus of all points where a scatterer might lie which results in a single bounce multipath component with delay τ_i is an ellipse with $a = c\tau_i/2$, $f_{focus} = d/2$, and $b = \sqrt{f_{focus}^2 - a^2}$

Combining Eqn. 92 and Eqn. 93 gives

$$(\cos\theta_d + \cos\theta_a)(\sin\theta_a + \sin\theta_d) + (\cos\theta_d - \cos\theta_a)(\sin\theta_a - \sin\theta_d) = \frac{2f_{focus}}{a}(\sin\theta_a + \sin\theta_d), \quad (94)$$

which may be rewritten as

$$\sin(\theta_a + \theta_d) = \frac{f_{focus}}{a}(\sin\theta_a + \sin\theta_d). \quad (95)$$

After considerable manipulation this may be solved for θ_a:

$$\theta_a = 2\tan^{-1}\left(\left(\frac{a - f_{focus}}{a + f_{focus}}\right)\cot\left(\frac{\theta_d}{2}\right)\right). \tag{96}$$

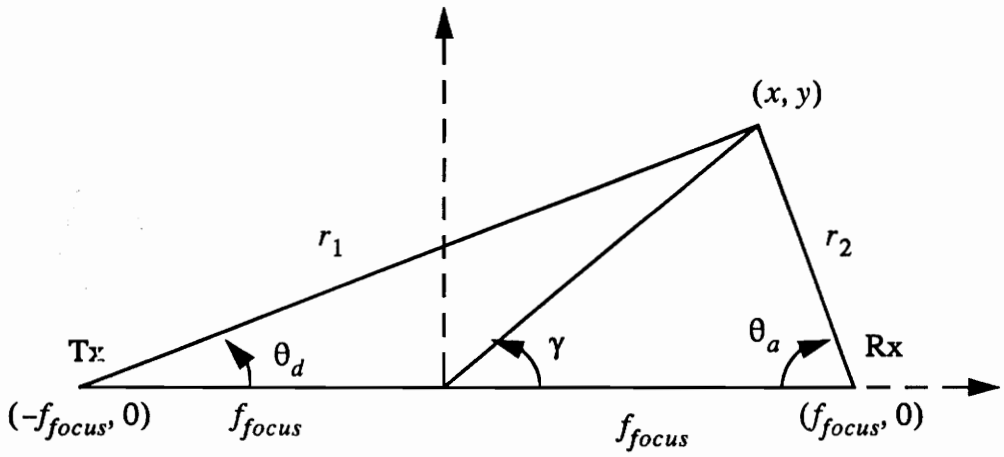

Figure 9. Geometry for Determining θ_a as a Function of θ_d

In deriving a statistical model for angle of arrival in single-bounce multipath channels [Joe95], we make the following assumption. *Let us assume that a single-bounce ray leaving the transmitter at a particular angle θ_d has the same probability of reaching the receiver as a ray leaving the transmitter from any other angle.* Thus, for a given single bounce ray arriving at the receiver, the probability density function describing the angle-of -departure from the transmitter is simply

$$p_{\theta_d}(\theta_d) = \frac{1}{2\pi} \qquad 0 \le \theta_d < 2\pi\,. \tag{97}$$

The probability density function for the angle of arrival is then given by

$$p_{\theta_a}(\theta_a) = \left.\frac{p_{\theta_d}(\theta_d)}{\left|\frac{dg(\theta_d)}{d\theta_d}\right|}\right|_{\theta_d = g^{-1}(\theta_a)}, \tag{98}$$

where

$$\theta_a = g(\theta_d) = 2\tan^{-1}\left(\left(\frac{a - f_{focus}}{a + f_{focus}}\right)\cot\left(\frac{\theta_d}{2}\right)\right), \tag{99}$$

with

$$\theta_d = g^{-1}(\theta_a) = 2\tan^{-1}\left(\left(\frac{a - f_{focus}}{a + f_{focus}}\right)\cot\left(\frac{\theta_a}{2}\right)\right), \tag{100}$$

we find

$$\frac{dg(\theta_d)}{d\theta_d} = -\frac{\left(\frac{a - f_{focus}}{a + f_{focus}}\right)\csc^2\left(\frac{\theta_d}{2}\right)}{1 + \left(\left(\frac{a - f_{focus}}{a + f_{focus}}\right)\cot\left(\frac{\theta_d}{2}\right)\right)^2} \tag{101}$$

Then

$$\left.\frac{dg(\theta_d)}{d\theta_d}\right|_{\theta_d = g^{-1}(\theta_a)} = \left(\frac{a - f_{focus}}{a + f_{focus}}\right)\frac{1 + \left(\frac{a + f_{focus}}{a - f_{focus}}\right)\tan^2\left(\frac{\theta_a}{2}\right)}{1 + \tan^2\left(\frac{\theta_a}{2}\right)}. \tag{102}$$

Recognizing that Eqn. 102 is always positive for reasonable values of a and f_{focus}, and substituting Eqn. 102 and Eqn. 97 into Eqn. 98 gives

$$p_{\theta_a}(\theta_a) = \frac{\alpha}{2\pi}\left(\frac{1 + \tan^2\left(\frac{\theta_a}{2}\right)}{1 + \alpha^2\tan^2\left(\frac{\theta_a}{2}\right)}\right) \qquad 0 \le \theta_a < 2\pi, \tag{103}$$

where

$$\alpha = \frac{a + f_{focus}}{a - f_{focus}}, \tag{104}$$

α is a measure of the eccentricity of the ellipse. For $\alpha = 1$, the focus of the ellipse is at the origin and the ellipse is a circle. For $\alpha = \infty$, the ellipse is a flat line along the x-axis.

The path length associated with the *i*th single bounce multipath component is $c\tau_i = d_i = 2a_i$. The excess delay associated with the *i*th multipath component, $\Delta\tau_i$, is the delay associated with the *i*th path in excess of the delay associated with the direct path. In terms of a and f_{focus}, this is

$$\Delta\tau_i = \frac{2(a_i - f_{focus})}{c}, \tag{105}$$

or

$$a_i = \frac{c\Delta\tau_i}{2} + f_{focus}. \tag{106}$$

Thus, f_{focus} is equal to half of the T-R separation and a_i is determined for each excess delay $\Delta\tau_i$. These quantities are used in Eqn. 104 to determine α which is used to determine the probability density function for the angle of arrival in Eqn. 103. A plot of the pdf of the angle-of-arrival is shown in Figure 10 for many excess delay times.

When the excess delay of a component is very large, $a_i \gg f_{focus}$, so that α is approximately unity. In this situation, the pdf of Eqn. 103 is approximately equal to Eqn. 97. In other words, for multipath components with large excess, delays, the angle-of-arrival is

approximately uniformly distributed between 0 and 2π. When the excess delay is very small, we have $a_i \approx f_{focus}$ so that α becomes very large. In this case the ellipse becomes a straight line. Thus Eqn. 103 presents a simple means of quantifying the behavior of the angle of arrival of multipath components in line-of-sight environments when no other information is available. This model may be used to supplement the work of Seidel and Rappaport in which the multipath channel is statistically characterized for omnidirectional antennas.

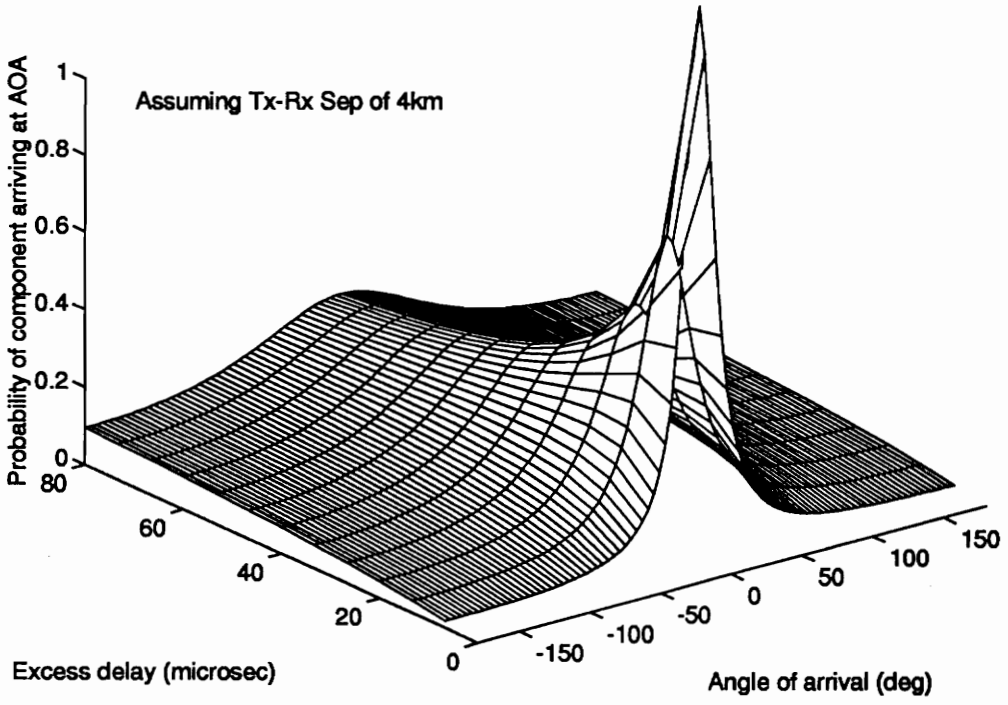

Figure 10. The probability density function for the angle of arrival of single bounce multi-path components as a function of excess delay for a T-R separation of 4 km

We recognize that the fundamental assumption to obtain Eqn. 97 ia simplistic. It may be more appropriate to consider scatterers which are uniformly distributed in space. Knowledge of the fact that the transmitting antenna is omnidirectional coupled with the

assumption that scatterers are uniformly distributed throughout space and that, for a specified excess delay, the scatterers associated with a particular multipath component must also lie on an ellipse, should be sufficient to develop another statistical model which may be more appropriate than the one presented here.

The channel model used in the simulation has one ellipse i.e., one delayed component. The delay profile is shown in Figure 11. The angles-of-departure of the multipaths is found by generating a uniform random variable between 0 and 2π. Then the angles-of-arrival of the multipaths are determined by using Eqn. 99. In the simulation, one multipath which power is 6 dB below the direct path is considered and the multipath component arrives after a delay of 30 μsecs.

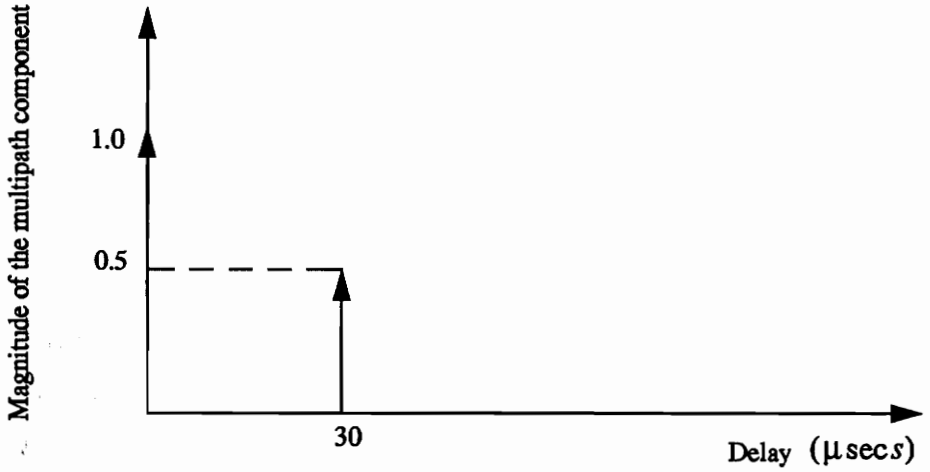

Figure 11. Delay Profile of the Channel

4.3 Performance Criteria

Mean-Squared Error (MSE) in the time domain is the most common performance measure used. This is a measure of the energy of the difference between the original signal vector and the reconstructed signal vector. Weightings can be a common occurrence in an attempt to better match perceptual performance to the distortion measure.

$$d(x,\hat{x}) = (x-\hat{x})^{t}\hat{W}(x-\hat{x}) = \frac{1}{k}\sum_{i=o}^{k-1} w_i (x_i-\hat{x}_i)^2. \quad (107)$$

To evaluate the performance of the algorithms for AMPS, the performance criterion used is the mean-squared error in the frequency domain of the demodulated signal with the array and without the array. MSE in the frequency domain is more appropriate for relating voice clarity than the time domain MSE. MSE in the frequency domain is defined as

$$d(f,\hat{f}) = \frac{1}{k}\sum_{i=o}^{k-1} w_i\left(f_i-\hat{f}_i\right)^2, \quad (108)$$

where f is the vector which has the frequency components, i.e., the normalized FFT points, of the original signal and the $\hat{f}$ is the vector which contains the frequency components of the recovered signal. w_i is the weighting function which depends on the window used. If all w_is are one, then the MSE in the time domain is same as the MSE in the frequency domain. The window is chosen such that all the frequency components from 300 Hz to 3.5 kHz are scaled by one, while the other components are notched out. For the IS-54 testing, bit error rate (BER) is used as the performance measure.

4.4 Performance of the Adaptive Array on AMPS and IS-54 Signals

Performance evaluation of the algorithms is carried out by first simulating AMPS and IS-54 signals. All the performance evaluations use the fixed channel model that is described in Section 4.2. Four sets of simulations are performed for each of the signal. The four sets are described below.

a) MSE vs. SNR (Signal to Noise Ratio)

This simulation set demonstrates the performance of the algorithms in a channel

which has AWGN (Additive White Gaussian Noise) and multipath components. The variable parameter is the signal-to-noise ratio (SNR). SNR is varied from 4 to 28 dB and the performance measure (MSE for AMPS and BER for IS-54) is plotted against SNR.

b) MSE vs. SIR (Signal to Interference Ratio)

This simulation set demonstrates the performance of the algorithms for a varying signal-to-interference ratio. The signal-to-noise ratio is maintained constant at 20 dB. SIR is varied from -20 dB to 20 dB and the MSE is plotted against SIR.

c) MSE vs. Different Number of Users

This simulation set demonstrates the capacity increase provided by adaptive arrays. The signal-to-noise ratio is maintained constant at 20 dB. The number of users is increased from 1 to 4. The signals-not-of-interest are maintained at 6 dB below the signal of interest.

d) MSE vs. Different Number of Antenna Elements

This simulation set demonstrates the performance of the array with different number of elements. There is one interferer, whose signal strength is 6 dB below the SOI. The signal-to-noise ratio is maintained constant at 20 dB. The number of elements is varied as 1, 2, 3, 4 and 8.

4.5 Implementation of the Algorithms

4.5.1 CMA Implementation

The Constant Modulus Algorithm (CMA) is implemented as explained in Section 3.3.2, but it uses least-squares algorithm (LS) instead of least-mean squares algorithm (LMS). The Least-Squares Constant Modulus Algorithm (LSCMA) is a block based algorithm i.e., it operates on a block of data containing 64 samples. Initialization of CMA is

vital to the operation of a CMA array. A CMA array should not be initialized with all-zero weights, because if initialized in this manner the output will be zero for all the time. The CMA array has one weight per antenna element. The received data is partitioned into contiguous non-overlapping blocks of length 64 samples, and LSCMA recursion is applied to eack block using weights provided from the previous block. The weights are updated over each block until the algorithm converges (for this research 4 updates are used). The algorithm converges within 2 milliseconds (100 samples of a signal which is sampled at 48 kHz). The convergence time is small enough to accommodate fast changes in the channel.

4.5.2 SCORE-Tapped Delay Line (SCORE-TDL) Implementation

The SCORE-TDL algorithm is implemented using recursive least-squares algorithm. The algorithm operates on samples of data instead of blocks of data. SCORE-TDL has 16 weights per antenna element. The number of weights per element is dependent on the cyclic-autocorrelation function of the SOI. The cyclic-autocorelation function is significantly high for a period equal to $2 \times T_o$, where T_o is equal to $1/$ frequency of the SAT. Since T_o is equal to 8 samples, the length of the FIR filter is 16. This structure incorporates only one periodicity, i.e., it exploits the spectral redundancy of the frequency components spaced by the SAT tone. Initialization of SCORE-TDL array is as vital as to the operation of a CMA array. The array can be initialized with all-zero weights.

4.5.3 TDAA Implementation

The time-dependent adaptive array is implemented using a recursive-least squares algorithm. The structure uses a tapped-delay line for each of the antenna elements. The length of the tapped-delay line is 16. The number of weights per element is dependent on the cyclic-autocorrelation function of the SOI. The cyclic-autocorelation function is significantly high for a period equal to $2 \times T_o$, where T_o is equal to $1/$ frequency of the SAT. Since T_o is equal to 8 samples, the length of the FIR filter is 16. This structure exploits multiple statistical periodicities. In the simulation, two periodicities are exploited,

i.e., it exploits the spectral redundancy of the frequency components spaced by the SAT tone and the frequency components spaced by twice the SAT tone. This time-dependent structure performs better than all the other structures.

4.6 Problems in Simulating Realistic Conditions

Realistic conditions are important in evaluating the performance evaluation of blind adaptive algorithms. Lack of proper channel models to calculate the angle-of-arrival of the multipath components at the array input poses a problem in creating realistic conditions. The simple model discussed in Section 4.2 is a first order approximation. This model does not take into account the effects of shadowing. Lack of statistics of the location of the users in a typical cellular environment is another drawback. In the simulations, the users in the cell are assumed to be uniformly distributed. The measure to gauge the performance of the array is the improvement in BER or MSE. There need not be a one-to-one relationship between BER improvement and cell capacity gain.

Setting up the simulation for IS-54 standard is more complicated than AMPS. There are three users in a each TDM frame. The location of the users in a cell is vital to carry out the test. The antenna beam has to track three different users in a serial fashion continuously. Beamforming for IS-54 signals is more difficult than with AMPS.

4.7 Discussion of the Results

Land mobile communication experiences classic forms of interference such as background noise, multipath propagation, and in-band interference from the surrounding systems. The degree of interference depends on the surrounding topography, number of users, cell structure, distribution of the users, allowable transmission powers, and degree of spectrum regulation. In this section, the performance of the blind adaptive algorithms under various channel conditions and the performance improvement brought about by the

increase of number of elements are examined. The main focus will be to examine the ability of the adaptive array to reject interference from co-channels.

4.7.1 Testing the CMA on AMPS Signal

The AMPS signal generated has a bandwidth of 30 kHz and the carrier is 0 Hz. All the signals in the simulation are complex baseband signals. The Constant Modulus Algorithm is tested on AMPS signals under various conditions and the results are discussed in this section.

4.7.1.1 Interference from Background Noise

Background additive white Gaussian noise is a problem for analog and digital communications. Adaptive arrays can significantly reduce the noise level by forming beam in the direction of the SOI and the noise contribution is only from the direction of the SOI. The simulation setup uses a linear array of four elements and each element is spaced by a distance of $\lambda/2$ from the adjacent element. Each element has a weight attached to it. The arrival angle of the SOI is 60 degrees. Figure 12 shows the radiation pattern of the array for every block of data. Each block of data consists of 64 samples (1.3ms). The radiation pattern of each block of data is overlaid on one another to show how the array is able to track the SOI. Initially all the weights are one, so the radiation pattern has a main beam at an angle of 90 degrees. As the algorithm converges, the radiation pattern shifts to 60 degrees in the direction of the angle of arrival of the SOI.

Figure 13 shows the convergence characteristics for the four array weights when the SNR is 5 dB. The weights converge within 15 blocks of data for this case and as the SNR increases, the convergence rate also increases. This is due to the fact that consistent statistical estimates require less data when the CNR is high. Figure 14 shows the spectral plots of the original voice signal, corrupted voice signal, and the reconstructed voice signal for

the case when CNR = 4 dB. It can be seen how close the reconstructed signal resembles the original signal. Figure 15 shows the performance improvement curve offered by the CMA array in the AWGN channel. The figure shows MSE (in the frequency domain of the demodulated voice signal) plotted against carrier to noise ratio for a system using a single antenna and for a system using a CMA array. CNR is varied from 4 to 28 dB in this test case. The CMA array provides nearly an improvement of one order of magnitude. The improvement in MSE is due to the fact that noise at each element is uncorrelated, while the SOI is correlated at each element. The array forms a beam in the direction of the SOI and the noise which comes from all the directions other than the direction of SOI is rejected. The improvement in MSE has approximately a one-to-one relationship with the improvement of SNR. As the CNR increases form 4 dB to 28 dB, the CMA array settles to a noise floor for high CNRs.

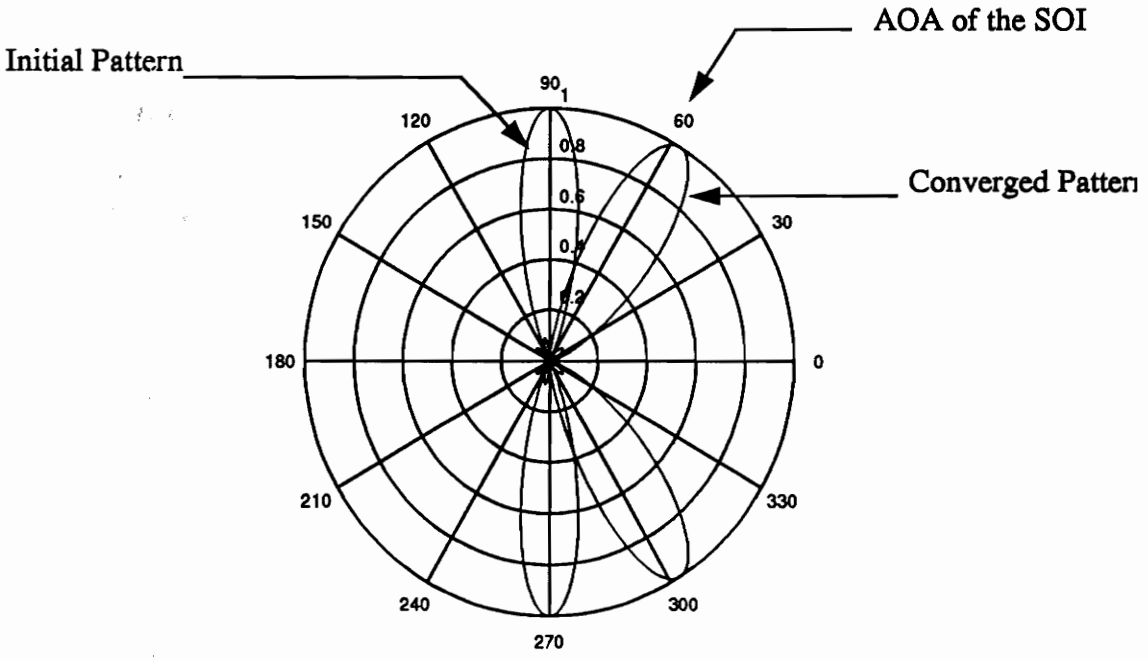

Figure 12. Radiation Pattern of the Array as the Algorithm Converges

Curves Show the Convergence Characteristics of each Weight of the Array

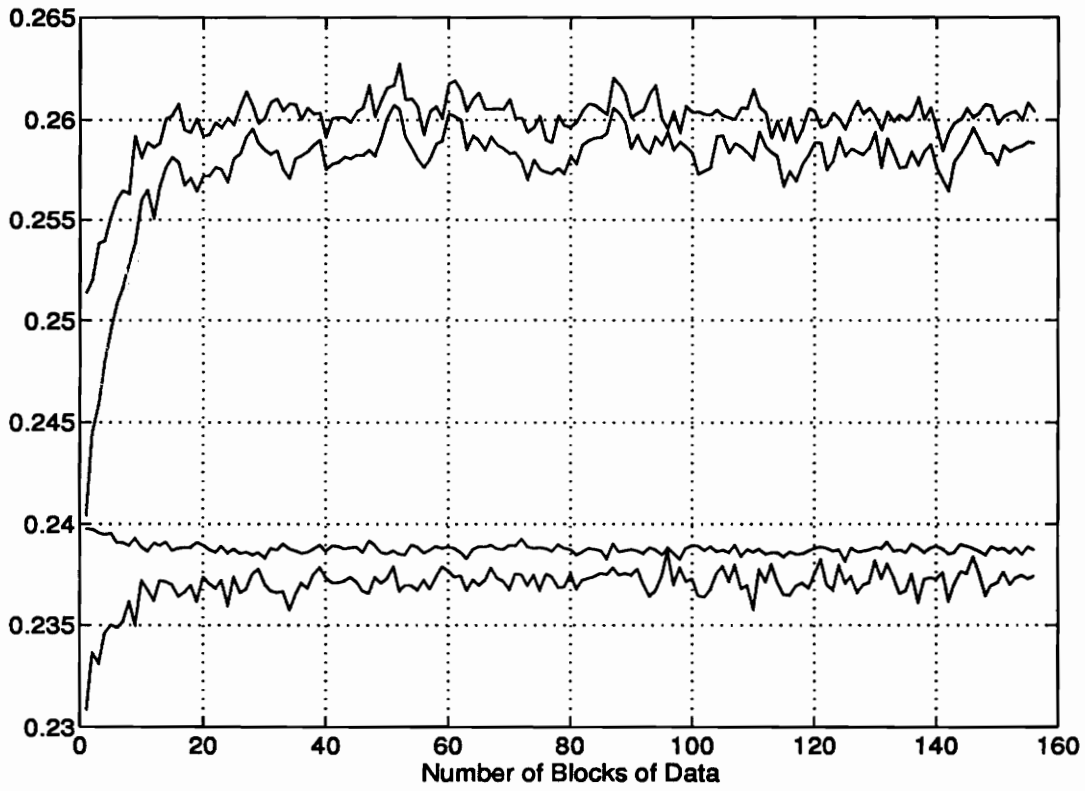

Figure 13. Convergence Curves for the Weights of the Array

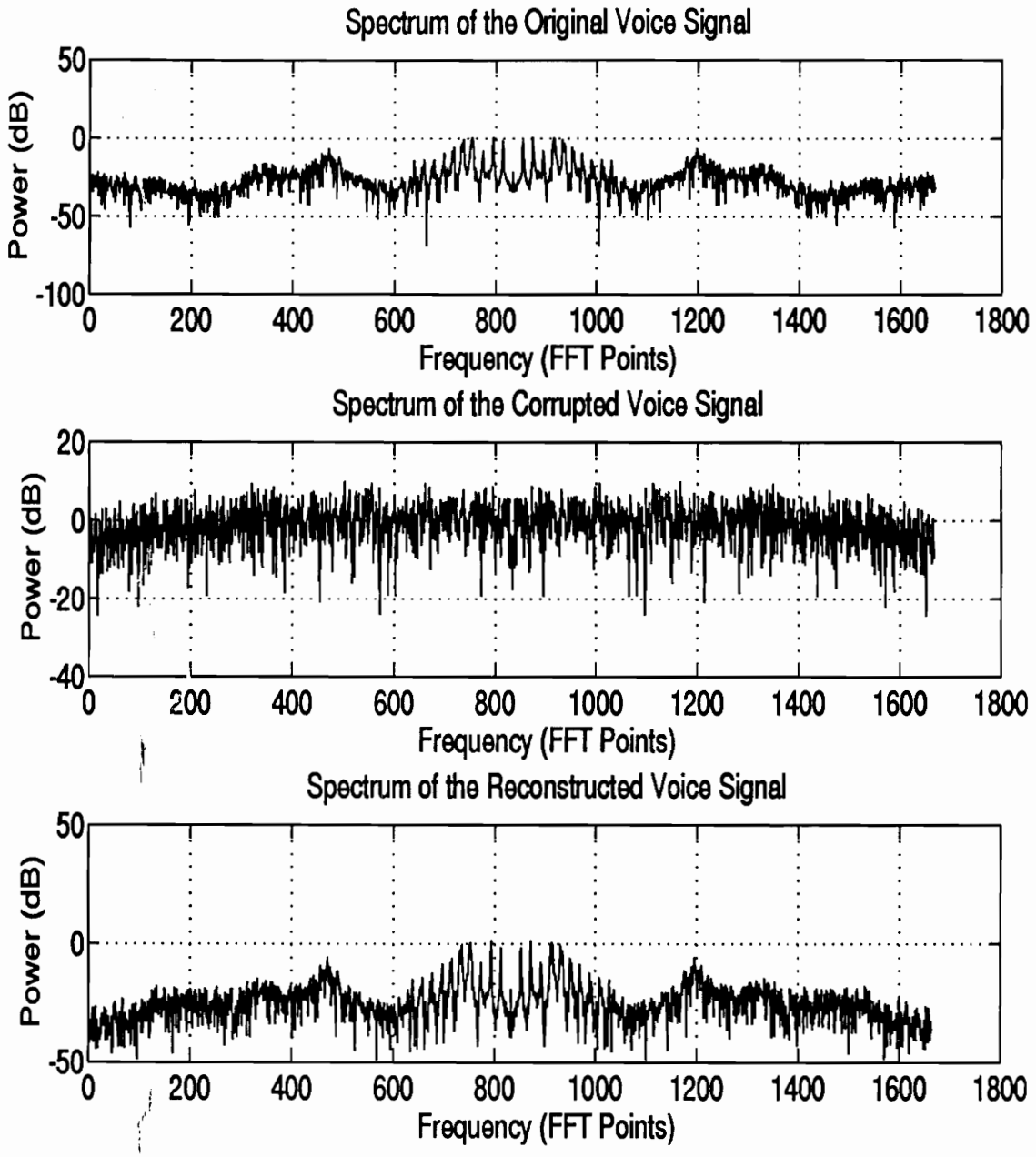

Figure 14. Frequency Domain Plots of the Original, Corrupted, and Reconstructed Voice Signals for CNR =4 dB.

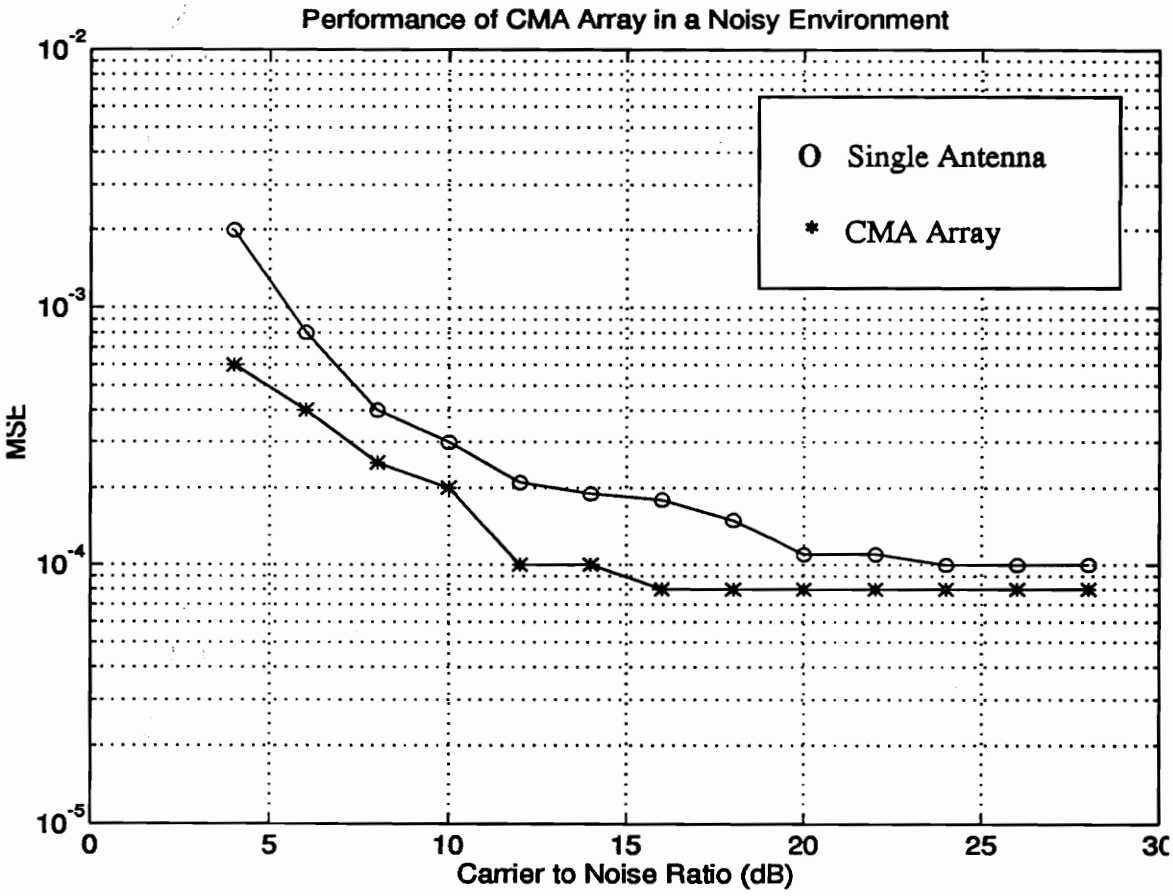

Figure 15. Comparison of MSE Curves of CMA Array with a Single Antenna

4.7.1.2 Interference from Co-Channel Users

Co-channel interference in the AMPS system is due to the interference from adjacent clusters. Any cluster is surrounded by six clusters and so there are six co-channel interferers in AMPS. AMPS adopted seven cell structure because, a mobile at the edge of a cell should have a Carrier-to-Interference Ratio (CIR) of 18 dB or above. A typical cell structure is shown in Figure 16.

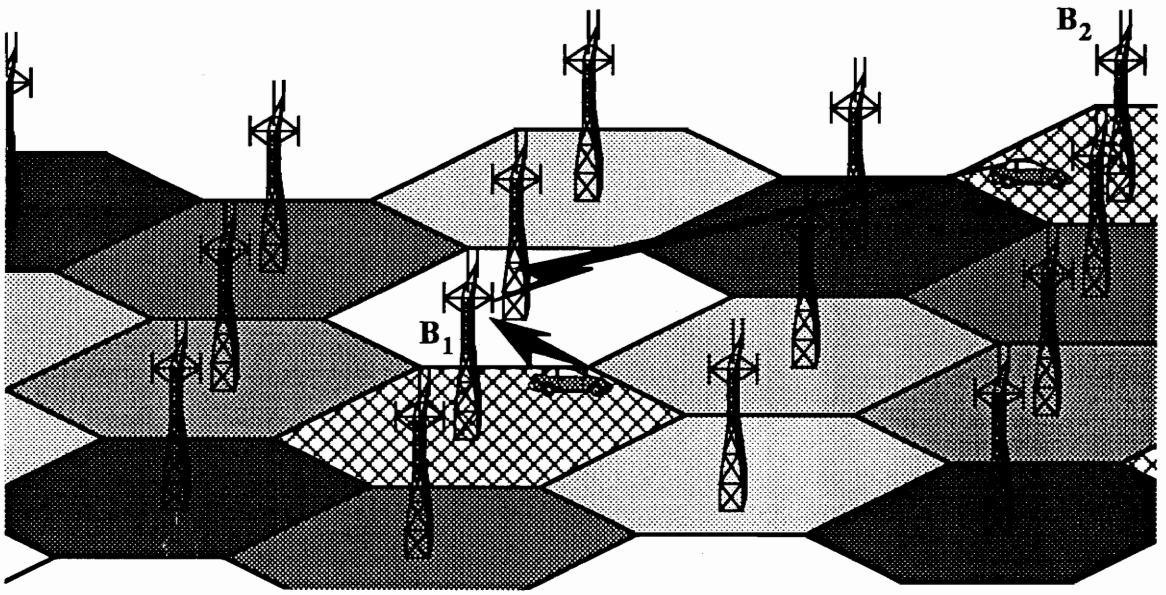

Figure 16. A cellular coverage region is split into many different cells where each cell has a base station. The shading in each cell represents the set of channels used in that cell. Cells with the same shading reuse the same channels. The figure shows a mobile subjected to co-channel interference.

The use of adaptive arrays at the base station enables the rejection of interference from a co-channel user. Clusters can be restructured to accommodate lesser number of cells and still can maintain the minimum required CNR. So the employment of adaptive arrays can increase the capacity of the cell tremendously.

Consider that the base station is located at the origin and signal from one user is received at 120^o and that of the interferer from 0^o

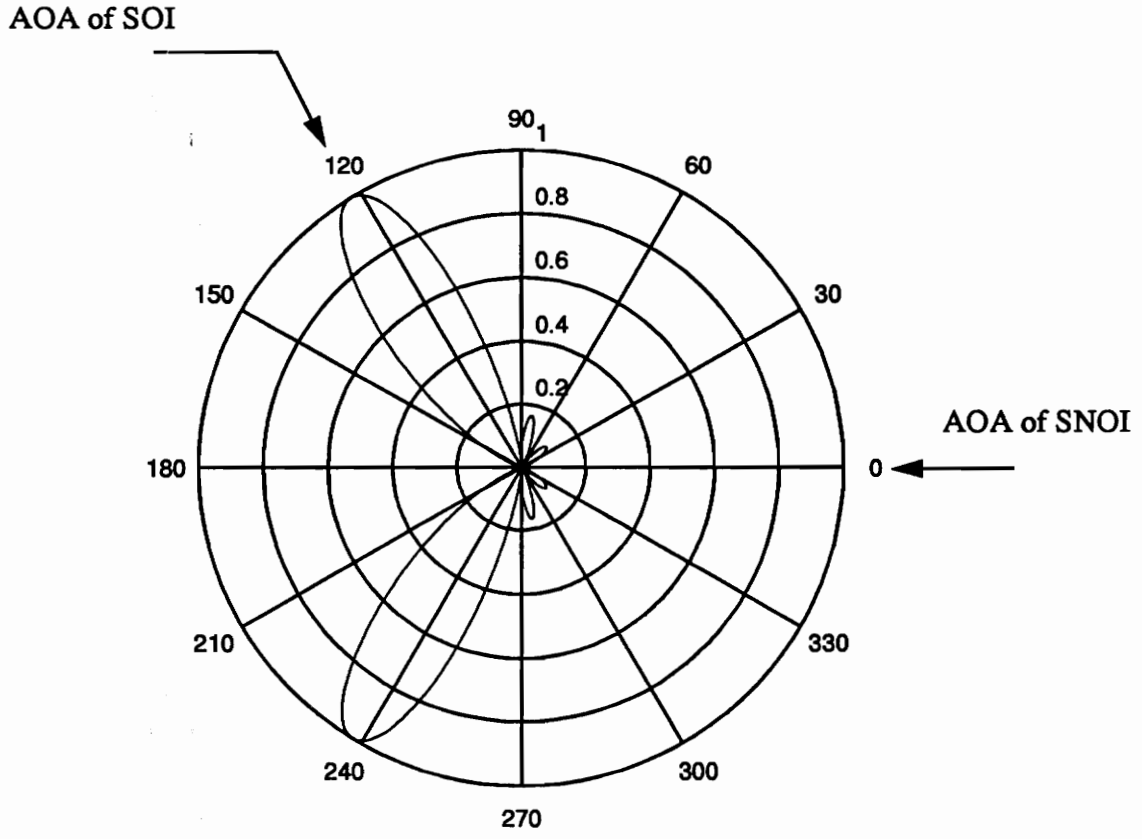

Figure 17. Radiation Pattern in the Presence of an Interferer

Figure 17 shows the radiation pattern of the linear array for the above mentioned condition. The array forms its main beam in the direction of the SOI and forms a null in the direction of the SNOI. The beamforming effectively mitigates the interference. The beam can track the SOI as it moves along and place a null in the direction of the interferer. This setup considers the condition where there is only one interferer. The SIR is varied

from 0 dB to 18 dB and the system performance is analyzed. Figure 18 shows the MSE (frequency domain) as a function of SIR (dB). The performance of the CMA array is compared with that of a single antenna. As the SIR increases from zero the improvement is dramatic. At an SIR of 2 dB, the array gives a two order improvement in the MSE to the link budget is improved by approximately 12 to 16 dB.

As the SIR increases above 6 dB, a consistent MSE improvement of one order of magnitude is obtained. CMA array does not perform well for negative SIRs, because in this region capture occurs. However, multitarget-CMA [Age89] can be used to track the SOI and the SNOI jointly and provide separate outputs at different ports. Using this structure, signals having an amplitude lesser than that of the interferer can also be tracked, i.e., the array can operate in the negative SIR region. Switching of signals from one port to the other can occur, i.e., interchange of SOI and SNOI can occur, but the SAT feature can be exploited to help determine which signal is at which port.

If there are multiple co-channel interferers, it means that more than one neighboring cluster is contributing to the interference. Figure 19 shows the setup for the simulation when there are three co-channel interferers. The angle-of-arrival of the SOI is 90 degrees. The three signals not of interest come from 0 degrees, 170 degrees, and 235 degrees, respectively. The signal strength of each SNOI is 6 dB below the signal strength of the SOI. In this test, a 4-element array is used and background noise is present.

The SNR is 20 dB and the interferers are introduced into the environment one by one. The Figure 20 show the MSE curves for different levels of interference. MSE is plotted against the number of users, and a comparison is made between the performance of the CMA array and that of a single antenna.

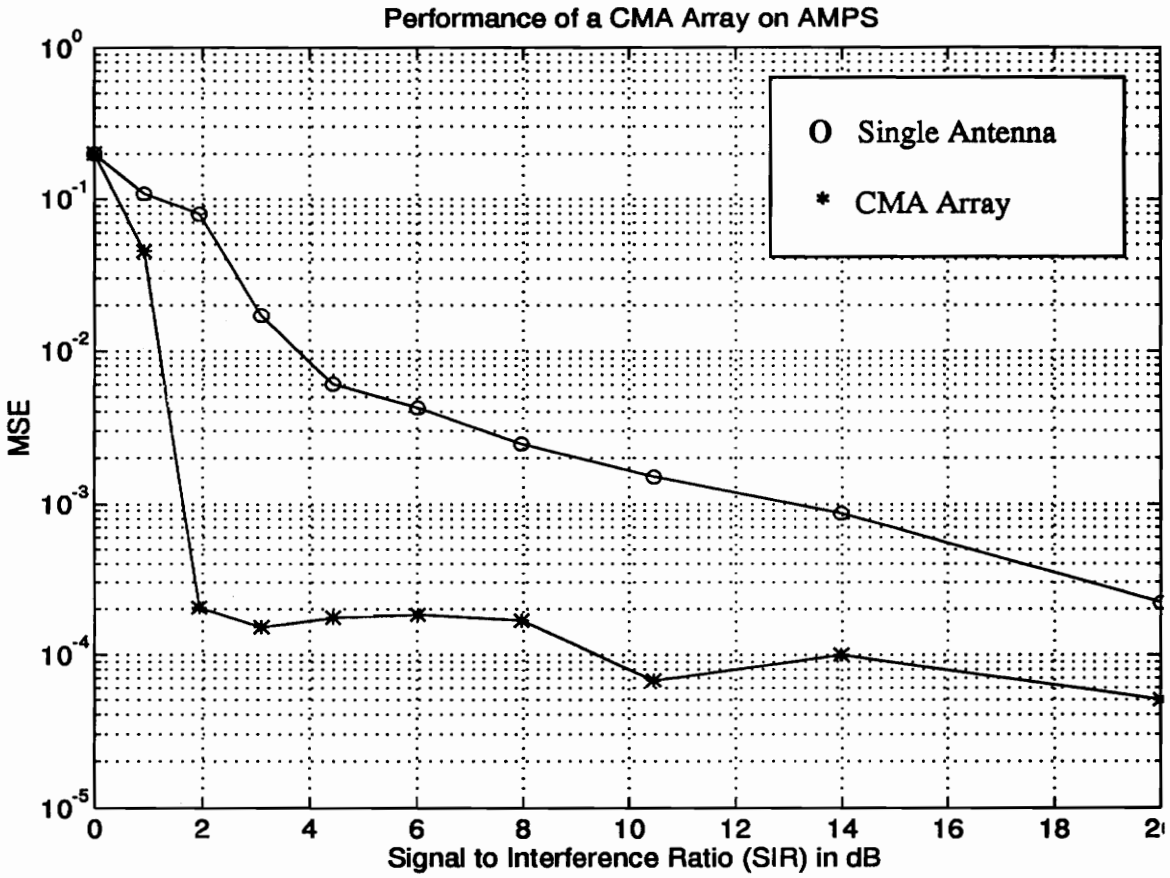

Figure 18. Performance Curves for CMA Array in the Presence of Interference (The linear array has 4 elements and the AOA of the SOI is 120 degrees and the AOA of the SNOI is 0 degrees)

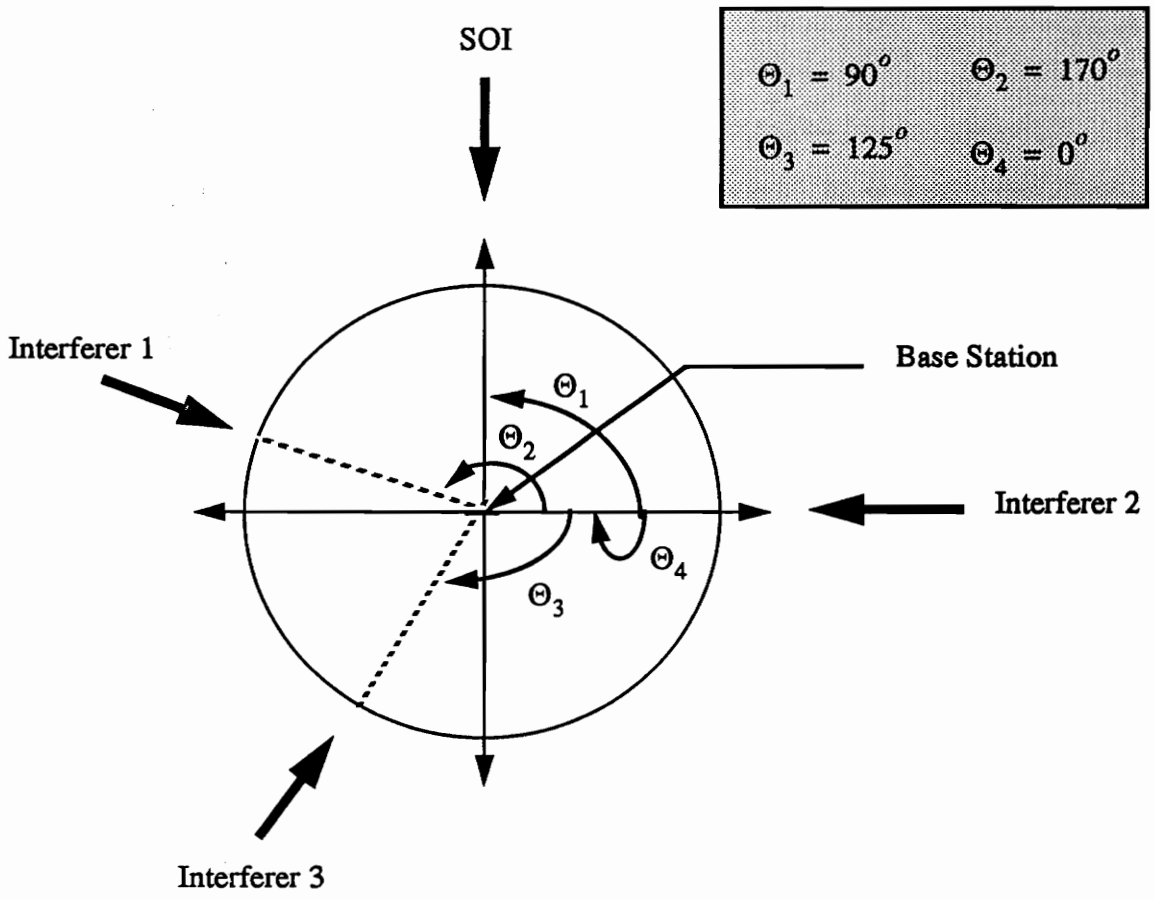

Figure 19. Figure Depicting Angle-Of-Arrivals of Different Users

The MSE curve for a single antenna shows a steady degradation in the performance as the number of co-channel interferers increase. But the CMA array is able to maintain an MSE of 10^{-4} irrespective of the number of users. The only constraint in this multi-co-channel interference environment is that the users should be located such that the array is able to resolve them in space. The resolution of the array is dependent on the number of elements, if the number of elements is large, the array can then form fine beams to track users who are close together.

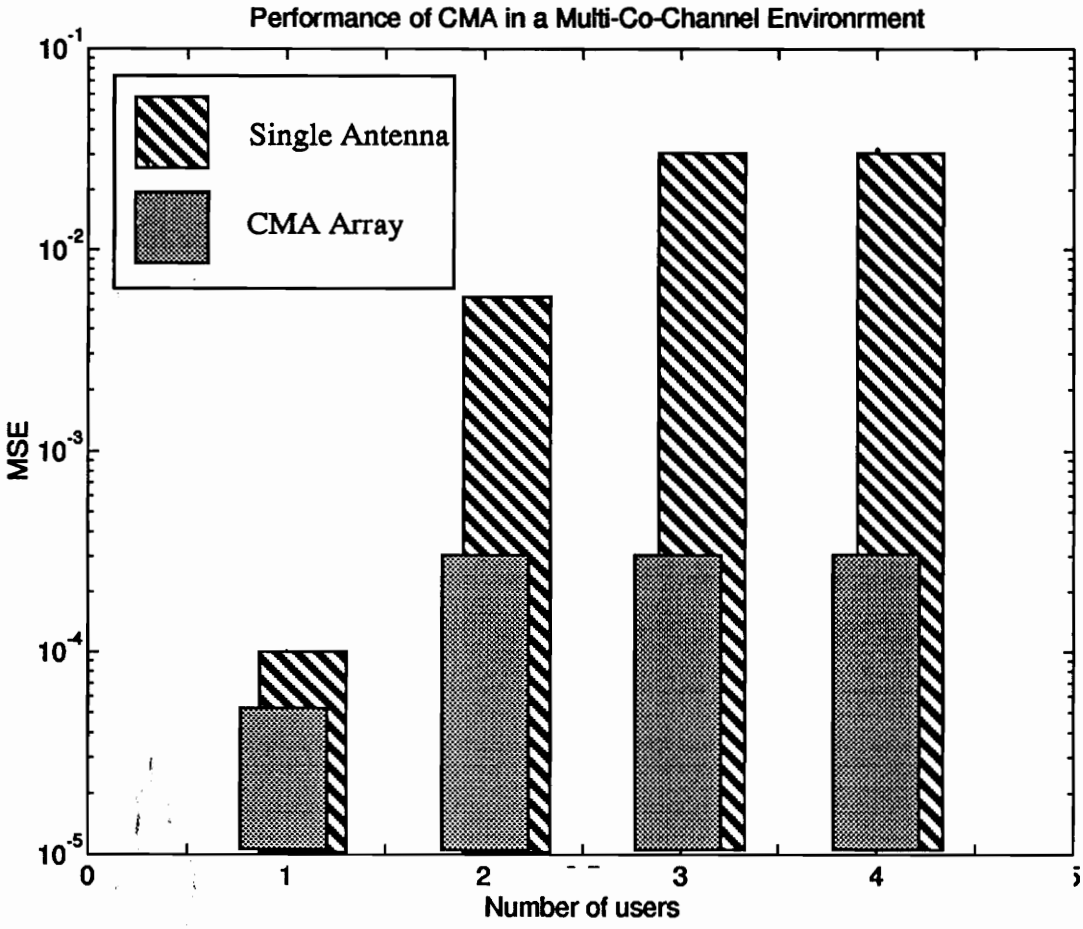

Figure 20. Bar Chart of MSE of a Four-Element CMA Array in a Multi-Co-Channel Environment

4.7.1.3 Effects of Increasing the Number of Elements on Interference from Co-channel Users

This section discusses the effects of increasing the number of elements in the array and analyzes the MSE improvement. The simulation setup is as follows. The base station receives signals from an in-cell user (SOI) and an out-of-cell interferer (SNOI). The AOA for the SOI is 90^o and the AOA for the interferer is 0^o. The power of the interferer is 6 dB below that of the SOI and the CNR with respect to the SOI is 20 dB. In the simulation the number of elements is increased from 1 to 8. Figure 21 shows the performance improvement obtained by the use of a multiple-element CMA array in an interference environment. The MSE decreases steadily as the number of elements is increased from 1 to 4. Since there is only one interferer to be suppressed, an array with two elements is sufficient to give an MSE of 10^{-4}. As the number of elements is increased to 3 the MSE decreases further, this is because the array has an excess degree of freedom to suppress (or take advantage of) the multipath (In this simulation the channel has only one multipath component). An array with 4 or 8 elements does not provide significant improvement over a 3-element array. A CIR improvement factor of 12 dB is provided by this array and so the 7-cell reuse pattern can reduced to a 3 or 4-cell pattern. A 7-cell pattern maintains a CIR of 18.1 dB for a channel with path loss exponent $n = 3.6$, and log normal standard deviation of 6.5 dB. A 3-cell reuse pattern can maintain a CIR of only 11.2 dB under the above mentioned channel conditions. Since the adaptive array can provide an improvement of 12 dB, a 3-cell reuse pattern can be used.

4.7.2 Testing SCORE-TDL on AMPS Signal

This section discusses the result of testing the SCORE-TDL array on AMPS signals under various conditions. It also explains the cyclostationary properties of AMPS signals.

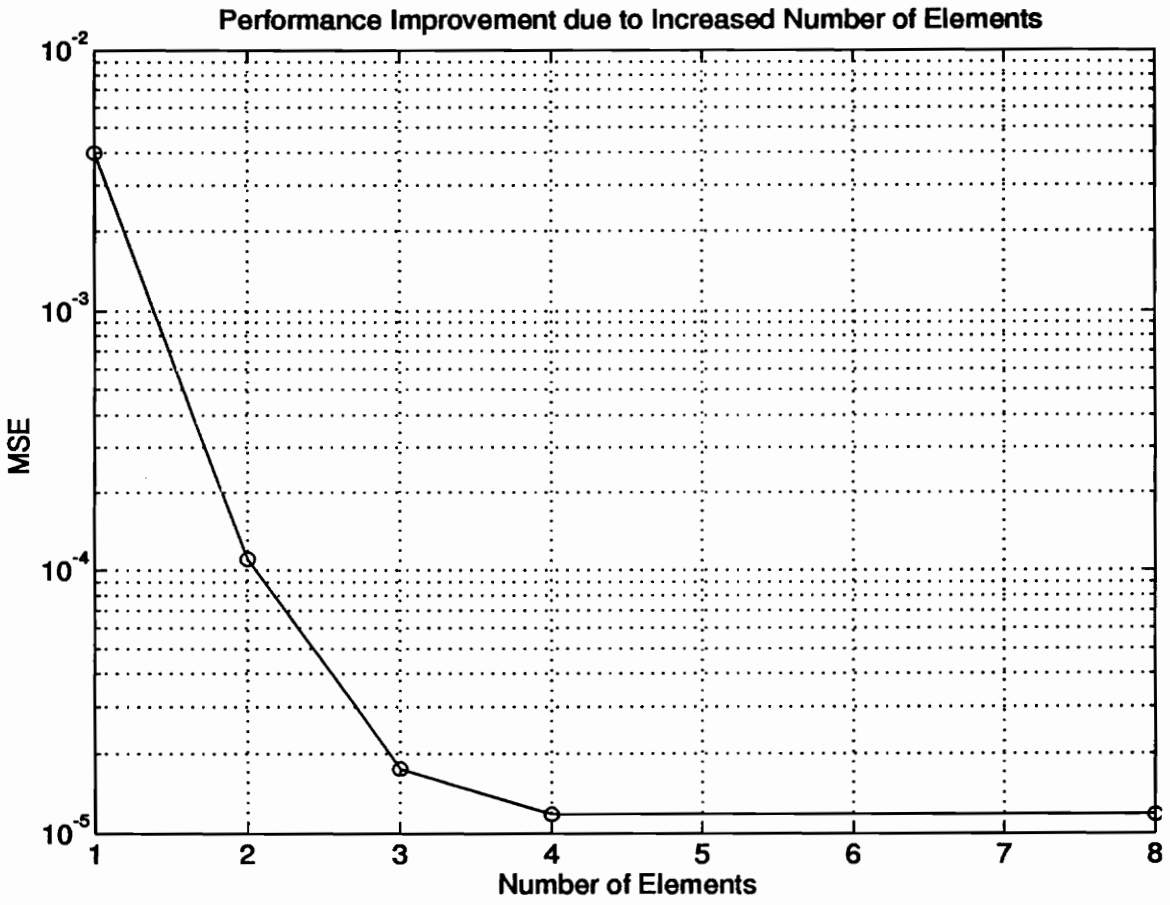

Figure 21. Performance Improvement Curves for Increased Number of Elements

4.7.2.1 Cyclostationary Characteristics of AMPS

AMPS signals exhibit cyclostationarity due to the presence of the Supervisory Audio Tone (SAT) [Ron94]. Supervision is defined as the process of detecting changes in the switch-hook state caused by the customer in classical land-line telephone system.
A cellular telephone has to ensure that adequate RF strength is received and maintained during a call. Signaling Tone (ST) and the SAT are used to avoid a false supervisory indication caused by the co-channel interference. Three frequencies are allocated for SAT signalling: 5970 Hz, 6000 Hz, 6030 Hz. The cell site sends out a SAT and receives a SAT, if the SATs are same then the loop is connected. The AMPS system has a frequency reuse factor of 7, i.e., a cluster of seven cells uses seven different frequencies and it is repeated in the next cluster. Each cluster uses one of the three SAT frequencies. Thus, the three-SAT scheme provides supervision and reduces the chance of misinterpreting an interferer as the desired signal. SAT is a simple tone that is added with the voice. The SAT produces a maximum frequency deviation of 2 kHz. Since all three SAT frequencies lie above the voice band, the SAT can be easily be removed after demodulation.

An AMPS signal can be expressed as

$$x(t) = Re\left\{ e^{j\left(\omega_c t + \beta f_m \int v(t)\, d(t) + k\sin(2\pi f_{sat} t) \right)} \right\} \tag{109}$$

or as

$$x(t) = Re\left\{ e^{j\left(\omega_c t + \beta f_m \int v(t)\, d(t) \right)} e^{j\{k\sin(2\pi f_{sat} t)\}} \right\} \tag{110}$$

where ω_c is the carrier frequency

β is the voice modulation index which is 3 for AMPS

f_m is the maximum frequency of the voice signal

k is the modulation index for SAT which is $1/3$

f_{sat} is the frequency of the SAT which is either 5970 Hz, or 6000 Hz, or 6030 Hz.

The following is a proof that AMPS signal exhibit cyclostationary property.

Let the signal be $s(t)$ given by

$$s(t) = e^{j\left(\omega_c t + \beta f_m \int v(t)\, d(t)\right)}, \tag{111}$$

and the term $e^{j\{k\sin(2\pi f_{sat}t)\}}$ can be expanded using Bessel functions

$$e^{j\{k\sin(2\pi f_{sat}t)\}} = \sum_{n=-\infty}^{\infty} J_n(k)\, e^{jn2\pi f_{sat}t} \tag{112}$$

where

$$J_n(k) = \frac{1}{2\pi}\int_{-\pi}^{\pi} e^{j\{k\sin(2\pi f_{sat}t)\}}\, e^{-jn2\pi f_{sat}t}\, d(2\pi f_{sat}t)\,. \tag{113}$$

Note that n is an integer and

$$J_n(k) = \begin{cases} J_{-n}(k), & n \text{ is even} \\ -J_{-n}(k), & n \text{ is odd} \end{cases}. \tag{114}$$

Based on the definition in Eqn. 112, it can be shown that the cyclic autocorrelation for the signal $x(t)$ to be

$$R_{xx}^{\alpha}(t) = \begin{cases} R_{ss}^{\alpha}(t) \sum_{n=-\infty}^{\infty}\sum_{m=\infty}^{\infty} J_n(k)\, J_m(k)\, e^{2\pi f_{sat}(\tau/2)\,(-j(n-m))}, & \text{for } \alpha = (n+m)f_{sat} \\ 0, & \text{for others} \end{cases} \tag{115}$$

The cycle frequency is at multiples of the SAT frequency and the cyclic spectrum is the Fourier transform of the cyclic autocorrelation.

$$S_{xx}^{\alpha}(f) = \int_{-\infty}^{\infty} R_{xx}^{\alpha}(t)\, e^{-j2\pi ft} dt$$

$$= \sum_{n=-\infty}^{\infty} \sum_{m=-\infty}^{\infty} J_n(k) J_m(k) S_{ss}\left(f + \frac{(n-m)}{2} f_{sat}\right) \qquad (116)$$

where $S_{ss}(f)$ is the spectrum of the FM signal which does not include SAT.

Combining Eqns. 114 and 116, it can be shown that when $(n-m)/2$ is not an integer number, the contribution from these terms to $S_{xx}^{\alpha}(f)$ is zero. The cyclic spectrum consists of replicated versions of the original FM voice signal with different weightings given by the Bessel coefficients.

4.7.2.2 Interference from Background Noise

This section discusses the behavior of the SCORE-TDL array in a noisy environment. The SCORE-TDL array exploits the spectral redundancy in the signal as explained in Section 3.4. Since Gaussian noise is a purely stationary process, it exhibits no spectral correlation [Gar87]. Thus, cyclostationary processing is able to exploit the spectral correlation of the *signal of interest* (SOI) in order to extract it from Gaussian noise. Figure 22 shows the performance improvement curves provided by the SCORE-TDL array with two elements over a single element.

The AMPS signal used in this test has a SAT at 6.0 kHz and so there is spectral redundancy at spacings of 6.0 kHz. The SCORE-TDL array exploits only one spectral periodicity. Noise is not spectral correlated and moreover noise in one element of the array is uncorrelated with that of the other elements, so the SCORE-TDL array can perform better than the single element.

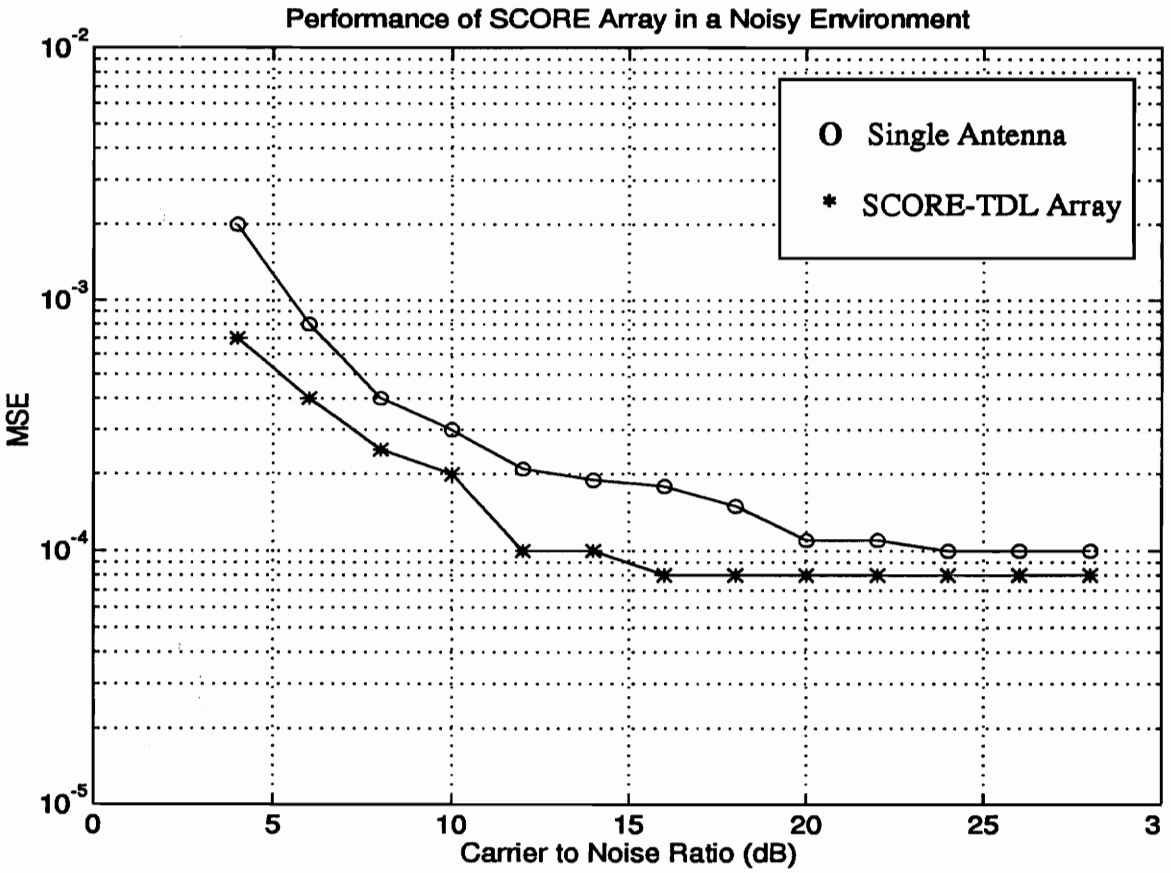

Figure 22. Performance Curve for SCORE-TDL Array in a Noisy Environment

4.7.2.3 Interference from Co-Channel Users

This section discusses the performance of the SCORE-TDL array in an interference environment. The simulation setup is similar to the one used to test CMA array. The implementation of the SCORE-TDL array is different from the conventional SCORE array. The conventional array has a weight in each element of the array. But the structure implemented to reject interference in this simulation has a tapped-delay line attached to each of the element. This new structure, the SCORE-Tapped Delay Line (SCORE-TDL), out-performs the conventional array in the presence of interferers. This structure exploits temporal diversity which is not the case in the conventional SCORE array.

The simulation setup has one interferer and the *signal to interference ratio* (SIR) is varied from -20 dB to 20 dB. The SNR of the SOI is 20 dB. The SOI has a SAT at 6.0 kHz and the SNOI has a SAT at 6.03 kHz. Both the signals exhibit spectral redundancy, but their cyclic periods are different and this feature is used to separate these two signals. Figure 23 shows the MSE performance of the SCORE-TDL array in the above mentioned environment. In the positive SIR region, the spectral properties of the SOI is stronger than that of the SNOI and the SCORE-TDL processor exploits the spectral correlation properties of the SOI to enhance the SOI. Thus, the SCORE-TDL array using a frequency shift of 6 kHz, acts as a beamformer in the positive SIR region. In the negative SIR region, the spectral properties of the SNOI is stronger than that of the SOI and the SCORE-TDL processor exploits the spectral correlation properties of the SNOI to remove the SNOI. Thus, the SCORE-TDL using a frequency shift of 6.03 kHz, array acts as a null-steering array in the negative SIR region.

Using a single antenna, Figure 23 and 24 show a steep decrease in the post and pre-demodulated MSE as the SIR increases. In the region of SIR -6dB to 6dB, the demodulated voice signal in completely inaudible without the adaptive array. As the SIR decreases below -6 dB, the interferer captures the receiver. The MSE (Figure 23) curve for the

SCORE-TDL array shows that the MSE is below 10^{-3} for most of the positive SIR region.

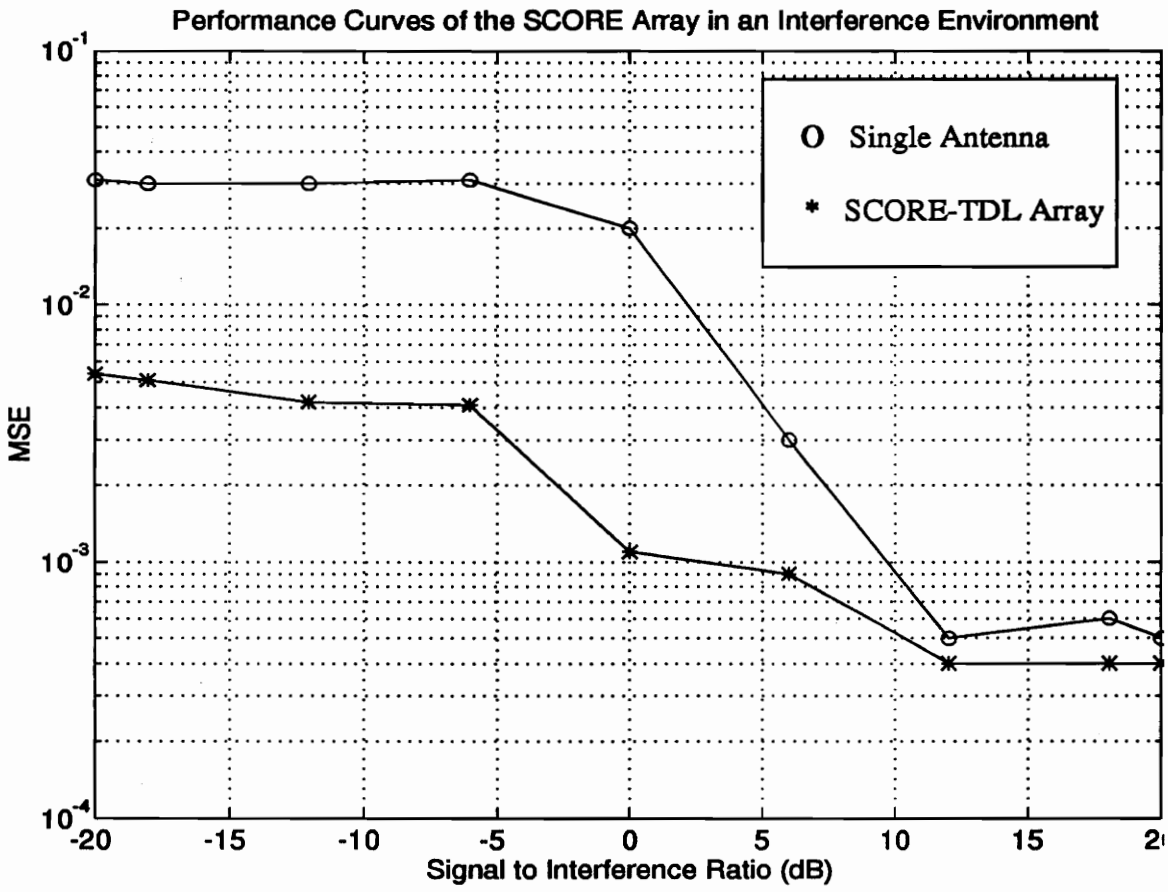

Figure 23. Post-Demodulated MSE Curves of the SCORE-TDL Array in an Interference Environment

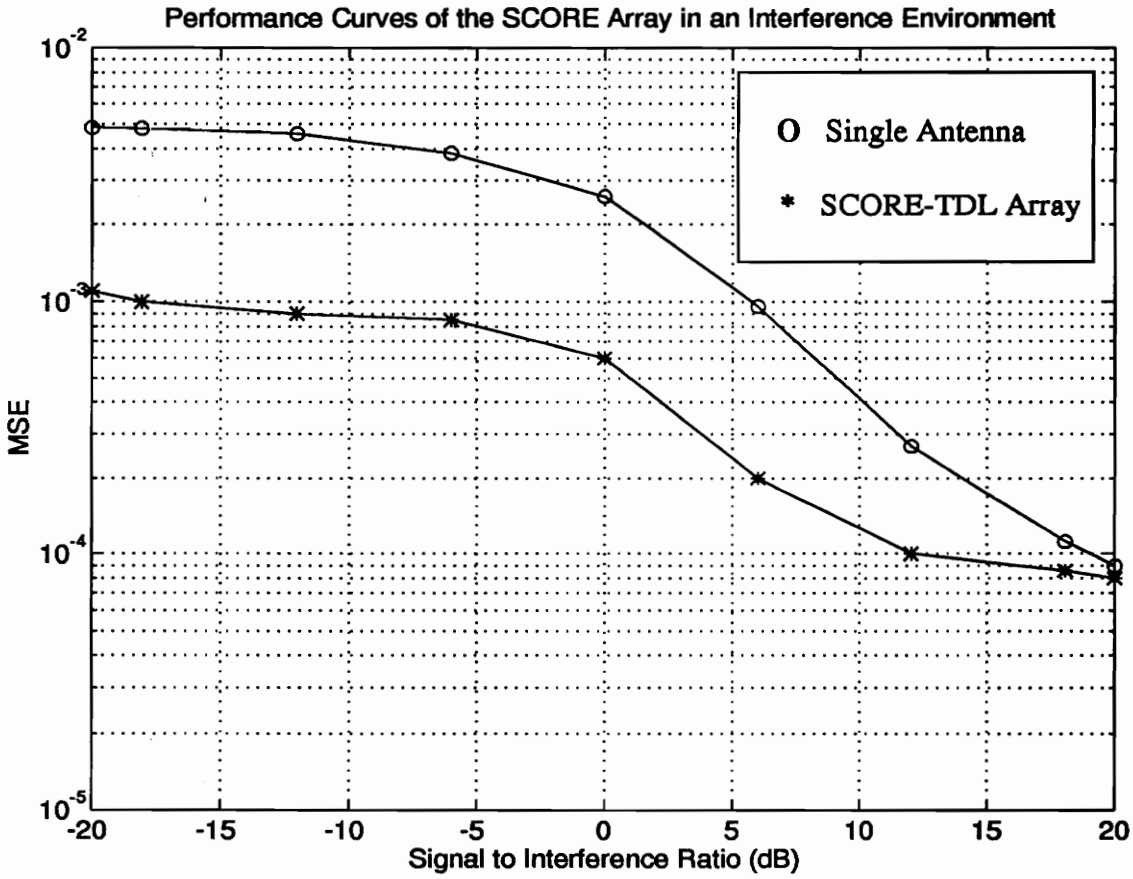

Figure 24. Pre-Demod MSE Curves of the SCORE-TDL Array in an Interference Environment

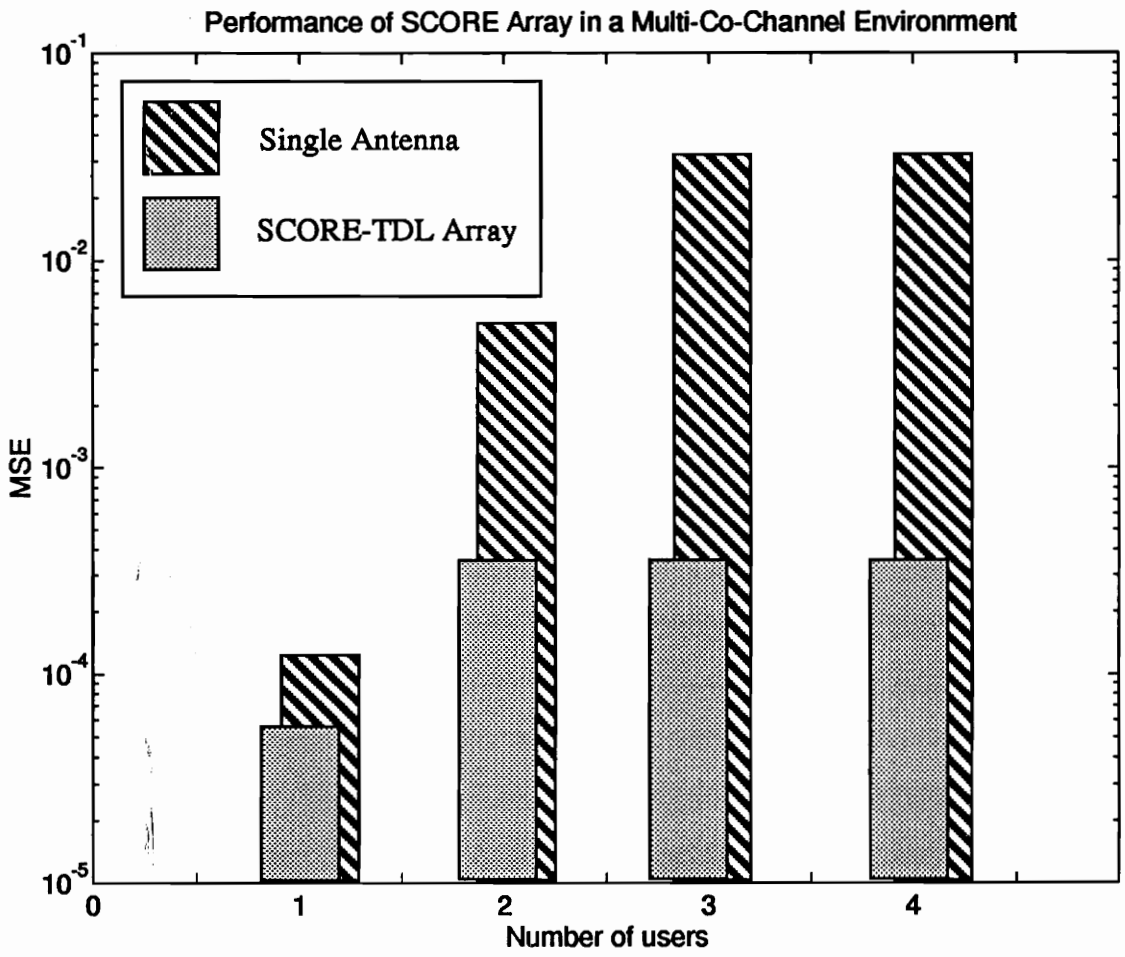

Figure 25. Bar Chart of MSE of the SCORE-TDL Array in a Multi-Co-Channel Environment

In the negative SIR region, the null-steering SCORE-TDL array is able to perform better than a single element and it is able to maintain an MSE lower than the MSE of the single element. Note at input SIR of 11 dB (typical SIR at the boundary of a 3-cell reuse) the adaptive array produces an output MSE equivalent to a single antenna with an input SIR of 18 dB (typical SIR at the boundary of a 7-cell reuse). Thus the capacity can be greatly increased without sacrificing quality of service. In an environment where there are multiple co-channel users, the simulation setup is similar to the one used in the testing of the CMA array. The signal strength of the interferers are 6 dB below the desired user. The performance of the SCORE-TDL array, as shown in Figure 25, is similar to the performance of the CMA array.

4.7.2.4 Effects of Increasing the Number of Elements on Interference from Co-channel Users

This section discusses the effects of increasing the number of elements in the array. The simulation setup is as follows. The base station receives signals from an in-cell user (SOI) and an out-of-cell interferer (SNOI). The AOA for the SOI is 90^o and the AOA of the interferer is 0^o. The strength of the interferer is 6 dB below that of the SOI and the CNR of the SOI is 20 dB. The channel comprises of a direct path and a multipath component. In the simulation the number of elements is increased from 1 to 8. Figure 26 shows the performance improvement obtained by the use of multiple-element SCORE-TDL array in an interference environment. The MSE decreases steadily as the number of elements is increased from 1 to 4. Since there is only one interferer to be suppressed, an array with two elements is sufficient to give an MSE of 10^{-4}. As the number of elements is increased to 3, the MSE decreases further. An array with 4 or 8 elements does not provide significant improvement over a 3-element array.

4.7.3 Testing TDAA on AMPS Signal

This section discusses the testing of the TDAA on AMPS signals. The TDAA exploits spectral redundancy like SCORE-TDL array, but the difference is that this structure exploits multiple statistical periodicities in the signal and the filter response is periodically time-varying. AMPS signals, as shown in Section 4.7.2.1, are spectrally redundant for frequency separations of $\pm f_{sat}, \pm 2f_{sat}, \pm 3f_{sat} \pm \ldots\ldots$. The spectral coherence strength of AMPS signals is not very strong, so exploiting more than two cyclic periodicities is not beneficial and in fact two primary periodicities supply the bulk of the gain. In this simulation, the TDAA exploits cyclic periodicities due to $\pm f_{sat}$. Each element in the array has 2 branches to exploit 2 periodicities.

4.7.3.1 Interference from Background Noise

This section discusses the behavior of the TDAA in a noisy environment. The TDAA exploits the spectral redundancy in the signal as explained in Section 3.4. Since Gaussian noise is a purely stationary process, it exhibits no spectral correlation [Gar87]. Thus, cyclostationary processing is able to exploit the spectral correlation of the *signal of interest* (SOI) in order to extract it from Gaussian noise. Figure 27 shows the performance improvement curves provided by the TDAA over a single element.

The AMPS signal used in this test has a SAT at 6.0 kHz and so there is spectral redundancy at spacings of 6.0 kHz. TDAA exploits multiple spectral periodicities and uses time-dependent filtering, and so it can perform better than the SCORE-TDL array, which uses one spectral periodicity and a time-independent filtering. Noise is not spectral correlated and more over noise in one element of the array is uncorrelated with that of the other elements, so the TDAA can perform better than the single element by nulling noise sources.

4.7.3.2 Interference from Co-Channel Users

This section discusses the performance of the TDAA in an interference environment.

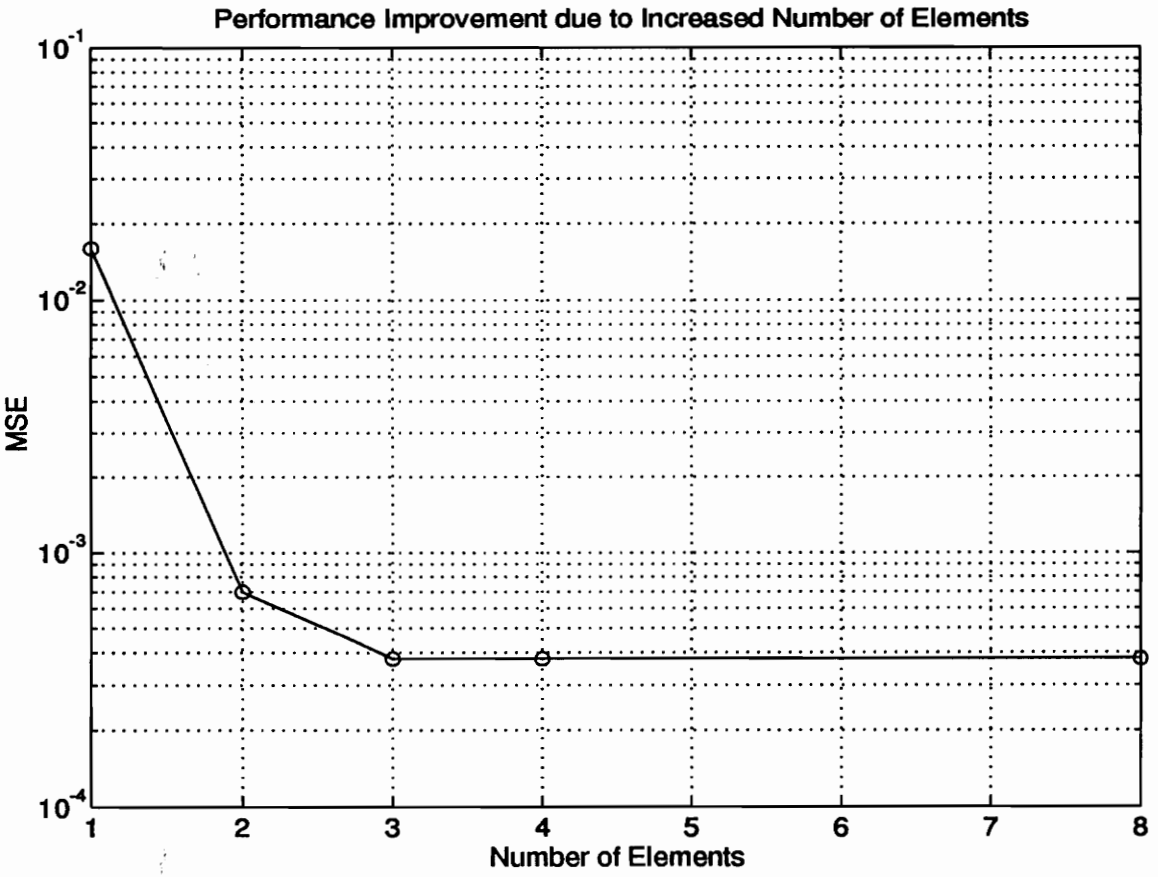

Figure 26. Performance Improvement due to Increased Number of Elements

The TDAA can spatially separate the SOI from the SNOI only when the SAT of the SOI is different from the SAT of the SNOI. The simulation setup is similar to the one used to test the CMA array for co-channel interference rejection. TDAA is implemented as explained in Section 4.5.3. The SOI has a SAT at 6.0 kHz and the SNOI has a SAT at 6.03 kHz. Both signals exhibit spectral redundancy, but their cyclic periods are different and this feature is used to separate these two signals. Figure 28 shows the post-demod MSE performance of the TDAA in the above mentioned environment. In the positive SIR region, the spectral properties of the SOI is stronger than that of the SNOI and the TDAA processor using frequency shifts of 6 kHz and -6 kHz, exploits the spectral periodicities of the SOI to dig out the SOI from the corrupted signal. The TDAA acts as a beamformer in the positive SIR region. In the negative SIR region, the spectral periodicities of the SNOI is stronger than that of the SOI and the TDAA processor using frequency shifts 6.03 kHz and -6.03 kHz, exploits the spectral periodicities of the SNOI to estimate the SNOI subtract the SNOI from the corrupted signal to retrieve the SOI. The TDAA acts as a null-steering array in the negative SIR region. A cascade of the beamformer and a null-steering array can provide nearly uniform performance irrespective of the value of the SIR.

The TDAA is able to maintain an MSE below 10^{-3}, irrespective of the SIR. The TDAA can perform satisfactorily even at an SIR value of -20 dB. This array provides superior performance to SCORE-TDL and CMA arrays. For higher SIRs, the performance difference between the SCORE-TDL and the TDAA decreases. For low SIRs, the TDAA is able to maintain an MSE much lower than the SCORE-TDL array. Figure 29 shows the pre-demod MSE performance curves for TDAA.

The simulation setup to test the performance of the TDAA array in a multiple co-channel environment is identical to the ones used in the testing of the CMA and SCORE-TDL array. The signal strength of the interferers are 6 dB below the signal strength of the desired user. The performance of the TDAA, as shown in Figure 30, is similar to the performance of the SCORE-TDL array, this is due to the fact that, the performance difference

between SCORE-TDL array and TDAA decreases for SIRs greater than 6 dB.

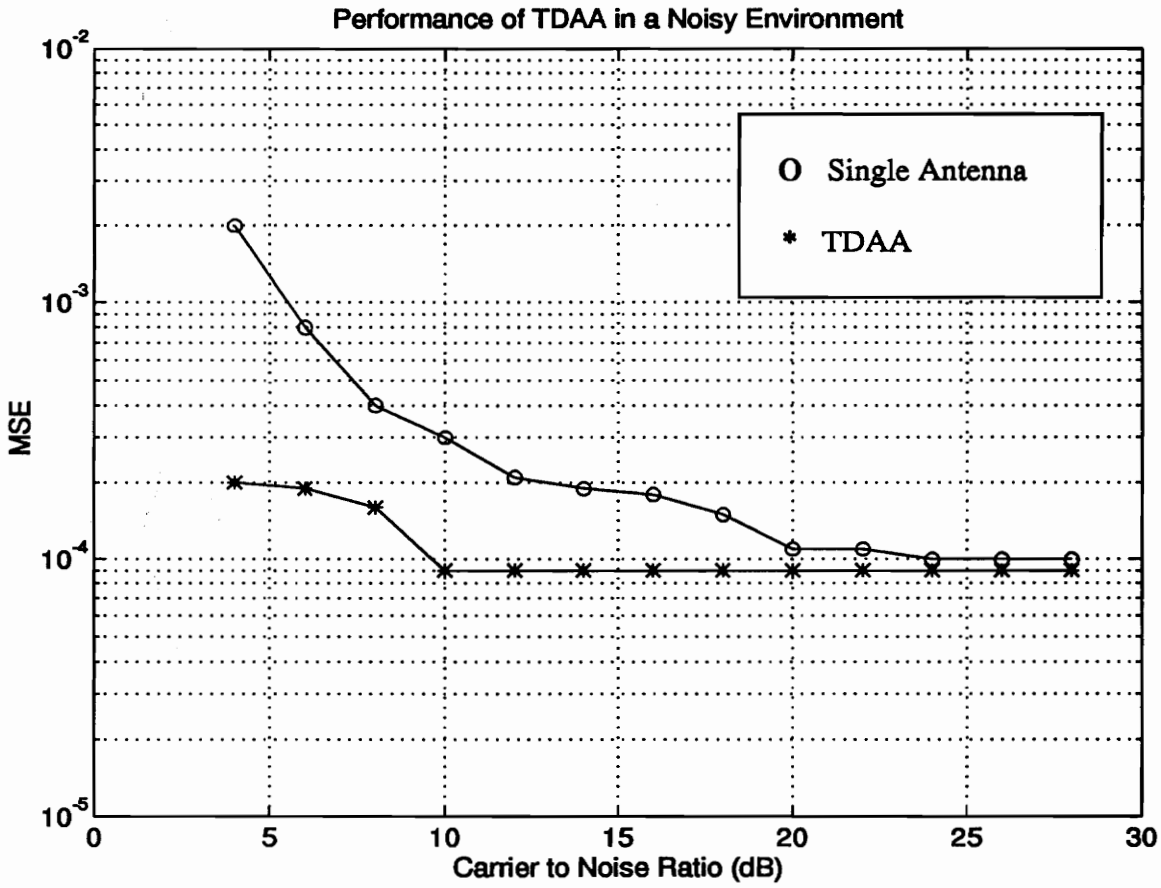

Figure 27. Performance Curve for TDAA in a Noisy Environment

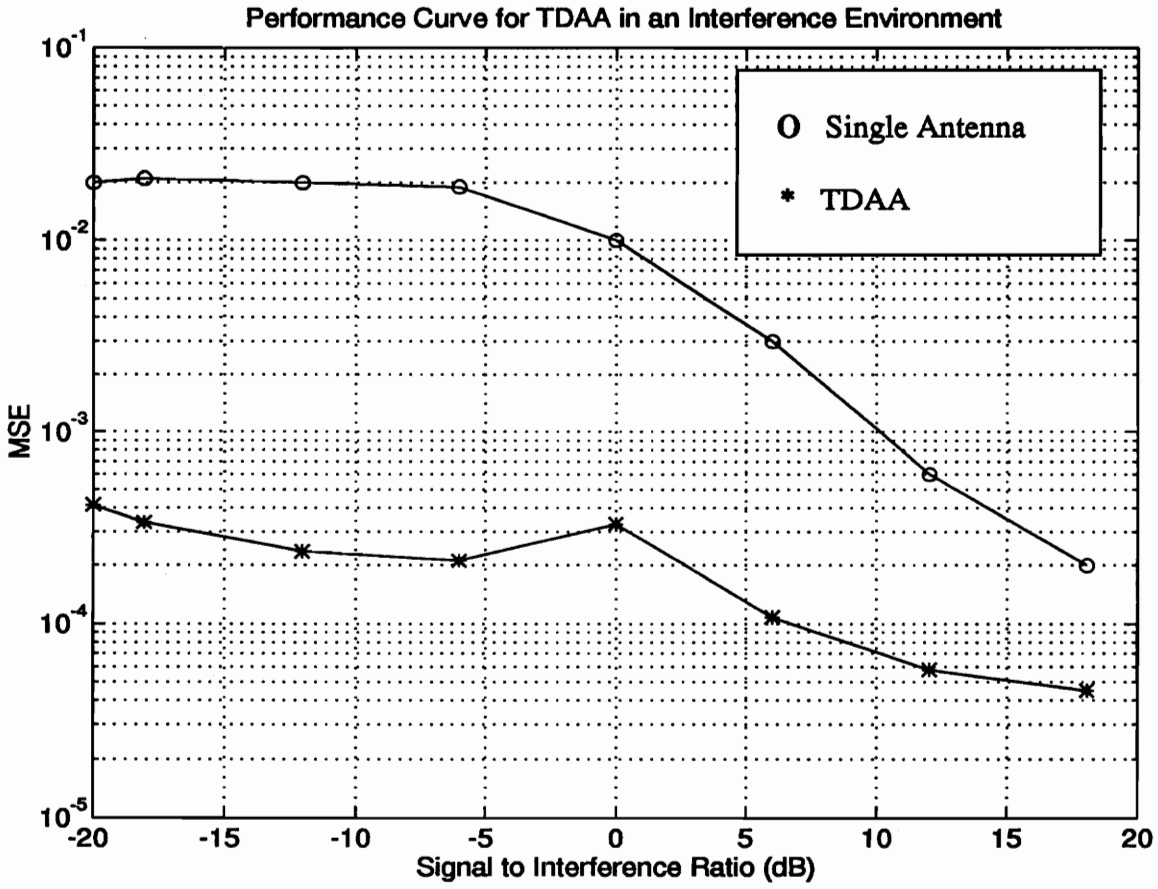

Figure 28. Pre-Demod MSE Curve for TDAA in an Interference Environment

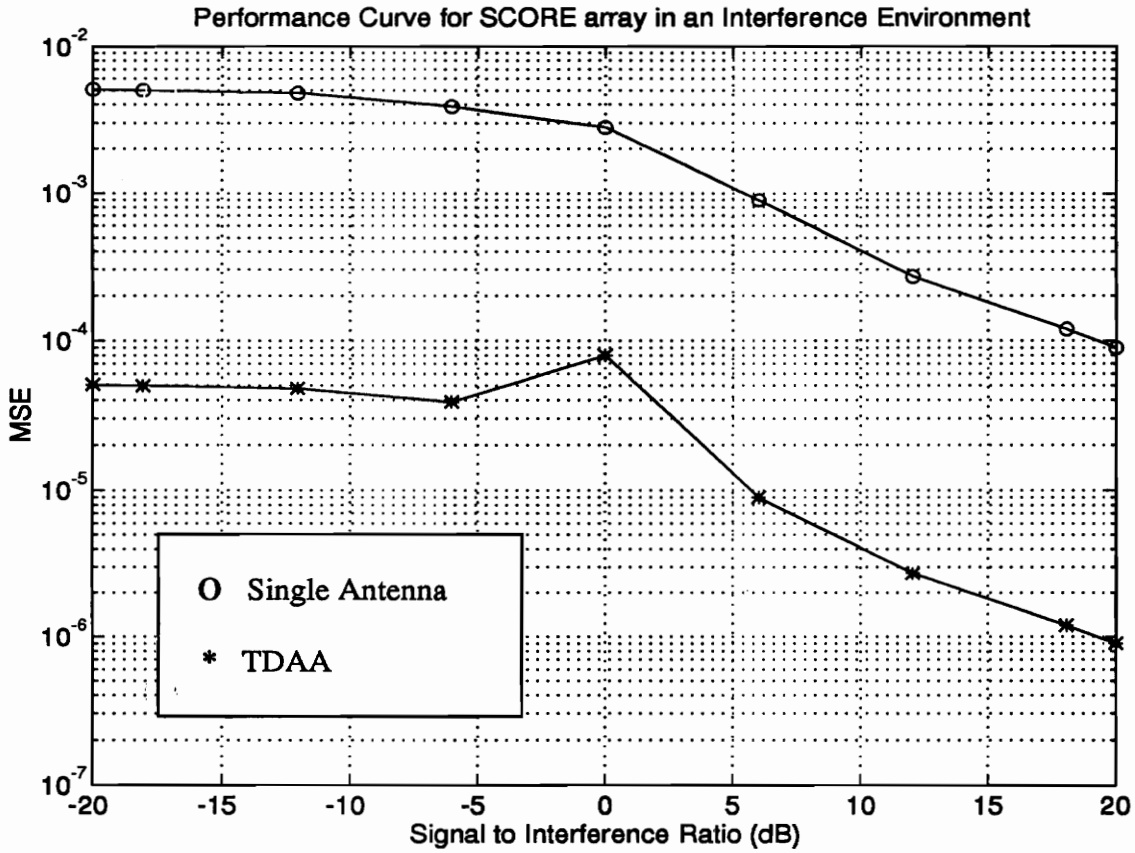

Figure 29. Post-Demod MSE Curve for TDAA in an Interference Environment

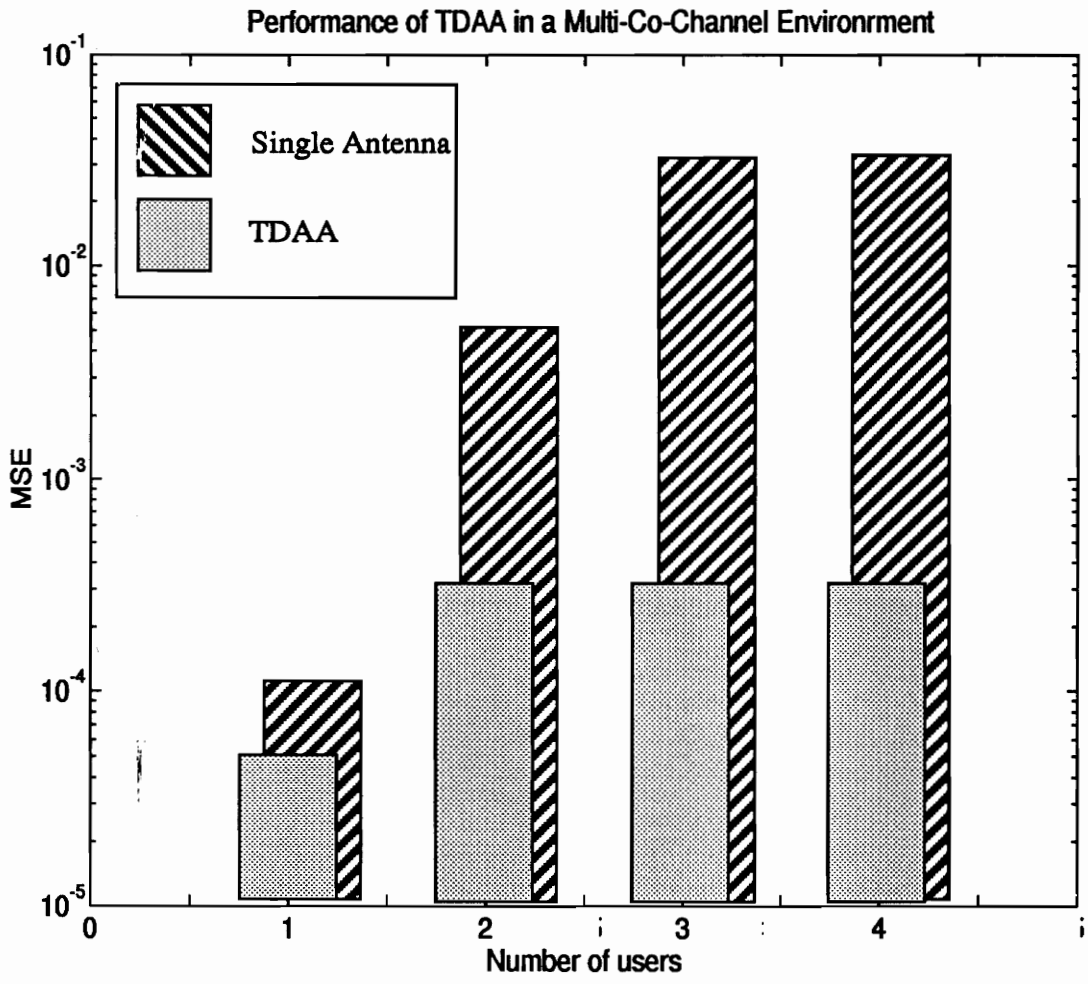

Figure 30. Bar Chart of MSE for TDAA in a Multi-Co-Channel Environment

4.7.4 Testing CMA on IS-54 Signal

Applying adaptive arrays to IS-54 is complicated than for AMPS. For example, for IS-54 are three users operating in a time frame and the array has to form a beam that switches over the three time slots. The AOA and the propagation characteristics for each user is different from that of other users. One approach for this problem is to save the weights for a particular user and recall these weights when the particular user starts transmitting again. A user transmits two bursts of data each spanning 6.67 ms within a frame and does not transmit for a time interval of 13.3 ms between bursts. The propagation characteristics of the channel changes within the time slot of 13.3 ms and so the above mentioned solution is only a sub-optimal solution for this problem.

The IS-54 signal simulated satisfies all the physical specifications of the standard. The simulation is setup as described below. The simulation takes into account one and two co-channel interferers. Figure 31 shows the simulation setup to test the CMA array on IS-54 signals. The mobile units are marked as 1 through 9, and the base stations as B_1, B_2, B_3. Table 3 shows the AOAs for different users at the base station B_1.

Table 3: AOA for Different Users

User Number	Angle-of-Arrival (degrees)
1	100
2	170
3	225
4	55
5	50
6	35
7	350
8	355
9	335

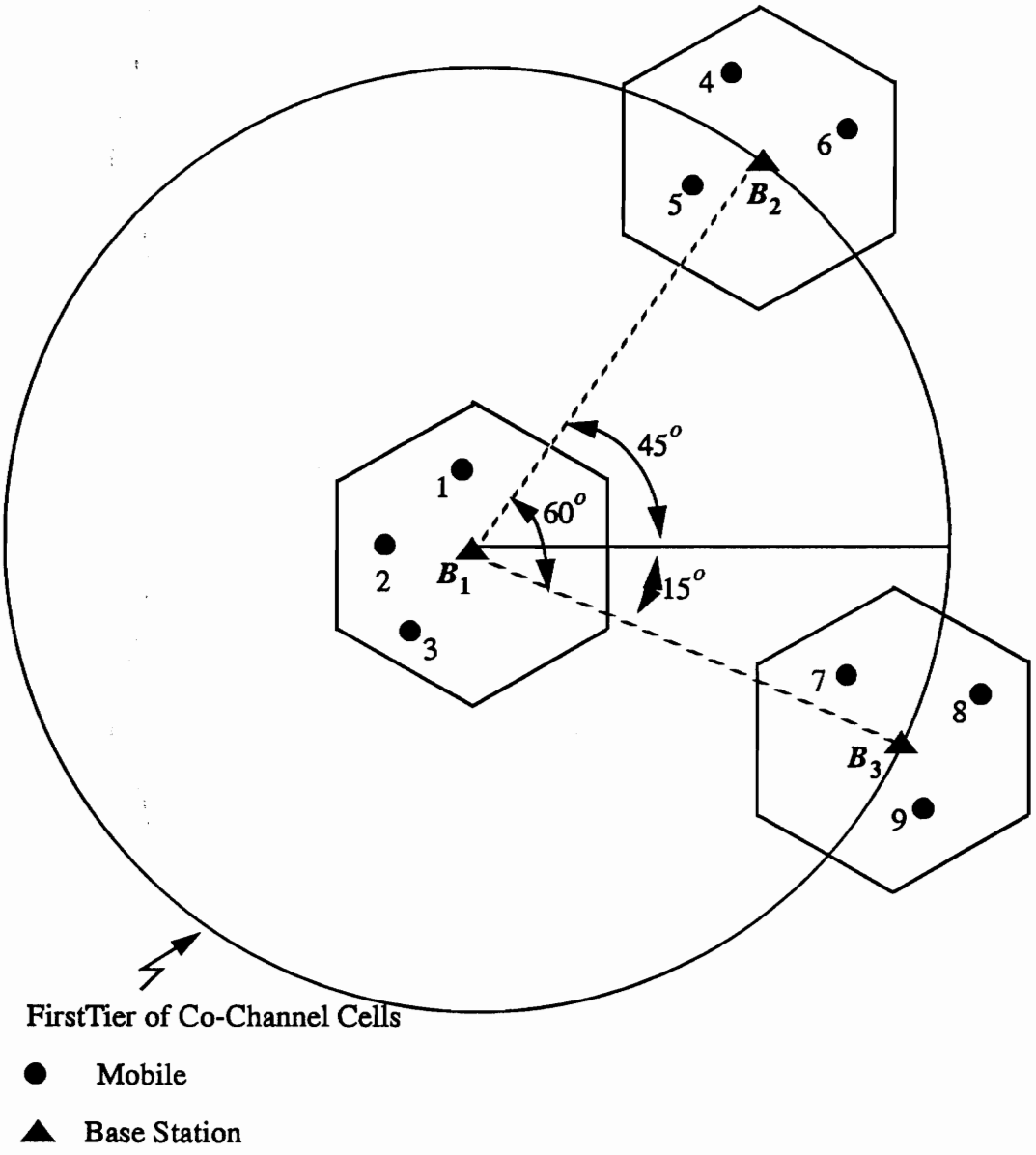

Figure 31. The Setup Used to Test the CMA Array on IS-54 Signals

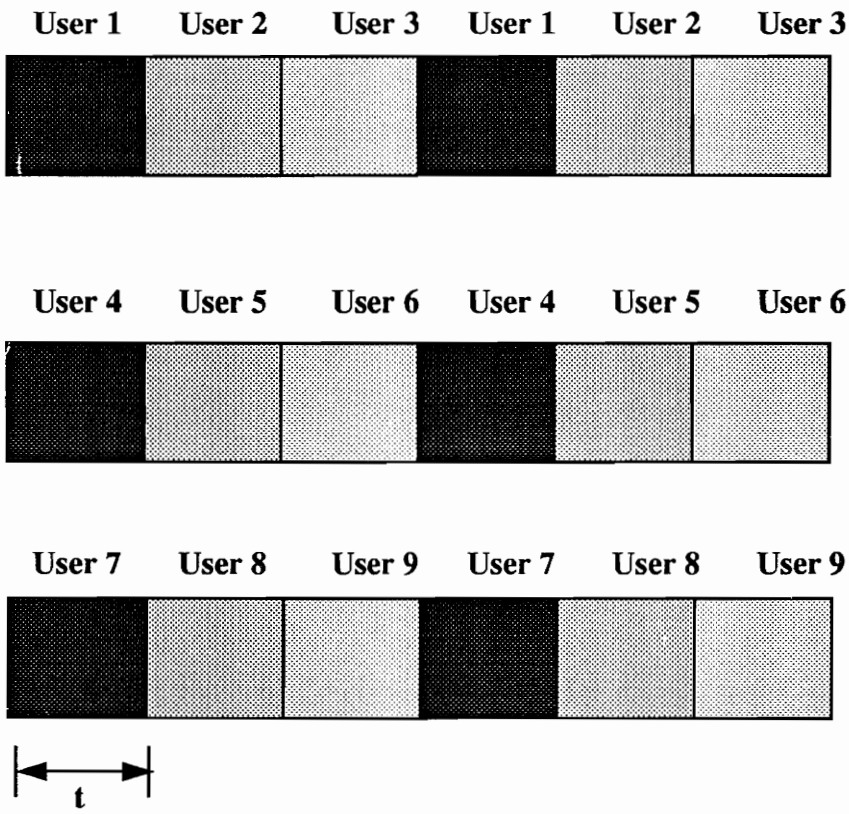

t = 6.67 ms

Figure 32. The Structure of the Time Frame for the Desired User and Two Co-channel Users, Users with the Same Shade Transmit Simultaneously.

There are three groups of mobile units that transmit simultaneously. The conflicting time slots are (1, 4, 7), (2, 5, 8), and (3, 6, 9). The time frame structure of these users is shown in Figure 32. The following is the discussion of the results obtained by employing CMA array at the base station B_1 in a noise and interference environment.

4.7.4.1 Interference from Background Noise

This section analyzes the performance of the CMA array on IS-54 signals in a noisy environment. The channel is a simple additive white Gaussian noise channel. The BER curves for each user in a time frame are plotted in Figures 33, 34, 35 and are compared with that of a single antenna. Figures shows that there is a BER improvement of one order of magnitude for a lower *carrier-to-noise ratio* (CNR) and as the CNR increases above 10 dB, there is not much improvement in the BER. The BER curves for three different users are very similar. Thus, in a noisy environment, a CMA array can provide improvement of one order of magnitude in the BER.

4.7.4.2 Interference from Co-channel Users

In a co-channel interfered environment, the CMA array has to form beams in the direction of all the three desired users. If it fails to form the beam in the right direction, burst errors occur due to capturing of the signal-not-of interest. This disadvantage limits the application of CMA array in a co-channel interference environment. The remedial measure for this problem is to incorporate the initial DOA of the signals from the desired users into the initial weight vectors. Beamforming for IS-54 signals has to be performed in two steps, the first step is to find a coarse measure of the DOA of the signal from the desired user and the second step is to allow the CMA algorithm to take over the beamforming operation. Multi-target CMA is another method to reject interference when the SIR is negative and identification bits in a frame can be used to prevent switching of signals between ports.

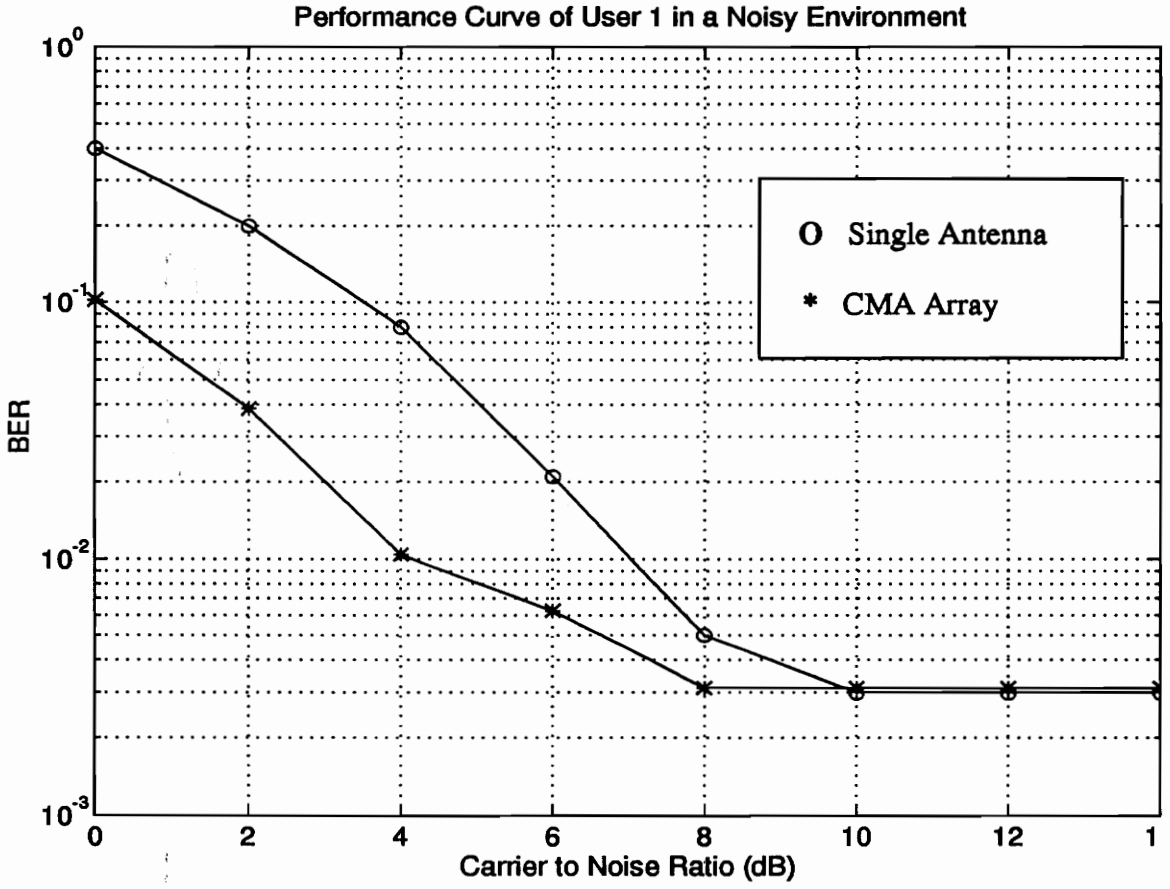

Figure 33. Performance Curve for User 1 in a Noisy Environment

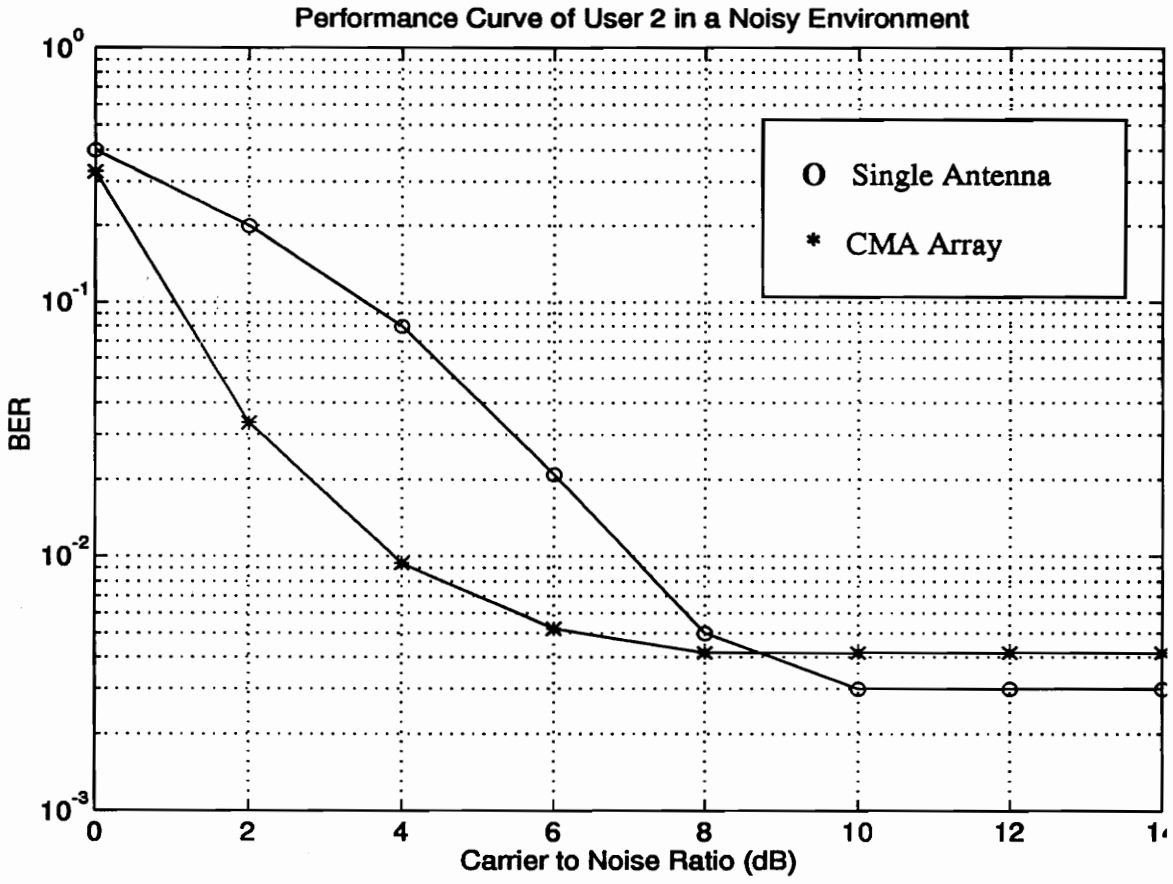

Figure 34. Performance Curve for User 2 in a Noisy Environment

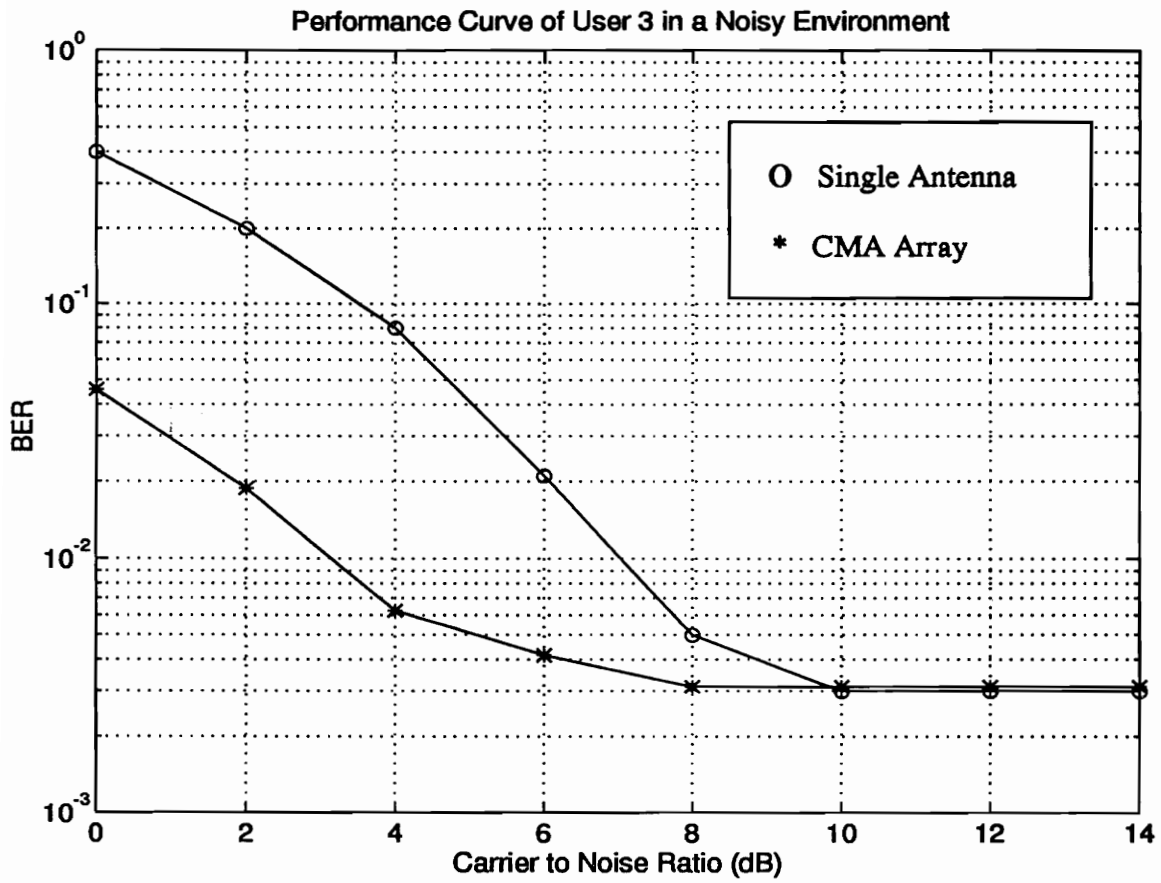

Figure 35. Performance Curve for User 3 in a Noisy Environment

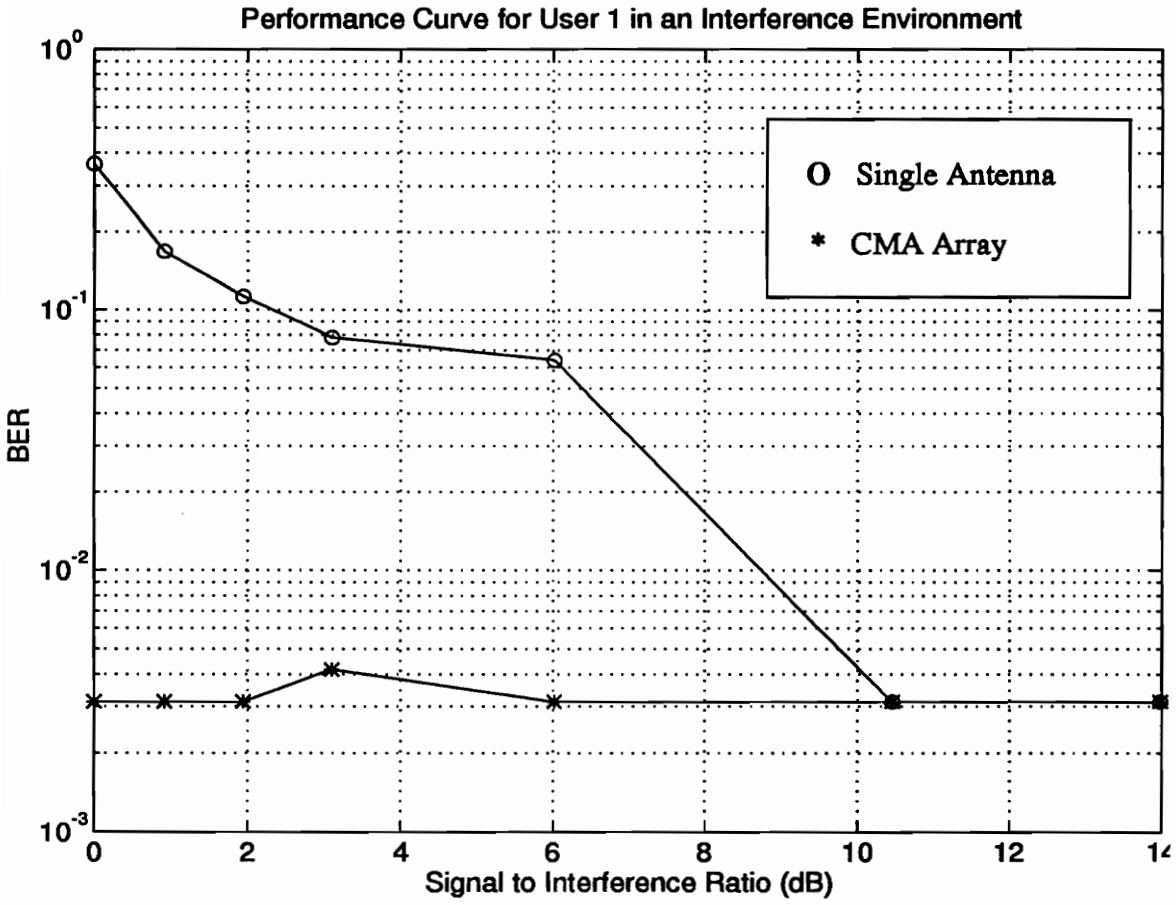

Figure 36. Performance Curve for User 1 in an Interference Environment

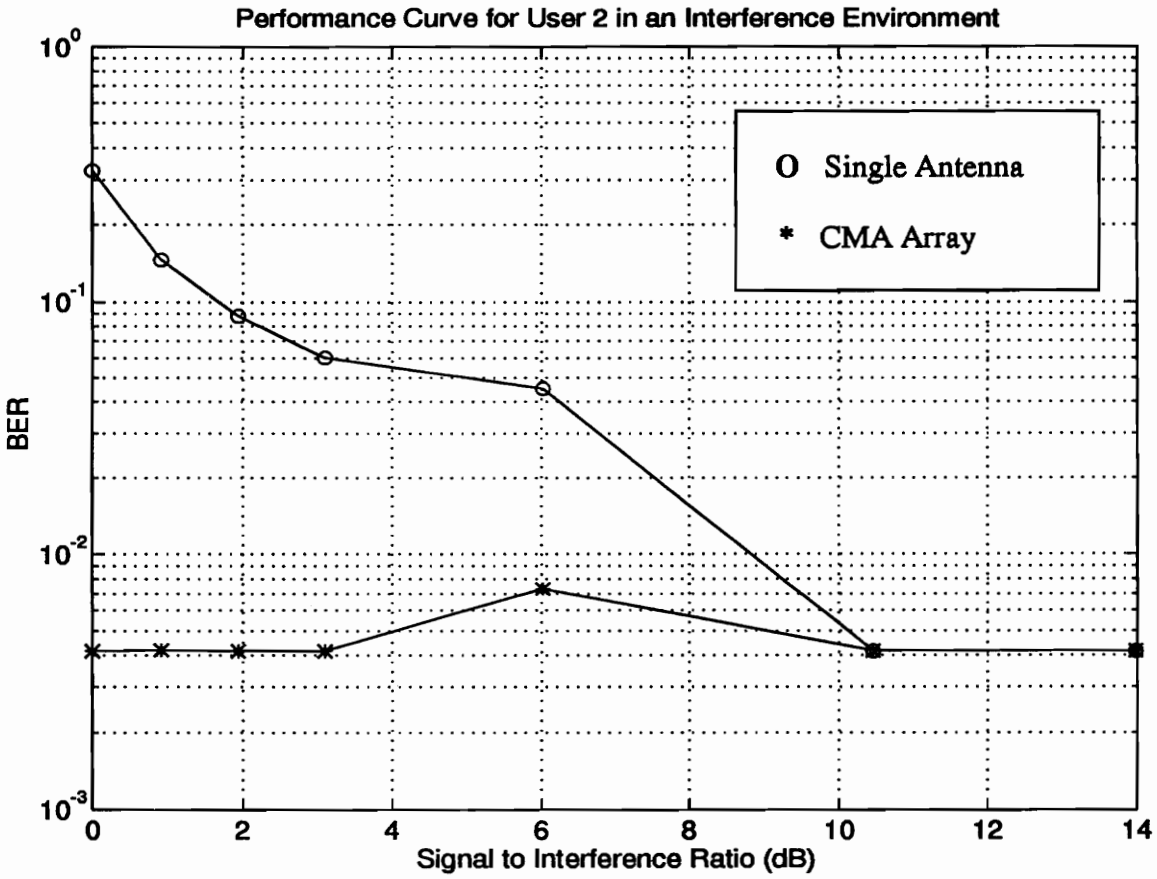

Figure 37. Performance Curve for User 2 in an Interference Environment

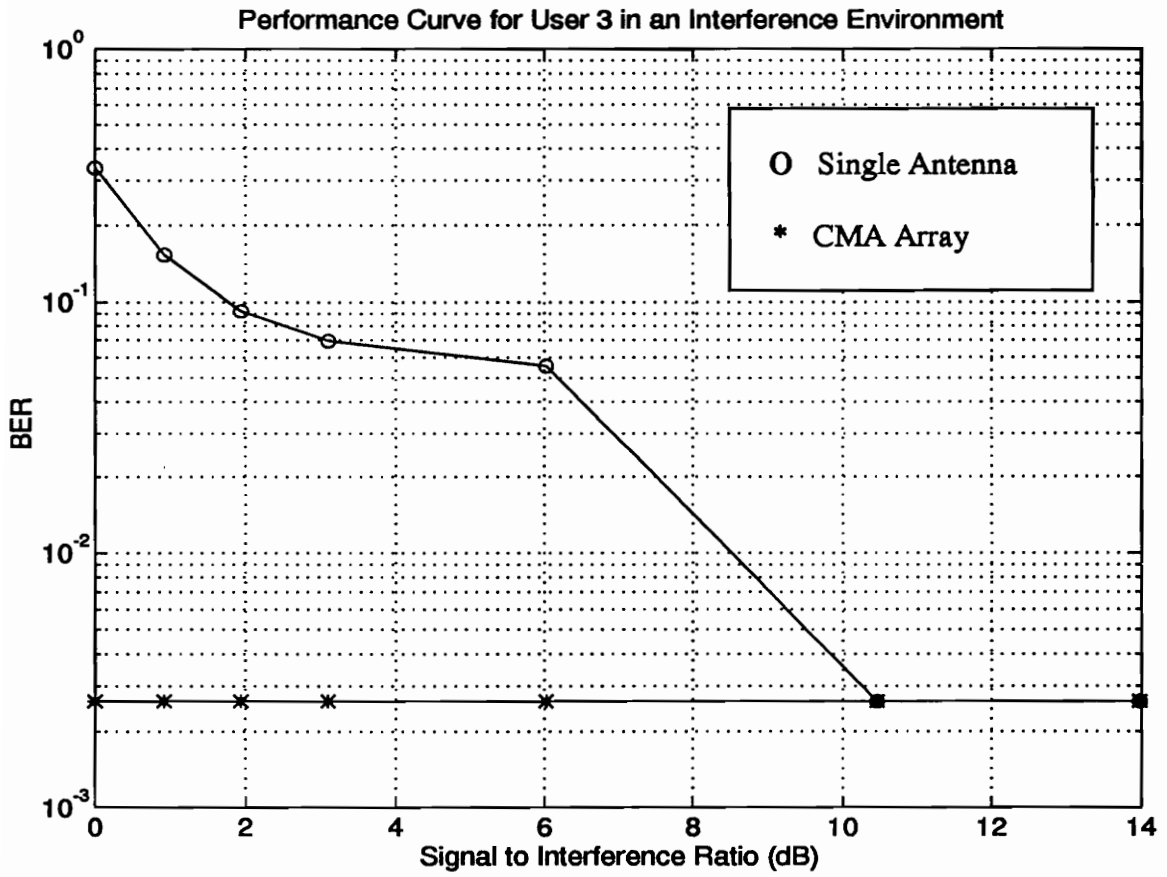

Figure 38. Performance Curve for User 3 in an Interference Environment

The initial knowledge of the DOA is assumed to be known with an error of $\pm 60^{o}$ (due to sectorization) in the simulation carried out and CMA array starts with the knowledge of the initial DOA. The initial DOAs for users 1, 2, and 3 are chosen to be 160^{o}, 230^{o}, and 165^{o}. The SIR for this test is varied from 0 to 14 dB and the CMA array is able to maintain a BER of less than 10^{-3} for all the users irrespective of the SIR, as shown in Figures 36, 37, and 38.

Test results of the CMA array for IS-54 signals in an environment which has multiple interferers is discussed in this section. One and two interferers are considered in this simulation and the CMA array which has an *a priori* knowledge of the DOA performs very well even when there are two interferers. The signal strength of the interferers is 6 dB below the SOI and the users are distributed as shown in Figure 31. Figure 39 shows the performance improvement obtained by employing CMA array in a multi-co-channel environment. The array maintains a constant BER irrespective of the number of interferers. The array can even work in the negative SIR region, because of the fact that the weights are initialized using knowledge of the initial DOA.

4.7.4.3 Effects of Increasing the Number of Elements on Interference from Co-channel Users

This section discusses the effects of increasing the number of elements in the array and analyzes the BER improvement. The simulation setup is as follows. The base station receives signals from an in-cell user (SOI) and an out-of-cell interferer (SNOI). The strength of the interferer is 4.46 dB below that of the SOI and the CNR with respect to the SOI is 20 dB. In the simulation the number of elements is increased from 1 to 8 and the performance is analyzed for the above described environment. Figure 40 shows the performance improvement obtained by the use of multiple-element CMA array in an interference environment. The BER decreases as the number of elements is increased from 1 to 2 and there is no improvement as the number of elements increases from 2 to 8.

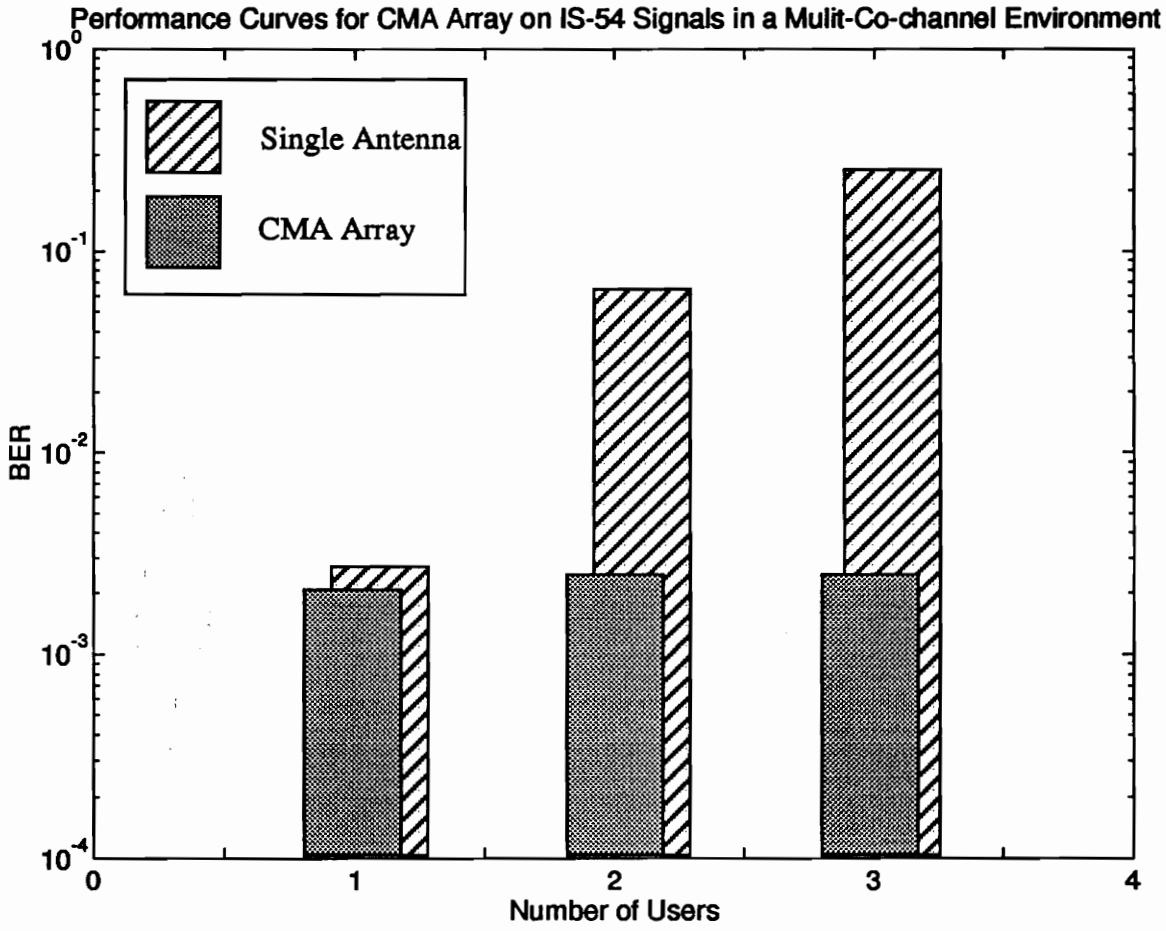

Figure 39. Performance Curve for CMA Array on IS-54 Signals in a Multi-Co-Channel Environment

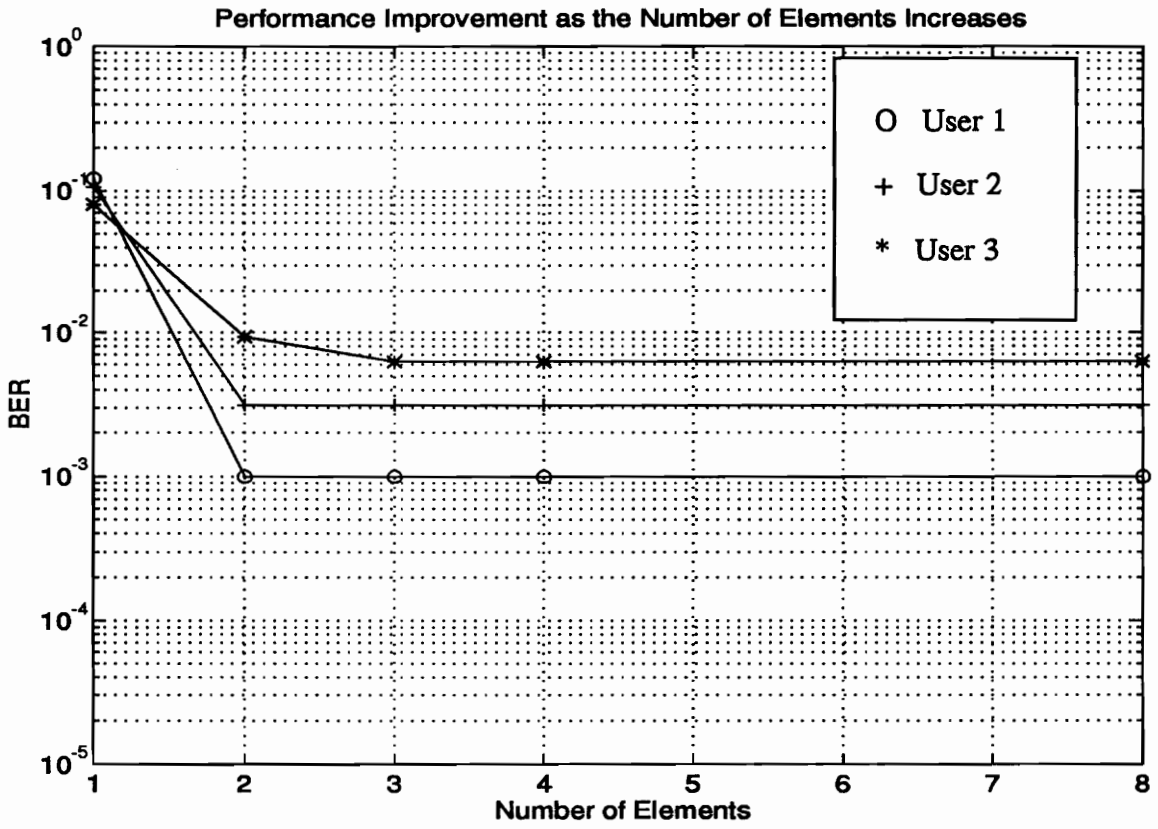

Figure 40. Performance Curves for CMA Array in an Interference Environment as the Number of Elements Increases

The BER curves for all the three users are superimposed and shown in Figure 40. Each user has a different irreducible BER, this is because the propagation characteristics for each user are different.

4.8 Summary

The CMA array, SCORE-TDL array and TDAA have been tested extensively under different conditions. The results have been compiled in Section 4.7. This section summarizes the results obtained and compares the performance of various arrays in an identical interference environment. Figure 40 shows the MSE curves for various arrays as the SIR is varied from - 20 to 20 dB. CMA array performs very well in the positive SIR region, but it falls apart in the negative SIR region and it performs no better than the single element. SCORE-TDL array performs better than both CMA array and the single element in the negative SIR region. In the positive SIR region SCORE-TDL array performs better than the single element, but it is not better than CMA array. TDAA provides the superior MSE performance irrespective of the SIR.

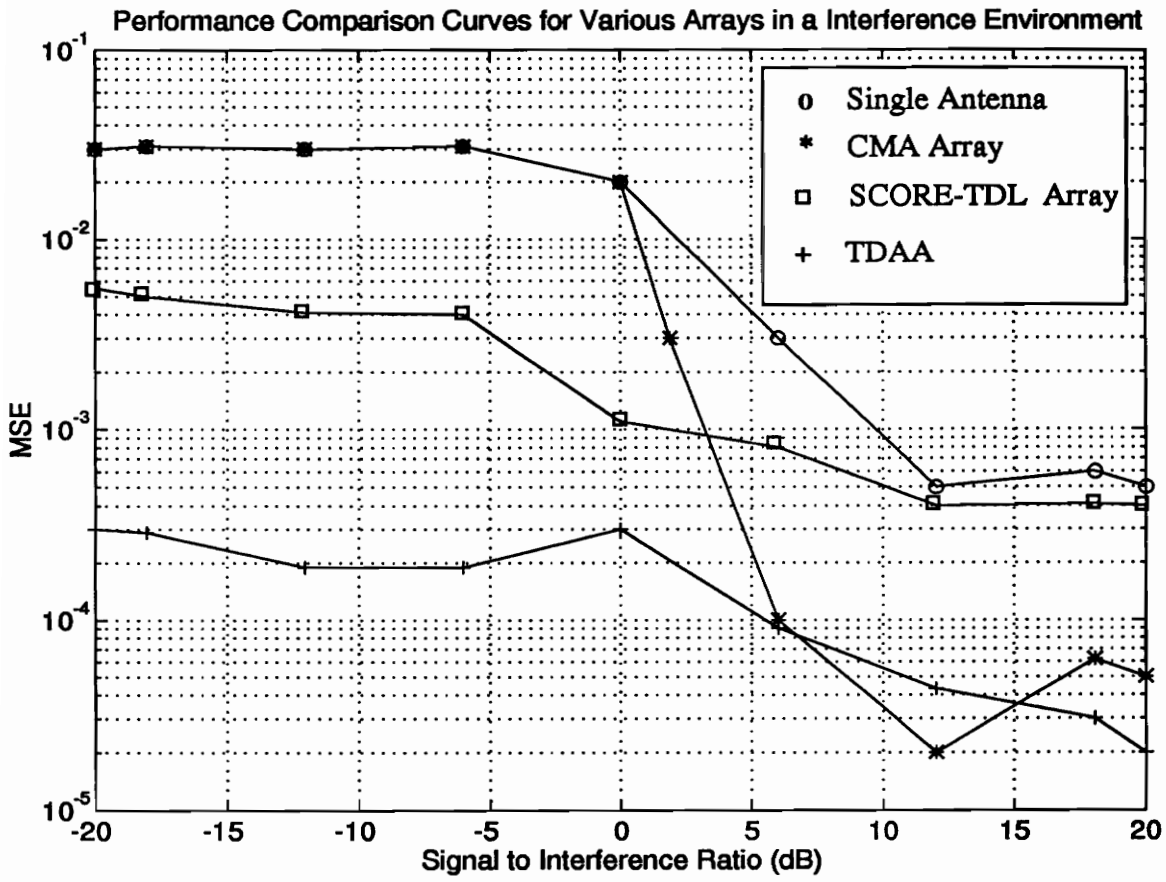

Figure 41. Performance Comparison Curves for Various Arrays in an Interference Environment (The linear array has 4 elements and the AOA of the SOI is 90 degrees and the AOA of the SNOI is 0 degrees)

Chapter 5

Conclusions and Future Work

The focus of this research is to show that by employing adaptive antenna arrays in the base station, interference can be greatly reduced and thus the capacity of the cell can be increased. The antenna arrays are trained by algorithms which are blind, i.e., those algorithms do not require training sequences. Extensive testing has been conducted using standard signals like AMPS and IS-54. The test results are compiled in Chapter 4. The results clearly show that by employing adaptive antenna arrays in the base station, an enormous reduction in interference is possible and thus an increase in the cell capacity can be achieved. The interference rejection capability tends to be proportional to the number of elements in the array. The interference rejection capability of the array is also dependent on the algorithm which drives the array. We found that the time-dependent adaptive array (configured as a spectral correlation predictor) performs better than the CMA and SCORE algorithms, especially when the signal-to-interference ratio (SIR) is very low. The only disadvantage with TDAA is that it is computationally very intensive compared to CMA and SCORE arrays. Typical improvement in MSE indicates a three cell reuse pattern might be possible compared to a seven cell reuse pattern for equivalent call quality.

Complexity is another factor which has to be taken into account. The CMA array seems to be the least computationally complex algorithm. TDAA is the most computationally complex algorithm. There are problems in applying the SCORE array and the TDAA to IS-54 and IS-95 signals. Since all users in the IS-54 and IS-95 systems use the same signal parameters, there is no easily recognized unique feature pertaining to cyclostationarity that enables us to identify a particular user.

The channel model proposed by [Lib95] is based on the relationship between the delay of the multipath and the AOA. This is a very simple model which assumes that all rays that originate from the mobile reach the base station. Complex models that take into account shadowing could be developed in a future research effort. Knowledge about the distribution of the users, i.e., knowledge of how realistic traffic condition, will be beneficial to set up realistic conditions.

This study has focussed on employing the adaptive arrays at the base station. The reason is that, the reverse link is the weak link and the adaptive arrays are most likely to be employed first in the base station. The use of the adaptive arrays in both the base station and the mobile is the ultimate goal. However, there are problems implementing the array in the mobile: the cost of the array, the space occupied by the array and the processor and the life of the battery that supports the processors.

Future work should focus on developing new blind adaptive algorithms. These new algorithms should exploit spatial, time and frequency diversities. Implementation of these algorithms in hardware and analyzing the performance of the array in a realistic channel are necessary future goals. The study so far has focussed on the improvement of the BER. Future work will involve more direct evaluation of the capacity increase brought about by these adaptive arrays. The complexity of the cellular system requires development of prototype systems before the issue of capacity gain can be fully resolved.

Nonlinear filtering techniques that exploit higher order cyclostationarity can be used to solve the interference problem in the case of IS-54 and IS-95 signals. Though the users have the same signal parameters, when the signal is passed through a nonlinear filter, hidden periodicities appear. If the signals from different users are mutually uncorrelated, then there exists minima in the performance function corresponding to the optimal extraction of each one of the different signals [Cas93].

Adaptive arrays can be classified as *smart, semi-smart,* and *moronic* antenna systems. *Smart antenna systems* are those which perform coherent combining. Smart antenna systems perform better than the other systems, however and the penalty is the cost and the complexity of the system. *Moronic antenna systems* are those which switch antenna elements based on the signal strength. These antenna systems are marginally better than the single element. The type of antenna systems is simple to implement. Future work will involve development of adaptive antenna arrays which are *semi-smart.* These systems are more intelligent compared to the moronic antenna systems and they function based on the principle of switched diversity, but the decision to switch is based on the spectral correlation strength of the SOI.

Appendix

Main Set of Matlab Programs

The following is the set of Matlab routines that manage all the simulation.

Setup_temp2.m - performs the first set of simulation for CMA

Setup_temp.m - performs the second set of simulation for CMA

Setup_temp3.m - performs the third set of simulation for CMA

Setup_temp1.m - performs the fourth set of simulation for CMA

Main1A.m - performs the first set of simulation for SCORE-tapped delay line structure

Main1.m - performs the second set of simulation for SCORE-tapped delay line structure

Main1B.m - performs the third set of simulation for SCORE-tapped delay line structure

Main1C.m - performs the fourth set of simulation for SCORE-tapped delay line structure

MainA.m - performs the first set of simulation for time-dependent adaptive array

Main.m - performs the second set of simulation for time-dependent adaptive array

MainB.m - performs the third set of simulation for time-dependent adaptive array

MainC.m - performs the fourth set of simulation for time-dependent adaptive array

References

[Age83] J. R. Treichler and B. G. Agee, "A new approach to multipath correction of constant modulus signals," *IEEE Trans. on ASSP.*, vol. ASSP-31, no. 2, pp. 459-472, April 1983.

[Age86] B. G. Agee, "The least-squares CMA: A new technique for rapid correction of constant modulus signals," *Proc. IEEE Internat. Conf. ASSP.*, pp. 953-956, April 1986.

[Age88] B. G. Agee, "Convergent behavior of modulus restoring adaptive arrays in Gaussian interference environments," *Proc. of the 22nd Asilomar Conf. on Signals, Systems and Computers,* Nov. 1988.

[Age88] B. G. Agee, S. V. Schell, and W. A. Gardner, "Spectral self-coherence restoral: A new approach to blind adaptive signal extraction," *Proc. IEEE*, vol. 78, pp.753-767, April 1990.

[Age89] B. G. Agee, "Blind separation and capture of communication signals using a multitarget constant modulus beamformer," *Proc. of IEEE MILCOM Conf.*, pp. 0340-0346, 1989.

[Age90] B. G. Agee and D. L. Young, "Blind capture and geolocation of general spatially self-coherent waveforms using multiplatform SCORE," *Proc. 24th Asilo-*

mar Conf. on Signals, Systems, and Computers, pp. 33-38, November 1990.

[Age93] B. G. Agee et al., "Simulation performance of a blind adaptive array for realistic channels," *Proc. IEEE Veh. Tech. conf.*, pp. 97-100,1993.

[Ber90] N. J. Bershad and S. Roy, "Performance of the 2-2 constant modulus adaptive algorithm for Rayleigh fading sinusoids in Gaussian noise", *Proc. IEEE Internat. Conf. ASSP.*, pp. 1675-1678, April 1990.

[Cas93] Luis Castedo et al., "A new cost function for adaptive beamforming using cyclostationary signal properties," *Proc. ICASSP*, pp. 284-287, 1993.

[Cha90] C. K. Chan and J. J. Shynk, "Stationary points of the constant modulus algorithm for real Gaussian signals," *IEEE Trans. ASSP.*, vol. ASSP-38, pp. 2176-2181, Dec. 1990.

[Edm89] Edmond Nicolau and Dragos Zaharia, *Adaptive Arrays*, Elsevier, New York, 1989.

[EIA90] "Cellular system dual-mode mobile station-base station compatibility standard," *Electronic Industries Association*, 1990.

[Fal90] D. D. Falconer, N. W. K. Lo, and A. U. H. Sheikh, "Adaptive equalization and diversity combining for a mobile radio channel," *Proc. IEEE GLOBECOM conf.*, pp. 923-927, 1990.

[Fer85] E. R. Ferrera, Jr., "A method for cancelling interference from a constant envelope signal," *IEEE Trans. on ASSP.*, vol. ASSP-33, pp.316-319, February 1985.

[Gar86] W. A. Gardner, "The spectral correlation theory of cyclostationary time-series," *Signal Processing*, vol. 11, no.1, July 1986.

[Gar91] W. A. Gardner, "Exploitation of spectral redundancy in cyclostationary signals", *IEEE Signal Processing Magazine*, April 1991.

[Gar92] W. A. Gardner, S. V. Schell, and B. G. Agee, "Multiplication of cellular radio capacity by blind adaptive spatial filtering," *Proc. IEEE Int'l. Conf. on Selected Topics in Wireless Comm.*, pp. 102-106, June 1992.

[Gar93] S. V. Schell and W. A. Gardner, "Maximum likelihood and common factor analysis-based blind adaptive spatial filtering for cyclostationary signals," *Proc. ICASSP*, pp. 292-295, 1993.

[Gil91] K. S. Gilhousen et. al, "On the capacity of a cellular CDMA System," *IEEE Trans. on Vehicular Technology*, vol. 40, no. 2, May 1991.

[God80] D. M. Godard, "Self-recovering equalization and carrier tracking in two-dimensional data communication," *IEEE Trans. on Communications*, COM-28(11): pp.1867-1875, Nov 1980.

[Goo86] Richard Gooch and John Lundell, "The CM array: An adaptive beamformer for the constant modulus signals", *Proc. ICASSP*, pp. 2523-2526, 1986.

[Goo88] R. P. Gooch and B. J. Sublett, "Joint spatial and temporal equalization in a decision-directed adaptive antenna system," *Proc. 22nd Asilomar Conf. on Signals, Systems, and Computers*, pp. 255-259, November 1988.

[Hay91] Simon Haykin, "*Adaptive filter theory*," Prentice Hall edition, 1991.

[Kam87] K. D. Kammeyer et al., "A modified adaptive FIR equalizer for multipath echo-cancellation in FM transmission," *IEEE Trans. J. Selected Areas of Comm.*, vol. SAC-5, pp. 236-237, Feb. 1987.

[Kai93] T. Kailath, A. Paulraj, and B. Khalaj, "Antenna arrays for CDMA systems with multipath," *Proc. MILCOM conf.*, 1993.

[Kik91] N. Kikuma et al., "Performance of CMA adaptive array optimized by the Marquardt method for suppressing multipath waves", *Electronics and Communications in Japan*, Part -1, vol. 75, no.9, 1992.

[Kwo92] O. W. Kwon et al., "Performance of constant modulus adaptive digital filters for interference cancellers", *Signal Processing*, vol. 26, no. 2, Feb. 1992.

[Lar85a] M. G. Larimore and J. R. Treichler, "The capture properties of CMA-based interference cancellers," *Proc. Asilomar Conf. Signals, Syst., Comput.*, pp. 49 -52, 1984.

[Lar85b] M. G. Larimore and J. R. Treichler, "Noise capture properties of the constant-modulus algorithm," *Proc. IEEE Internat. Conf. ASSP.*, pp. 1165-1168, March 1985.

[Lib95] Joseph C. Liberti, "CDMA Cellular Communications Systems Employing Adaptive Antennas", *Ph. D. dissertation*, Virginia Polytechnic Institute and State University, 1995 (to be published).

[Lib95] J. C. Liberti and T. S. Rappaport, "Analytical results for capacity improve-

ments in CDMA," *IEEE Trans. on Veh. Tech.*, vol. 43, No. 3, August 1994.

[Mon80] R. A. Monzingo and T. W. Miller, *Introduction to adaptive arrays*, New York:, Wiley 1980.

[Pic87] G. Picchi and G. Prati, "Blind equalization and carrier recovery using a "Stop-and-Go" decision directed algorithm," *IEEE Trans. on Comm.*, vol. com-35, no.9, September 1987.

[Rap89] T. S. Rappaport, "Indoor radio communications for factories of the future," *IEEE Comm. Magazine*, vol. 27, no. 5, pp. 15-24, May 1989.

[Sco90] T.S. Rappaport, S.Y. Seidel, and R. Singh, "900-MHz multipath propagation measurements for U.S. digital cellular radiotelephone," *IEEE Trans. on Veh. Techn.*, vol. 39, No. 2, pp.132-139, May 1990.

[Rap94] T. S. Rappaport et. al., "Path loss, delay spread, and outage models as functions of antenna height for microcellular system design," *IEEE Trans. on Veh. Techn.*, vol. 43, No. 3, July 1989.

[Ree87] J. H. Reed, "Time-dependent adaptive filters for interference rejection," *Ph. D. Dissertation*, Department of Electrical Engineering and Computer Science, UC, Davis, December 1987.

[Ree88] J. H. Reed, "A technique for sorting and detecting signals in interference," *Proc. MILCOM conf.*, pp. 425-430, 1988.

[Ron94] Rong He and J. H. Reed, "Spectral correlation of AMPS signals and its application to interference rejection," *Proc. MILCOM Conf.*,1994.

[Sat75] Y. Sato, "A method of self-recovering equalization for multilevel amplitude-modulation systems," *IEEE Trans. Comm.* vol. COM-23, pp. 679-682, June 1975.

[Sch93] S. V. Schell, "Blind adaptive spatiotemporal filtering for wide-band cyclostationary signals," *IEEE Trans. on Signal Processing*, vol. 41, no.5, May 1993.

[Sch88] S. V. Schell and B. G. Agee, "Application of the SCORE algorithm and score extension to sorting to the rank-L spectral self-coherence environment," *Proc. 22nd Asilomar Conf. on Signals, Systems, and Computers*, pp. 274-278, November 1988.

[Sha93] Sanyogita Shamsunder, "Exploiting cyclostationarity for range and bearing

estimation," *Proc. ICASSP*, pp. 280-283, 1993.

[Syl93] Sylvie Mayrargue, "Spatial equalization of a radio-mobile channel without beamforming using the constant-modulus algorithm," *Proc. ICASSP*, pp. 344-347, 1993.

[Tak91] Takeo Ohgane, "Characteristics of CMA adaptive array for selective fading compensation in digital land mobile radio communications", *Electronics and Communications in Japan*, Part 1, vol. 74, no. 9, 1991.

[Tak93] Takeo Ohgane, "An implementation of a CMA adaptive array for high speed GMSK transmission in mobile communications", *IEEE Trans. on Veh. Tech.* vol. 42, no 3, August 1993.

[Tre85a] J. R. Treichler and M. G. Larimore, "Convergence rates for the constant modulus algorithm with sinusoidal inputs," *Proc. 1985 IEEE Internat. Conf. ASSP*, pp. 1157-1160, March 1985.

[Tre85b] J. R. Treichler and M. G. Larimore, "The tone capture properties of CMA-based interference suppressors," *IEEE Trans. ASSP.*, vol. ASSP-33, pp. 946-958, August 1985.

[Tre80] J. R. Treichler, "Observability and its effects on the design of ML and MAP joint estimators," *IEEE Trans. on Inform. theory*, vol. IT-26, pp. 498-503, July 1980.

[Tre68] H. L. Van Trees, *Detection, Estimation, and Modulation Theory, Part I: Detection, Estimation, and Modulation Theory.* New York: Wiley 1968.

[Tre71a] H. L. Van Trees, *Detection, Estimation, and Modulation Theory, Part II: Nonlinear Modulation Theory.* New York: Wiley 1971.

[Tre71b] H. L. Van Trees, *Detection, Estimation, and Modulation Theory, Part III: Radar-Sonar Signal Processing and Gaussian Signals in Noise*. New York: Wiley 1968.

[Tug93] J. K. Tugnait and R. Swaminathan, "On improving the convergence of CMA adaptive filters," *Proc. ICASSP*, pp. 340-343, 1993.

[Wid67] B. Widrow et al., "*Adaptive antenna systems*," Proc. IEEE, vol. 55, no. 12, pp. 2143-2159, Dec. 1967.

[Win83] J. H. Winters, "Switched diversity with feedback for DPSK mobile radio sys-

tems," *IEEE Trans. Veh. Tech.* vol. VT-32, pp. 134-150, February 1983.

[Win84] J. H. Winters, "Optimum combining in digital mobile radio with cochannel interference," *IEEE Trans. Veh. Tech.* vol. VT-33, pp. 144-155, August 1984.

[Win93] J. H. Winters, "Signal acquisition and tracking with adaptive arrays in the digital mobile radio system IS-54 with flat fading," *IEEE Trans. on Veh.Tech.*, vol 42, no. 4, November 1993.

[Win94] J. H. Winters, "The impact of antenna diversity on the capacity of wireless communication systems," *IEEE Trans. on Comm.*, vol. 42, no. 2/3/4, Feb. / March/April 1994.

Vita

Paul Petrus was born on August 6, 1970, in Pondicherry, India. He received his B. Tech degree in Electrical Engineering with distinction in May'91 from Pondicherry University, Pondicherry. He received the award for the best outgoing student for the class of'91. He started his M. S. at Virginia Tech in Spring'93. In Summer'93, he joined MPRG, where he works with Dr. Reed on interference cancellation techniques.